Marker Studies of the Solid State Formation of $CrSi_2$ on Pd_2Si

Johan André Mars

Marker Studies of the Solid State Formation of $CrSi_2$ on Pd_2Si

by

Johan André Mars

dissertation submitted in partial fulfilment of the requirements for the degree of

Master of Technology
(M.Tech.)

in the School of Science at the

Peninsula Technikon

Internal Promotor: Mr John Farmer, Peninsula Technikon, Bellville

External Promotor: Dr René Pretorius, National Accelerator Centre, Faure

February 1998

ACKNOWLEDGEMENTS

This dissertation was completed with the guidance and generous help of a number of people to whom I wish to express my sincere gratitude:

- Dr R. Pretorius, my external promotor, for his guidance, participation and supervision of the investigation, encouragement and stimulating discussions and constructive criticism;
- Mr J. Farmer, my internal promotor for his support, advice and the interest he maintained throughout this study, as well as fruitful discussions;
- Dr C. Churms and Mr C. Theron for their continuous support, assistance and expertise during this investigation;
- Messrs K. Springhorn, N. Stoddart and C. Doyle for their efficient operation of the accelerator during experiments;
- Dr T. K. Marais, Mrs G. Stone and Messrs S. Hendricks, C. Cloete, W. Cloete and W. Gordon for their friendship and encouragement;
- My wife Marlene and children Brandon, Caraigne and André for their endearing love and moral support;
- To my Creator, whom I am forever thankful for the health and ability He has given me.

I declare that

Marker studies of the solid state formation of $CrSi_2$ on Pd_2Si

is my own work and that all the sources I have used or quoted have been indicated and acknowledged by means of complete references.

SYNOPSIS

The chemical system, Si < >| Pd | Cr, was investigated to study the formation of $CrSi_2$ on polycrystalline Pd_2Si, formed on Si<100> and epitaxial Pd_2Si formed on Si<111>. To ascertain the reaction mechanism during the formation, tantalum was used as an inert marker, since it does not participate in the reaction and is readily measured by Rutherford Backscattering Spectrometry (RBS). This investigation was performed in two parts. In the first part, the tantalum was inserted in the Pd_2Si layer to determine which species; palladium or silicon diffuses during $CrSi_2$ formation. In the second part, the marker was inserted in the $CrSi_2$ layer to determine whether chromium or silicon moves. In addition, the effect of marker thickness on the growth of $CrSi_2$ was investigated.

The samples were prepared by electron gun evaporation in vacuum, the elements being deposited on the particular silicon substrates. This was followed by the thermal treatment of the samples at temperatures of 400, 425, 450, 475, 500 and 550^{0}C. Normal and dynamic Rutherford backscattering spectrometry was used to characterize the thin film structures.

If the marker, when inserted in the Pd_2Si layer, should move towards the Pd_2Si | $CrSi_2$ interface then, the formation of $CrSi_2$ would be due to the dissociation of Pd_2Si. In this case Pd_2Si dissociates into Pd and Si and the Si diffuses to the interface of $CrSi_2$ and Cr to form $CrSi_2$, whereas the Pd diffuses to the Si < > | Pd_2Si interface to regrow Pd_2Si. However, if the marker position remains constant with respect to the Pd_2Si layer it can be concluded that the formation of $CrSi_2$ is due to the movement of Si from the substrate to the interface of $CrSi_2$ and Cr to form $CrSi_2$. If the marker when inserted in the $CrSi_2$ should move towards the sample surface then the chromium diffuses to the interface of $CrSi_2$ and Pd_2Si to react with the silicon, forming $CrSi_2$. If the marker does not move with respect to the $CrSi_2$ layer, then silicon diffuses and reacts with the chromium to form $CrSi_2$.

It was found that at the reaction temperatures of 500 and 550 ^{0}C, the $CrSi_2$ forms within the first minute of the chemical system attaining the temperature. At 550 ^{0}C, the $CrSi_2$ layer formation was completed before the temperature could be reached. During the growth of $CrSi_2$ on (a) Pd_2Si - Si <100> and on (b) Pd_2Si - Si <111> at the lower reaction temperatures, the marker position did not significantly change with respect to the Pd_2Si layer. It could be therefore concluded that the growth of $CrSi_2$ is predominantly due to silicon diffusion from the substrate through the Pd_2Si layer. Some initial palladium diffusion was found to occur during the early stages of $CrSi_2$ formation on both epitaxial Pd_2Si and non-epitaxial Pd_2Si. The initial palladium diffusion is independent of the temperature at which the reaction proceeds. In this instance, the silicon diffusion is slightly higher for growth on the non-epitaxial Pd_2Si than on epitaxial Pd_2Si. The thick (10Å) marker causes nearly twice as much initial palladium diffusion than in the case of the thin (5Å) marker.

The growth kinetics of $CrSi_2$ was found to be linear and there is no marked difference between the growth rates on the epitaxial and non-epitaxial Pd_2Si. However, when the marker thickness was increased from 5 to 10Å the time taken for growth to initiate was longer in the case of the thick marker than for the thin marker. In this instance, the growth rate of $CrSi_2$ when using a thick (10Å) marker differed only marginally from the growth of $CrSi_2$ for a thin (5Å) marker.

The degree of lateral non-uniformity of the Si < >|Pd_2Si interface was found to increase with an increase in the reaction temperature. For formation on epitaxial Pd_2Si, the degree of interface roughness (~ 40%) was higher than the degree of interface roughness (~20%) during formation on non-epitaxial Pd_2Si. In the case of the thick (10Å) marker, the degree of interface roughness was less and remained constant during the initial stages of $CrSi_2$ formation on non-epitaxial Pd_2Si. This is because more palladium diffusion mechanism occurs during the early stages and silicon is not derived from the substrate.

The thin (5Å) marker did not move when inserted in the $CrSi_2$ layer. Hence, it could be concluded that silicon is the diffusing species in the $CrSi_2$ layer during its formation. The marker however, has a marked effect on the kinetics of $CrSi_2$ formation and the temperature had to be increased to 800^{0}C before any reaction could take place.

CONTENTS

1. BACKGROUND AND SCOPE OF INVESTIGATION

1.1 Introduction......1

1.2 Solid State Reactions......2

1.3 Thin Films......6

1.3.1 Thin film growth......6

1.3.2 Application of thin films......8

1.4 Metal-Silicon Interactions......9

1.4.1 Silicide formation......9

1.4.2 Formation kinetics......10

1.4.3 Formation sequence......13

1.5 Diffusion......19

1.5.1 Solid state diffusion......19

1.5.2 Theory of diffusion......19

1.5.3 Basic diffusion mechanisms......24

1.5.4 Diffusing species..25

1.5.5 Marker studies..27

1.6 Formation of $CrSi_2$ on Pd_2Si..28

1.6.1 Pd_2Si formation..28

1.6.2 $CrSi_2$ formation..30

1.6.3 Si< >|Pd|Cr system..30

1.7 Scope of the Investigation..31

2. EXPERIMENTAL METHODS..33

2.1 Sample Preparation..33

2.1.1 Wafer preparation..33

2.1.2 Vacuum deposition..33

2.2 Sample Characterisation..35

2.2.1 Normal Rutherford backscattering spectrometry (RBS)..............35

2.2.1 *In situ* real time Rutherford Backscattering Spectrometry...........40

2.2.2 Measurement and data manipulation..41

3. COMPUTER SIMULATIONS..42

3.1 Introduction....42

3.2 Rump Simulation Software.... 42

3.3 Phase Identification....44

3.3.1 Palladium silicide phases.... .44

3.3.2 Chromium silicide phases....44

3.4 Mechanisms and Diffusing Species....45

3.5 Simulation of Marker Movement....47

3.6 Optimisation of Experimental Parameters....50

3.6.1 Pd thickness....51

3.6.2 Cr thickness....54

3.7 Simulation of the Marker Movement in $CrSi_2$ 55

3.8 Interface Roughness....56

4. FORMATION OF $CrSi_2$ ON Pd_2Si....61

4.1 Introduction....61

4.2 Non-epitaxial Pd_2Si....62

4.2.1 Kinetics....62

4.2.2 Diffusion mechanism....64

4.2.3 Interface roughness....67

4.3 Epitaxial Pd_2Si....68

4.3.1 Kinetics....68

4.3.2 Diffusion mechanism....70

4.3.3 Interface Roughness....72

4.4 Effect of Marker Thickness....74

4.4.1 Kinetics....74

4.4.2 Diffusion mechanism....75

4.4.3 Interface Roughness....77

4.5 Comparison of Results....79

4.5.1 Kinetics....79

4.5.2 Diffusion mechanism....80

4.5.3 Interface Roughness....80

4.6 Diffusion in $CrSi_2$ Layer....81

5. SUMMARY and CONCLUSIONS....82

Appendix A..86
K values for Rutherford backscattering spectrometry

Appendix B..87
Thicknesses that react

Reference Index..89

LIST OF TABLES AND FIGURES

Tables

Table [1.1] Summary of deposition methods for silicide formation 7

Table [1.2] Main types of reactions for the order of the reaction 12

Table [1.3] Values for the Heat of Formation of Cr – Si binary system................15

Table [4.1] Growth rates of $CrSi_2$ on Pd_2Si – Si <100>....................................63

Table [4.2] Growth rates of $CrSi_2$ on Pd_2Si – Si <111>....................................69

Table [4.3] Growth rates for thick marker compared...................................74

Table [6.1] List of K values for RBS...86

Table [6.2] Thicknesses of metals that would react to form silicides..................87

Figures

Figure [1.1] Diagram of the mechanism of $NiAl_2O_4$ formation 4

Figure [1.2] Phase diagram of the Pd – Si binary system................................10

Figure [1.3] Phase diagram of the Cr – Si binary system................................11

Figure [1.4] Effective Heat of Formation diagram for Cr – Si binary system..........18

Figure [1.5] Flux of matter or property down a concentration gradient..................20

Figure [1.6] Interaction of two metals to form a silicide...................................21

Figure [1.7] Illustration of interstitial mechanism 25

Figure [1.8] Illustration of vacancy diffusion mechanism...................................26

Figure [1.9] Illustration of grain boundary diffusion mechanism 26

Figure [1.10] Diagram of the diffusion of metal A into the interface....................27

Figure [2.1] Representation of the Ultra High Vacuum evaporation system 34

Figure [2.2] Diagram of the conceptual layout of backscattering spectrometry......36

Figure [2.3] Layout of a dynamic backscattering system................................41

Figure [3.1] Simulated backscattering spectrum of Pd – Si binary phases.............45

Figure [3.2] Simulated backscattering spectrum of Cr – Si binary phases.............46

Figure [3.3] Illustration of Ta marker movement for two possible mechanisms during $CrSi_2$ formation..48

Figure [3.4] Simulation of marker movement during Si diffusion mechanism........48

Figure [3.5] Simulation of marker movement during Pd diffusion mechanism.......49

Figure [3.6] Theoretical simulation of marker movement for both.....................50 Si and Pd diffuse mechanism

Figure [3.7] Determination of the relative positions of the elements...................51

Figure [3.8] Optimisation of Pd_2Si thickness 52

Figure [3.9] Optimisation of Ta marker position in the Pd_2Si layer 53

Figure [3.10] Illustration of change in marker position with increase in front Pd_2Si layer thickness 54

Figure [3.11] Determining the resolution of Cr and Pd peaks.............................55

Figure [3.12] Plot of the resolution distance against thickness of $CrSi_2$ layer 56

Figure [3.13] Mechanism for marker movement in $CrSi_2$ layer 57

Figure [3.14] Illustration of the two mechanisms, identifying the diffusing species in $CrSi_2$ 58

Figure [3.15] Illustration of a typical sample structure.......................................59

Figure [3.16] Composite spectra of sample structures used by PERT to obtain The best fit for the layer...59

Figure [4.1] Graph of growth in thickness on Pd_2Si – Si <100>........................62

Figure [4.2] Arrhenius plot of growth rates on Pd_2Si – Si <100>........................63

Figure [4.3] RBS spectra to indicate inward movement of the marker 64

Figure [4.4] Representation of *in situ* real time RBS spectra at 425 ^{0}C 65

Figure [4.5] Illustration of marker movement during growth on Pd_2Si – Si <100> 66

Figure [4.6] Illustration of % silicon diffusion on Pd_2Si – Si <100> 67

Figure [4.7] Degree or Interface Roughness on Pd_2Si – Si <100>..........................68

Figure [4.8] Growth of $CrSi_2$ on Pd_2Si – Si <111>...69

Figure [4.9] Arrhenius plot of growth rates on Pd_2Si – Si <111>..........................70

Figure [4.10] Backscattering spectra showing the inward movement of the marker during growth on Pd_2Si – Si <111>.....................................71

Figure [4.11] *In situ* real time RBS spectra during growth on Pd_2Si – Si <111>..........71

Figure [4.12] Marker movement during growth on Pd_2Si – Si <111>......................72

Figure [4.13] Illustration of % silicon diffusion on Pd_2Si – Si <111>........................73

Figure [4.14] Illustration of Interface roughness on Pd_2Si – Si <111>.......................73

Figure [4.15] Growth rate on thick and thin markers compared 75

Figure [4.16] Backscattering spectra for growth on Pd_2Si – Si <111> using a thick marker...76

Figure [4.17] *In situ* real time RBS using a thick marker......................................77

Figure [4.18] Degree of silicon diffusion mechanism for a thick marker....................78

Figure [4.19] Marker movement in the presence of the thick marker 79

Figure [4.20] Illustration of degree of Interface roughness when using a thick marker...79

Figure [4.21] RBS spectra indicating Si diffusion in $CrSi_2$ 81

CHAPTER 1

BACKGROUND AND SCOPE OF INVESTIGATION

1.1 Introduction

The advent of personal computers gave microelectronics new technological importance. For this reason, it is referred to as the most revolutionary industry of the twentieth century. The silicon chip is the most important component in the microelectronics industry. It is a small sliver of single crystal silicon upon which microelectronic circuitry is printed and etched. This generated considerable interest in the solid state interaction between thin-films, which is the basic interaction in most semiconductor systems. Silicides, formed by the interaction of silicon and metals, are used extensively as metallisation in microelectronic devices. (Metallisation is the laying down of conducting tracks on integrated circuits). Metal-silicide systems have favourable characteristics such as good thermal stability and low electrical resistivity (Nicolet & Lau, 1983:330). These characteristics facilitate the manufacture of the silicon-based micro-electronic devices. Clearly any study contributing positively to such a large industry will give rise to substantial savings in time and money, internationally.

In this study the solid state chemistry of the Si< >/Pd/Cr thin film system, specifically the formation of $CrSi_2$ on previously formed Pd_2Si, will be investigated. In the first part of this study, tantalum will be inserted in the Pd_2Si layer to act as an inert marker and in the second part it will be inserted in the $CrSi_2$ layer. These markers do not participate in the reaction at the specified temperature (Nicolet & Lau, 1983:359). Therefore, as the solid-state interaction takes place, any change in the position of the marker will give rise to important information such as to the identity of the diffusing species. The mechanism of diffusion

and diffusing species, which then will be determined by the study, will contribute to the basic understanding of solid state interaction of thin metal films with semiconductors. This information is also of paramount importance in the design of silicide-based micro-electronic devices, as the feature size of these devices shrinks to sub-micron dimensions. At these dimensions, knowledge of diffusion species and mechanism can guide the fabrication and design in order to minimise subsequent device failure.

1.2 Solid State Reactions

Most solids do not react at room temperature at an appreciable rate and over a reasonable time-scale (West, 1984:5). The reaction can therefore not be monitored adequately. It is thus necessary to heat the reactants to relatively high temperatures, often between 200 to 1500°C, to bring about a reaction. This indicates that both thermodynamic and kinetic factors are important in solid state reactions (West, 1984:5). The thermodynamic factors show whether the reaction is feasible and the kinetics factors indicate the rate at which the reaction is likely to occur. One can appreciate the complexity with which reactions in the solid state occur and the difficulty when heating the reactants to such high temperatures. Solid state reactions are seldomly discussed in general texts. Since it forms the basis of this investigation, a more in-depth study of these reactions is necessary.

A solid state reaction occurs when local transport of matter is seen in crystalline phases (Schmalzried, 1981:11). The transport of matter in the solid state and the reactivity of solids are dependent on the mobility of the individual particles in the lattice. A perfectly ordered crystal can ideally only be moved as a whole. Motion of the individual particles from their lattice sites cannot occur without the aid of crystal defects.

There are generally three classes of solid state reactions: (Schmalzried, 1981:11)

- Homogenous reactions
- Reactions in single phase inhomogeneous systems

- Heterogeneous reactions

1.2.1 Homogeneous reactions

As an example, in a compound, of the formula AB_2O_4 (Cotton, Wilkinson & Gauss, 1987:132-3; West, 1984:5), which crystallises in a spinel structure, the ions can be arranged in two limiting cases. Firstly, in the normal spinel, the divalent cations are located on the regular lattice. These cations have a tetrahedral symmetry and the trivalent B cations, found on the lattice sites, have an octahedral symmetry. Secondly, in the inverse spinel structure, half of B cations are found on the regular lattice, having a tetrahedral symmetry. The other half is located with the A cations on regular lattice sites with an octahedral symmetry. When the temperature of the spinel crystal changes, a local redistribution of A^{2+} and B^{3+} cations takes place:

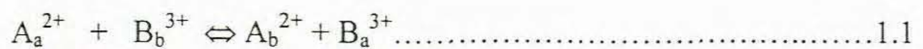

$$A_a^{2+} + B_b^{3+} \Leftrightarrow A_b^{2+} + B_a^{3+} \quad \text{..........} 1.1$$

The ions of the one sub-lattice seek out the vacancies in the other sublattice and a reversal of positions occurs. This process takes place by means of diffusional steps and no compositional, but only structural change occurs.

1.2.2 Reactions in an inhomogeneous single phase system

This class of solid state reactions occurs by a diffusional process in a single-phase system with a concentration gradient. As an example, consider iron packed with graphite. At 950°C, carbon atoms diffuse into the interstices of the face-centred cubic iron, down the concentration gradient from the surface into the interior of the iron. In a similar manner semi-conductors can be doped (i.e. add low concentrations of foreign materials) to control their electrical conduction properties.

1.2.3 Heterogeneous reactions

A heterogeneous solid state reactions occurs when two substances react with one another to form one or more products, the product(s) being separated by a phase boundary. Consider as an example the reaction of the crystals NiO and Al_2O_3 to form the $NiAl_2O_4$ spinel. The crystals are in close contact over a shared interface. After the necessary heat treatment, the crystals have partially reacted to form a layer of $NiAl_2O_4$ at the interface, shown schematically in **figure [1.1]**.

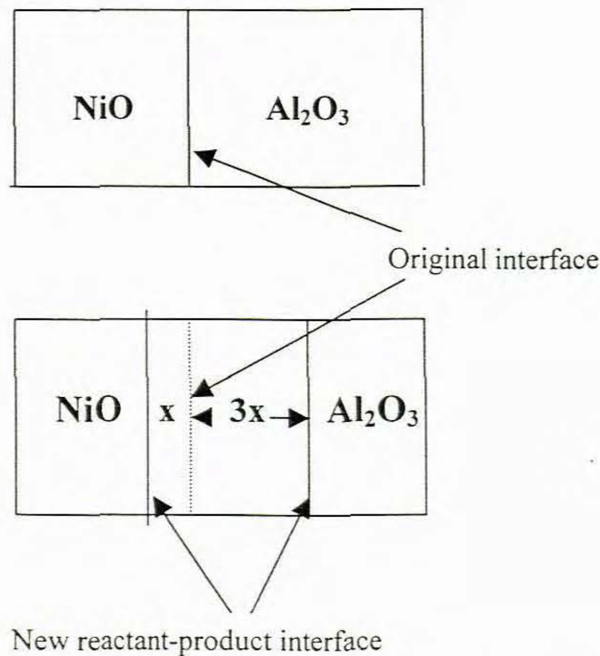

Fig. [1.1] ***Conceptual diagram of the mechanism of formation of $NiAl_2O_4$ by the interdiffusion of the cations from NiO and Al_2O_3 based on schematics in West, 1984:6***

Nuclei of $NiAl_2O_4$ are formed in the first stage of the reaction. The nucleation process is difficult since the structure of the reactants and that of the product differs considerably. There is a large amount of structural organisation when the product forms. This factor adds to the difficulty of nucleation. Bonds break and reform and atoms migrate at times distances that are large on the atomic scale. At a sufficiently high temperature, Ni^{2+} and Al^{3+} ions have enough energy to be displaced from their normal crystal lattice sites. These ions

diffuse through the crystal. Ni^{2+} ions diffuse from the NiO layer towards the interface and Al^{3+} ions diffuse from the Al_2O_3 layer to form $NiAl_2O_4$. Subsequent counter diffusion of Ni^{2+} and Al^{3+} must occur through the existing $NiAl_2O_4$ product layer to the new reaction interfaces. There are now two interfaces - the NiO | $NiAl_2O_4$ interface and the $NiAl_2O_4$ | Al_2O_3 interface. If the rate-limiting step for the reaction is the diffusion of Ni^{2+} and Al^{3+} ions through the $NiAl_2O_4$ layer, then diffusion flux will slow as the product thickness increases. At the two interfaces the reactions are:

At the NiO | $NiAl_2O_4$ interface

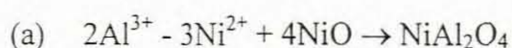

(a) $2Al^{3+} - 3Ni^{2+} + 4NiO \rightarrow NiAl_2O_4$

At the $NiAl_2O_4$| Al_2O_3 interface

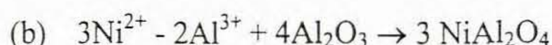

(b) $3Ni^{2+} - 2Al^{3+} + 4Al_2O_3 \rightarrow 3\ NiAl_2O_4$

The overall reaction is:

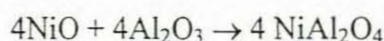

$4NiO + 4Al_2O_3 \rightarrow 4\ NiAl_2O_4$

Reaction (b) gives three times more of the product than reaction (a). The interface on the Al_2O_3 side subsequently moves at three times the rate of the interface of the NiO side. The reaction rate is controlled by (West, 1984:6,7):

- The transport of matter to the reaction interface,
- Reaction at the interface and
- The transport of matter away from the interface.

The slowest of these processes is the rate-controlling step (Atkins, 1995:885-6).

In the analysis of the reaction rate by using the rate laws, the concept of reaction order – the power to which the concentration of the component is raised in the rate law – is helpful. The rate of change in the concentration of product is proportional to the *n*th power or order of the reactant(s) i.e.

$$dC/dt = k\,c^{-n} \qquad \text{1.2}$$

where C is the concentration of the product(s), k is a proportionality constant, the rate constant, c the concentration of the component, n the power to which the concentration of the component is raised and t the time. In a zeroth order reaction, when $n = 0$ equation [1.2] becomes

$$dC/dt = k \Rightarrow \int dC = k\int dt \Rightarrow C = kt \qquad \text{1.3}$$

The concentration of the product is thus linearly related to time. For the formation of $NiAl_2O_4$, the interdiffusion of the cations (Ni^{2+} and Al^{3+}) through the spinel is the rate controlling step and the rate of formation of the product is inversely proportional to the concentration, i.e. $dC/dt = 1/C$. Here $n = 1$ and the concentration of the product depends on the square root of time.

In this section only one of the general principles of solid state reactions viz. reaction conditions was discussed. Other principles such as structural considerations must be considered when deciding on a reaction mechanism.

1.3 Thin Films

1.3.1 Thin film growth

The factors that influence the growth of thin films depend on the deposition techniques. A comparison of the different deposition methods is given in **table [1.1]**. The factors that influence film growth are:

- The type and condition of substrate (polycrystalline or amorphous etc.),
- The presence of any residual gas in the deposition chamber, e.g. oxygen, methane and other inert gasses,

Table [1.1] *Summary of the deposition methods for the formation of silicides (From Nicolet and Lau, 1983:337)*

	Vacuum evaporation		Nonreactive sputtering		
	One source (metal)	Two sources (metal and Si)	One source (silicide target)	Two sources (metal and Si)	Chemical vapor deposition (CVD)
Substrate	Si	Any	Any		Any
Substrate temperature during deposition	~Room temperature (RT)		~100–≳300°C		High
Possibility to control substrate temperature	Good		Fair		Good
Compatibility with photoresist (liftoff)	Good		Fair to poor		Nil
Soft x rays	Filament: no E-gun: Yes		Yes		No
Purity of deposition	Good		Mediocre	Fair	Good
Control of stoichiometry	None	Demanding	None	Good	Demanding

- The presence of charged particles near the atoms being deposited,
- Chemical reactions that can take place between the substrate and the atoms during the deposition.

In this study, vacuum evaporation by an e-gun was used to prepare the samples. When fabricating exposed metal oxide semi-conductors (MOS), the soft x-ray background that is associated with e-gun evaporation can be avoided by vacuum evaporation of a substance from a filament. Many of the factors such as control over the substrate temperature, compatibility with photo-resist and the purity of the deposition are within the control of the experimenter. After deposition, the simplest configuration is a uniform layer on a flat surface that is much larger than the thickness of the film. The sample (substrate and layer) is now subjected to a heating process. Film growth depends on factors such as the crystallo

graphic orientation of the substrate and the temperature. Characteristics that should be considered are the melting temperature of the layer and the eutectic point.

1.3.2 Application of thin films

The applications of thin film technology found its roots in the electroplating industry (West, 1984:33). The primary aim was the protection of metals against corrosion or chemical attack. Examples are the galvanisation of iron (Fe) with tin (Sn). This prevents the oxidation of Fe to Fe_2O_3 by water and air (Cotton, Wilkinson & Gauss, 1987:494-7). Protective coatings can be formed on refractory metals for protection from oxidation at high temperatures. Other applications of thin films are in data storage on compact- and magnetic disks, in metallurgical coatings for corrosion inhibition and optical coatings. The structure and properties of deposited thin films depend on the surface used for deposition and growth. Thorough characterisations of the surface, as to the crystallographic orientation, energy of desorption and dislocation and imperfection densities will yield an adequate description of the film properties.

Silicide films are used in integrated silicon devices as part of the contact that joins an interconnecting line to the silicon substrate in a contact window and for interconnections. In contacts for interconnections, the flow of electric current is mainly perpendicular to the silicide layer and across the silicide-silicon interface. The electrical characteristics of the contact are of prime importance. It is desired to express these characteristics in terms of parameters such as barrier heights, ideality factor or contact resistivity. In interconnections, the current flows mainly along the plane of the thin film. The characteristics of importance are the carrier concentration, carrier mobilities and electromigration. Silicides are used as interconnects since its metallic nature provides good electrical conduction. Silicides can also withstand high-temperature oxidising ambients, which cannot be withstood by refrac-

tory metals. Furthermore, the silicides have small grain sizes, which is desirable for good line definition upon etching and are they compatible with poly-silicon gate technology.

1.4 Metal-Silicon Interactions

Most metals, whether alkali, alkali-earth, transition or rare-earth metals are able to form silicides (Nicolet & Lau, 1983:334). The alkali- and alkali-earth metals have only one or two electrons in their outer orbital and thus have low ionisation energies. These metals are therefore chemically very reactive. (They react violently when in contact with water (Liptrot, 1983:174; Cotton, Wilkinson & Gauss, 1987:244,269)). This characteristic is undesirable in integrated circuits and these metals are therefore seldomly used in the manufacturing process. Transition metals, when subjected to a process of solid-phase reaction with silicon as the substrate, give well-defined uniform silicide layers. In this study, the typical thickness of the silicides is of the order of 100 to 1000 Å.

1.4.1 Silicide formation

Each transition metal can form numerous compounds with the silicon substrate with which it reacts. It is therefore extremely important to ascertain:

- which of the silicides are actually formed,
- the temperature at which they are most likely to form
- the kinetics of formation
- the diffusing species and the diffusing mechanism during formation.

For instance, the compounds that can form from the interaction of Si and Pd are PdSi, Pd_2Si, Pd_3Si, Pd_9Si_2, and Pd_5Si as can be seen in **figure [1.2]**, in which the phase diagram of the palladium-silicon binary system is depicted.

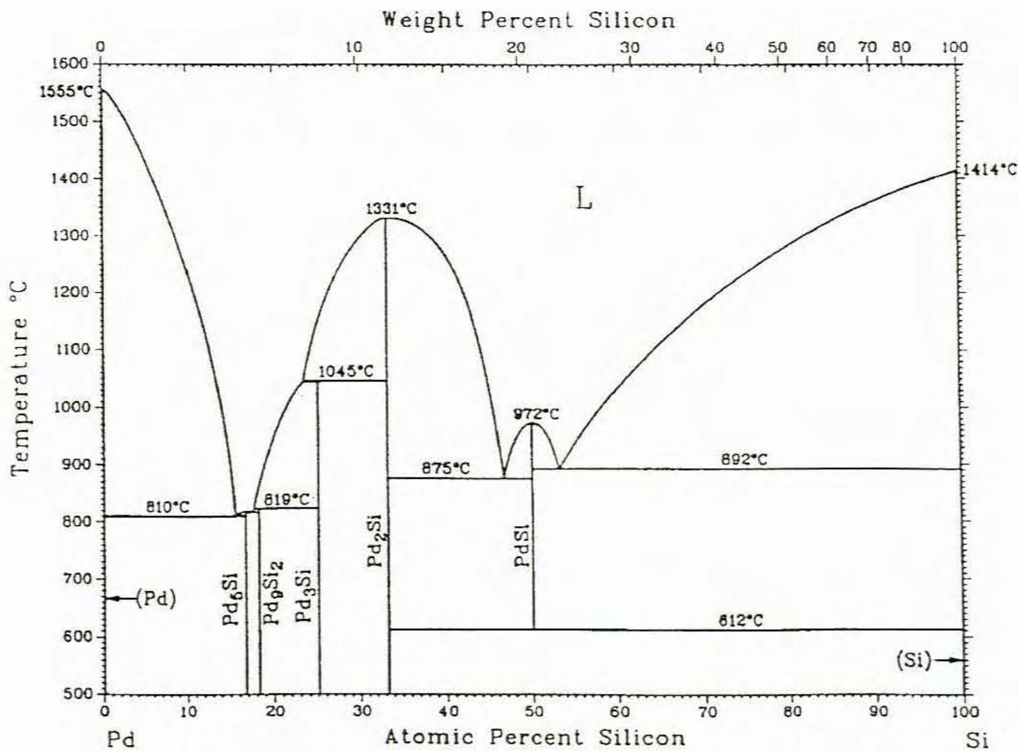

Figure [1.2]. ***The phase diagram of the Pd – Si binary system.(From Baxi and Massalski, 1991:350)***

The compounds that may be formed by the interaction of Cr and Si are $CrSi_2$, CrSi, Cr_5Si_3 and Cr_3Si, as can be seen in the phase diagram of the Cr – Si binary system, given in **figure [1.3]**.

1.4.2 Formation kinetics

The type of silicide formed and the temperature at which it forms will have an immense impact on the kinetics of the Si <> | Pd | Cr chemical system. In section [1.3.1], it was pointed out that the temperature, crystallographic orientation and the condition of the substrate would affect the growth in thickness of the silicide layer. In this investigation, single-crystal silicon-substrates were used.

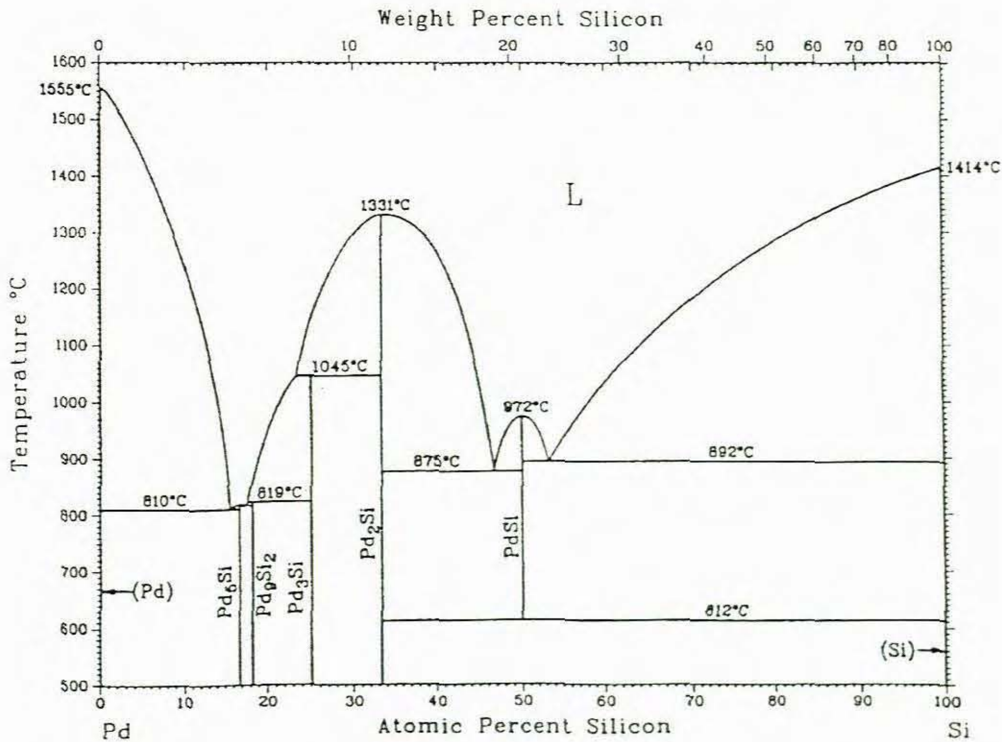

Figure [1.2]. ***The phase diagram of the Pd – Si binary system.(From Baxi and Massalski, 1991:350)***

The compounds that may be formed by the interaction of Cr and Si are $CrSi_2$, CrSi, Cr_5Si_3 and Cr_3Si, as can be seen in the phase diagram of the Cr – Si binary system, given in **figure [1.3]**.

1.4.2 Formation kinetics

The type of silicide formed and the temperature at which it forms will have an immense impact on the kinetics of the Si < > | Pd | Cr chemical system. In section [1.3.1], it was pointed out that the temperature, crystallographic orientation and the condition of the substrate would affect the growth in thickness of the silicide layer. In this investigation, single-crystal silicon-substrates were used.

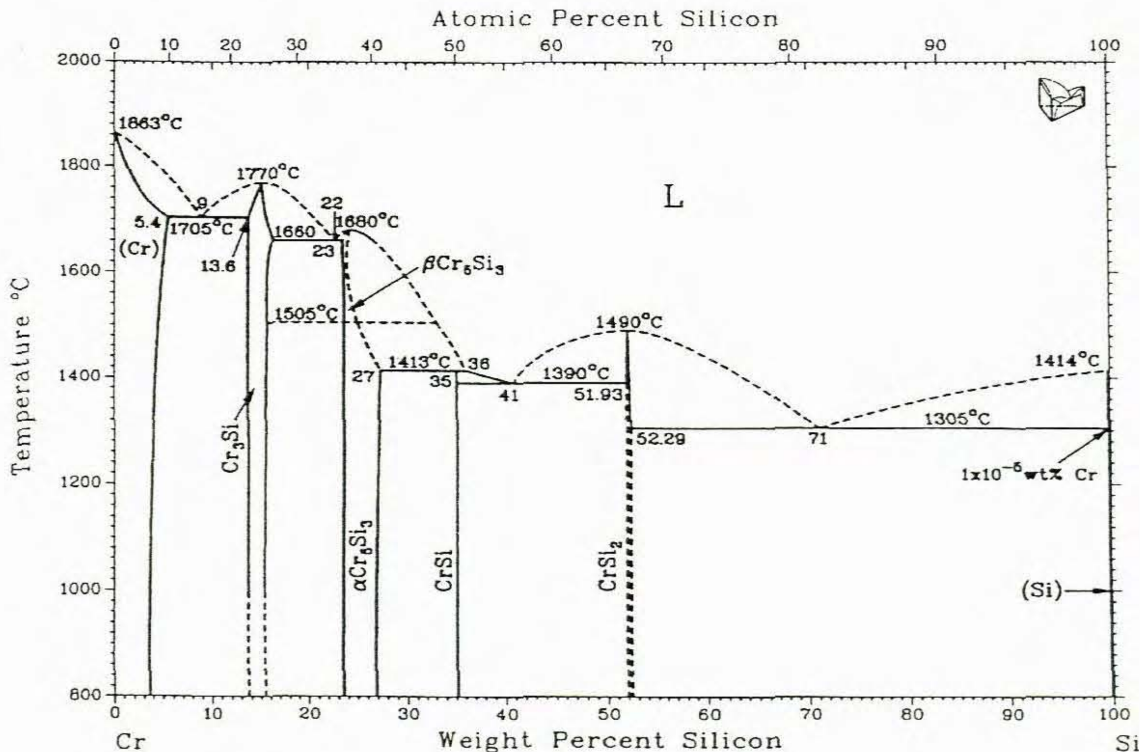

Figure [1.3] *Phase diagram of the Pd – Si binary system. (From Moffat, 1997:7/87)*

The kinetics of formation will undoubtedly be expressed by the laws of rate of formation or rate laws, as commonly known. In this instance, the formation rate can be defined in terms of the order of the reaction, (Atkins, 1995:866). **Table [1.2]** gives a summary of the main reaction types. In the integrated form, the first equation of the rate-laws in **table [1.2]** represents a linear relation between the thickness of product formed and the time elapsed. The rate of change in thickness is therefore independent of the initial amount of the product. The integrated form of the second equation expresses the dependence of the thickness of product, at an arbitrary time, to the initial thickness. In the third equation, two reactants participate in the reaction and the final thickness of product is dependent on the initial

Table [1.2] ***Main types of reactions, for the order of the reaction, the corresponding rate-laws and the integrated forms of the rate-laws. A and B are the reactants, P the product, t the time, k_0 is a constant and x the amount (thickness) of product formed. The subscript 0 indicates the initial concentration.(From Atkins, 1995:867)***

	Reaction	Order	Rate law	Integrated Form
1.	$A \rightarrow P$	0	$dx/dt = k_o$	$k_o t = x$
2.	$A \rightarrow P$	1	$dx/dt = k_o[A]$	$k_o t = \ln \frac{[A]_0}{[A]_0 - x}$
3.	$A + B \rightarrow P$	2	$dx/dt = k_o[A] \times [B]$	$k_o t = \frac{1}{[B]_0 - [A]_0} \times \ln \frac{[A]_0([B]_0 - x)}{([A]_0 - x)[B]_0}$

amount of both the reactants. (It should be noted that these equations do not take into account the temperature at which the solid state reactions occur.)

There are two general categories for the formation kinetics of silicides (Nicolet & Lau, 1983:345-7). In the first category, the system shows lateral uniform growth with a well-defined temperature dependence and good kinetics. In the second category, the system shows laterally non-uniform growth and critical temperature dependence. In the first category for the solid state reactions, the formation kinetics can be linear or parabolic. If the formation kinetics is linear, then the growth is limited by interfacial interaction (Nicolet & Lau, 1983:345-7) and if parabolic then the growth is limited by diffusion. The reaction also takes place over a wide temperature range and the melting- or eutectic point is much higher than this temperature range. Examples of parabolic formation kinetics are the growth of Pd_2Si, Ni_2Si, Pt_2Si, and NiSi and linear formation kinetics is found in the growth of $CrSi_2$, $MoSi_2$, and $TiSi_2$. It is further emphasised (Nicolet & Lau, 1983:345-7) that "...rates of the reaction and the morphology of the silicides generally depend on the details of deposition and annealing, but the mode of the process is independent". It is noteworthy

that, for the formation of silicides investigated, the formation kinetics has been expressed in terms of the growth rate by the two relations:

$$\text{thickness} \propto \text{time} \quad \Rightarrow dx/dt \propto t$$

$$\text{or} \quad \text{thickness} \propto \sqrt{time} \quad \Rightarrow dx/dt \propto t^{1/2}$$

1.4.3 Formation sequence

The driving force for a reaction to take place is the change in the free energy of the system. The relation of the free energy to these properties is expressed by (the Gibbs-Helmholtz) equation

$$\Delta G_T = \Delta H_T - T\Delta S_T \qquad \text{1.4}$$

G is the Gibbs free energy, S the entropy and H the enthalpy (heat) of formation. The subscript T denotes the temperature. The free energy is thus directly proportional to the difference in heat of formation and the product of T and the entropy of the system. The temperature dependence of the enthalpy and the entropy is related to the heat capacities. The relation between the enthalpy of formation and the heat capacity at constant pressure, C_p, of the phase is given by

$$C_P = \left(\frac{\partial H}{\partial T}\right)_p \qquad \text{1.5}$$

The subscript P indicates that the measurement was taken at constant pressure. The relation of the heat capacity at constant pressure and the heat capacity at constant volume (C_v) is given by

$$C_p - C_v = (\alpha^2/\kappa)TV \quad \text{.......} \quad 1.6$$

The compressibility (κ) for a solid is normally insignificant, but the volume change (α) may be considerable. It would therefore be erroneous to equate the heat capacity at constant volume to the heat capacity at constant pressure. Equation [1.6] can be rewritten as follows (Atkins, 1995:69):

$$C_p - C_v = n \cdot R \quad \text{.......} \quad 1.7$$

where n is the number of degrees of freedom and R is the universal gas constant ($R = 8.341\ J.K^{-1}.mol^{-1}$). The atoms in a solid are located in a fixed lattice. There are thus no rotational and or translational movements possible. However, three vibrational degrees of freedom exist (Kubaschewski & Alcock, 1979:181). The value of equation [1.8] is therefore approximately $25x10^{-3}kJ.K^{-1}.mol^{-1}$. This value also agree with the Dulong and Petit's rule which states that "the atomic heats of the elements generally approximates to the value of ~$25x10^{-3}kJ.K^{-1}.mol^{-1}$". For reactions in the solid state, there is then relatively no change in the heat capacity with temperature. The enthalpy of formation ΔH in equation [1.4] can therefore be approximated to ΔH_{298}, the standard heat of formation (at $25^{\circ}C$). This can be tested by calculating the temperature dependence of ΔH explicitly with the aid of

$$\Delta H_T \approx \Delta H_{298} + \int_{298}^{T} \Delta Cp\, dT \quad \text{.......} \quad 1.8$$

For example, the enthalpy of formation as a function of temperature for the phases of the Cr - Si binary system in the temperature range of 298 to 850 K can be calculated using

equation [1.8] and data for the heat capacities (Kubaschewski & Alcock, 1979:340-356). These calculations are given in **table [1.3]**. It is evident that the enthalpy of formation remains relatively constant over the temperature range.

Table [1.3] ***Values for the heats of formation, given in kJ(mol.atom)$^{)-1}$, of the phases of the Cr - Si binary system calculated from equation [1.9] and data for C_p from Kubaschewski & Alcock, 1979:340-356)***

Compound	ΔH_{298}	ΔH_{400}	ΔH_{500}	ΔH_{600}	ΔH_{700}	ΔH_{800}	ΔH_{850}
Cr_5Si_3	-35.0	-34.9	-34.9	-34.9	-34.9	-34.9	-34.8
CrSi	-30.2	-30.1	-30.1	-30.1	-30.0	-30.0	-29.9
$CrSi_2$	-25.8	-25.8	-25.8	-25.9	-25.9	-25.9	-25.9
Cr_3Si	-34.4	-34.4	-34.4	-34.3	-34.3	-34.3	-34.3

The influence of the entropy factor (ΔS) on the free energy can now be evaluated. Generally, for solid state reactions, the effect of the entropy term is quite small in comparison to the enthalpy of formation. The contribution of the entropy term, $T\Delta S$, to the Gibbs free energy change, $\Delta G°$, as a percentage of the enthalpy of formation, $\Delta H°$, has been calculated (Pretorius, Marais & Theron, 1993:10-11). These calculations were effected at a temperature $T=273+ 1/3t_{lm}$, where t_{lm} is the liquidus minimum (°C) of the binary phase. It was found in most cases that the contribution was less than 10%, which is insignificant compared to the accuracy of entropy and enthalpy of formation (Kubaschewski & Alcock, 1979:4). Therefore in solid state reactions, the Gibbs free energy $\Delta G°_T$ may be approximated quite well by $\Delta H°_{298}$ or

$$\Delta G_T^{\circ} \approx \Delta H_{298}^{\circ} \qquad 1.9$$

Where experimental values of ΔH_{298} are not available, other theories can be used to estimate the enthalpy of formation. The cohesion in alloys (Miedema, de Chatel & de Boer, 1979:1-28), a semi-empirical model, is based on a macroscopic atom picture in which free atoms are considered as a reference system. Another model is the application of the Redlich-Kister expression for the free energy (Baxi and Massalski, 1991:349-356). This expression applies to face centred cubic, diamond cubic and liquid forms.

In section [1.4.1] the number of silicides that can form in the Si<>|Pd|Cr system were discussed. The title of this investigation '.... **formation of $CrSi_2$ on Pd_2Si**' states that $CrSi_2$ forms on Pd_2Si and assumes that Pd_2Si is the phase of the binary system Pd – Si that forms and not the other phases of Pd - Si binary system. Further $CrSi_2$ is the phase that forms and $CrSi_2$ forms on top, which is after the formation, of the Pd_2Si. The phases that form are of cardinal importance to this study. It is necessary to discuss in detail the phase formation sequence for both Pd and Cr. The Effective Heat of Formation theory (Pretorius, Marais & Theron, 1993:1-28) is used to predict the phase that will form. In this theory, the effective heat of formation is related to the heat of formation by the equation

$$\Delta H^{eff} = \Delta H_f^{\circ} \times \frac{[X]_{eff}}{[X]_{com}} \quad \ldots\ldots 1.10$$

where ΔH^{eff} is the effective heat of formation, ΔH^0 is the standard heat of formation of the compound. $[X]_{eff}$ is the effective concentration and $[X]_{com}$ the compound concentration of the limiting element. The values of ΔH^{eff} and ΔH_f° are expressed in kJ (mol. atom)$^{-1}$.

The effective concentration of the limiting element is taken to be the composition of the lowest temperature eutectic in binary silicide systems. The system is said to have a congruently melting phase when the melting process occurs such that the chemical compo-

sition of the system remains the same. Similarly, the system has a non-congruent melting phase if there is a change in chemical composition. The Effective Heat of Formation model for predicting phase formation sequence in silicides (Pretorius, Marais & Theron, 1993:1-28) is then formulated as: ***In a binary silicide system, the phase to form first during metal-silicon interaction, is the congruent phase with the lowest (most negative) effective heat (enthalpy) of formation (ΔH^{eff}) at the concentration of the lowest eutectic temperature of the system.***

As an example let's assume that for the formation of $CrSi_2$ the effective concentration at the interface is 25% Cr. In this instance, Cr will be the limiting element. The ΔH° for $CrSi_2$ is –25.8 kJ (mol.atom)$^{-1}$ then

$$\Delta H^{eff}_{CrSi_2} = -25.8\left(\frac{25.0}{33.33}\right) = -19.35 \text{ kJ K}^{-1} \text{ (mol.atom)}^{-1}$$

The Effective Heat of Formation values for all the phases in the Cr – Si binary system are plotted in **figure [1.4]**, with the phase diagram (Moffat, 1997:7/87). From this figure, it can be deduced that $CrSi_2$ is the first phase of the Cr – Si binary system that forms. Similarly, for the Pd – Si binary system, it can be deduced that Pd_2Si is the first phase that forms. It should be noted that for Pd – Si interaction in the prediction of the effective heat of formation, the contribution of the entropy term is relatively higher than the values used (Kubaschewski & Alcock, 1979:340-356). Higher results, in which the contribution of the entropy term is 20% to the heat of formation, are obtained.

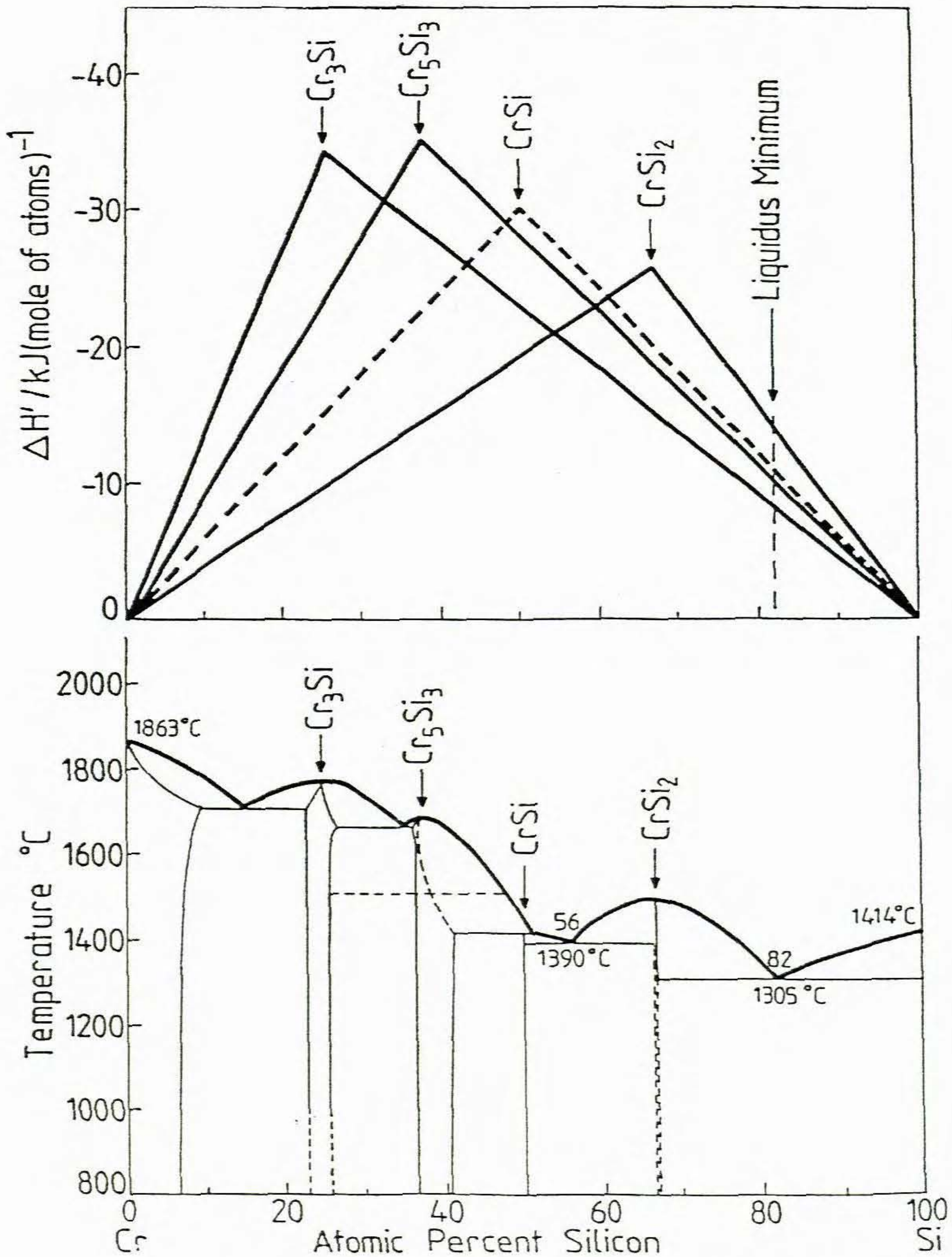

Figure [1.4] *The effective heat of formation diagram for compound phase formation (top) calculated from data in Pretorius, Marais & Theron, 1993:10-11 and the phase diagram (bottom) from Moffat, 1997:7/87 for the Cr – Si binary system. A linear relation exists between ΔH^{eff} and $[X]_{eff}$.*

1.5 Diffusion

Diffusion is the flow or transport of matter from one region to another. Examples of the transport of matter are:

- the effusion of a gas from a region of high pressure to a region of low pressure until the pressures in the two regions are equilibrated,
- when matter is displaced from a region of uniform composition to one of non-uniform composition, such as the diffusion of a radioactive isotope into a non-radioactive gas,
- when heat is applied to a system, the heat will be transported throughout the system until uniform temperature is attained and
- when a solid is dissolved in a solvent, the solid will be distributed uniformly in the solvent.

These examples indicate that diffusion is found in liquids and solids.

1.5.1 Solid state diffusion

In solids, the atoms in the crystal lattice are in continuous oscillation around their equilibrium positions. When sufficient heat is applied to the system it becomes energetically favourable for the atom(s) to be displaced ('jump') from the original site and a change in position occurs. This displacement of matter, in this manner, gives rise to solid state reactions.

1.5.2 Theory of diffusion

When matter is transported from one region to another, a measure of the rate of flow is necessary. The measure of the flow of matter will be referred to as the flux (J).

The flux (J) is therefore the amount of matter that passes through a unit area during a unit time as illustrated in **figure [1.5]**. The matter flows down a concentration gradient from a

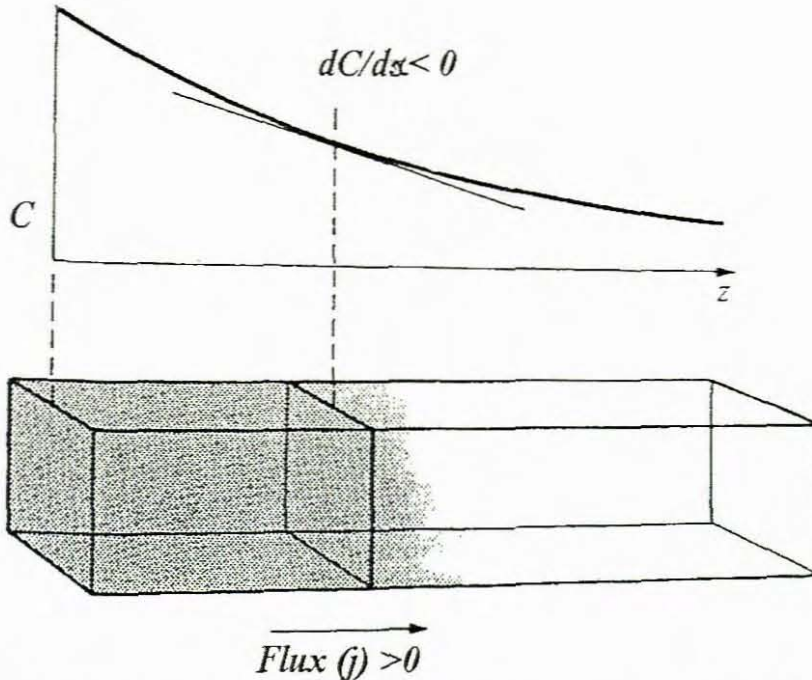

Figure [1.5]. ***The flux of matter or property down a concentration gradient.***

region of high concentration to one of low concentration the flux is expressed by

$$\Rightarrow J \propto dC/dx \qquad 1.11$$

and can be written as

$$J = -D\cdot(dC/dx) \qquad 1.12$$

D is the proportionality constant and termed the coefficient of diffusion with units of

Equation [1.13] is known as Fick's first law of diffusion. In the derivation of equation [1.13], it was assumed that the change in concentration was uniform, i.e. the concentration gradient is constant,

$$\Rightarrow d^2C/dx^2 = 0 \quad \text{.......} \quad 1.13$$

In sections [1.2] and [1.4], it was stated that the growth kinetics for most metal and silicide interactions is normally linear or parabolic. We can now assume that two compounds A and B, both metallic in nature, react to form a compound of the composition A_xB (**figure [1.6]**) and A, in this instance, is the diffusing species.

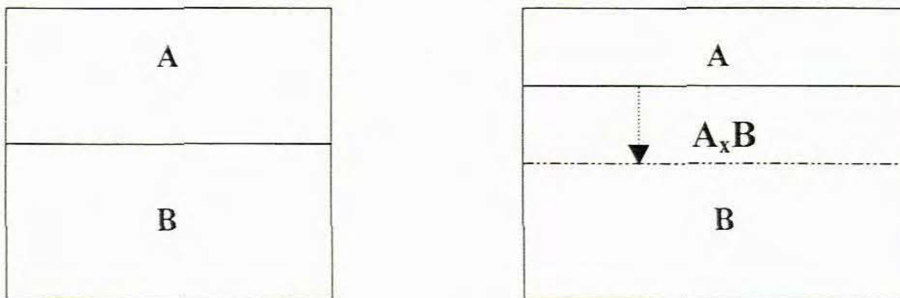

Figure [1.6] ***Conceptual diagram of the interaction of metals A and B to form the metal-silicide A_xB, after time t***

Atoms of A diffuse through A_xB to the interface of A_xB and B where further growth of A_xB takes place.

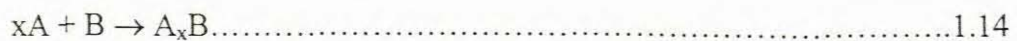

$$xA + B \rightarrow A_xB \quad \text{.......} \quad 1.14$$

Let's denote the concentration of atoms in A at the interface of A_xB and A as C_0 and the concentration of atoms of A at the interface of A_xB and B as C_i. The thickness of the inter-

posed layer A_xB is l. then according to equation [1.13] the flux of A diffusing down the concentration gradient is given by

$$J_1 = D \cdot \left(\frac{C_0 - C_i}{l} \right) \qquad 1.15$$

The rate at which equation [1.14] can occur determines the flux , J_2, of A atoms that can react with B to form A_xB. Hence for the flux J_2

$$\Rightarrow \quad J_2 \propto C_i \quad \Rightarrow \quad J_2 = k \cdot C_i \qquad 1.16$$

where k is the chemical reaction rate constant for the consumption of A in equation [1.14]. For equilibrium growth, these fluxes should be equal.

$$\Rightarrow \quad J_1 = J_2 \Rightarrow J = \left(\frac{DC_0 k}{D + kl} \right) \qquad 1.17$$

The growth rate, dl/dt (thickness per unit time) increase or change of the system, is then given by

$$\Rightarrow \quad \frac{dl}{dt} = \frac{J}{[A \cdot atoms]} = \left(\frac{DC_0 k}{[A \cdot atoms]} \right) \cdot \frac{1}{D + kl} \qquad 1.18$$

The square brackets denotes the concentration of atoms of A in the phase A_xB.

$$\Rightarrow \frac{dl}{dt} \propto \frac{Dk}{D + kl} \qquad 1.19$$

If k >> D/l then equation [1.19] becomes

$$\frac{dl}{dt} \propto \frac{D}{l} \quad \Rightarrow \quad l \propto t^{1/2} \quad \ldots 1.20$$

and when k << D/l

$$\frac{dl}{dt} \propto k \Rightarrow l \propto t \quad \ldots 1.21$$

Equation [1.20] shows that the reaction kinetics is parabolic and equation [1.21] shows that the reaction kinetics is linear. This concurs with equation [1.2]. When the atoms of A interact with the atoms of B, the frequency of interaction is denoted by Z_{AB}. The atoms must interact with an energy E_a, the activation energy, for a reaction to ensue (Atkins, 1995:878). The proportion of atoms that interact with the energy E_a must thus be multiplied by the frequency of interaction. This proportion is given by the Boltzmann distribution (equation [1.22]).

$$\frac{N_i}{N_j} = e^{(-(E_i - E_j)/RT)} \quad \ldots 1.22$$

where E is the energy, R the universal gas constant and N the population in the energy state. The subscripts i and j refer to the energy states. The rate of interaction (k), the growth of thickness per unit time is, therefore proportional to the exponential function of the energy and the temperature. This relation is expressed by (the Arrhenius) equation [1.23].

$$\Rightarrow k = Z_{AB} \cdot e^{\left(\frac{-E_a}{RT}\right)} \quad \text{.........} 1.23$$

Z_{AB} is the pre-exponential term and $e^{(-E_a/RT)}$ the exponential term. This expression takes in account the principle features of the reaction mechanism in that the atoms must interact – the pre-exponential term – and react only if the interactions are energetically sufficient – the exponential term. Substituting A for Z_{AB} and taking natural logarithms on both sides in equation [1.23], then

$$\Rightarrow \ln k = \ln A - \frac{E_a}{RT} \quad \text{.........} 1.24$$

When for a number of reactions the temperatures (T) and the growth rates (k) are known, equation [1.24] is used to plot ln k versus $\frac{1}{T}$, yielding a straight line. The y-intercept will give the natural logarithm of the pre-exponential factor and the slope will yield $-E_a/R$, from which the activation energy can be determined since R is a constant.

1.5.3 Basic diffusion mechanisms

From the theory of specific heat, the atoms are in continuous oscillation around their equilibrium positions. When it becomes energetically favourable, these atoms will move from their original positions. These displacements or jumps give rise to diffusion. There are various mechanisms (Schmalzried, 1983:67) that bring about the movement of atoms.

(i) Interstitial mechanism

An atom diffuses by interstitial mechanism (**figure [1.7]**) when it passes from one

interstitial site to another. The atoms that move by this mechanism are appreciably smaller than the matrix atoms.

(ii) Vacancy diffusion

In crystals, some of the lattice sites are not occupied. These unoccupied sites are termed vacancies. When an atom jumps from one vacancy site to another, the atom is said to diffuse by vacancy mechanism. The mechanism is illustrated **in figure [1.8]**.

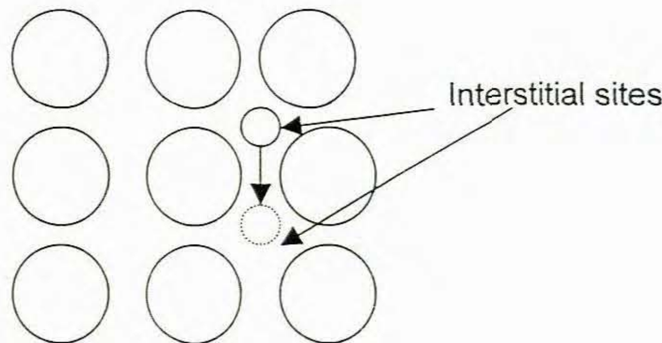

Figure [1.7] ***Illustration of the interstitial mechanism. The size of the interstitial atom is smaller than the size of the matrix atoms.(From Schmalzried, 1981:67)***

(iii) Grain boundary diffusion

The interfacial region between two grains is known as the grain boundary. The grain boundary provides a diffusion route to the moving atom. When an atom moves in a grain boundary, it is not necessarily confined to the boundary and can jump back into the surrounding lattice. **Figure [1.9]** depicts the grain boundary mechanism.

1.5.4 Diffusing species

Considering again the example in figure [1.7], where A reacts with B to form A_xB. In this figure, A is deposited on the inert substrate (SiO_2) and then B deposited on A.

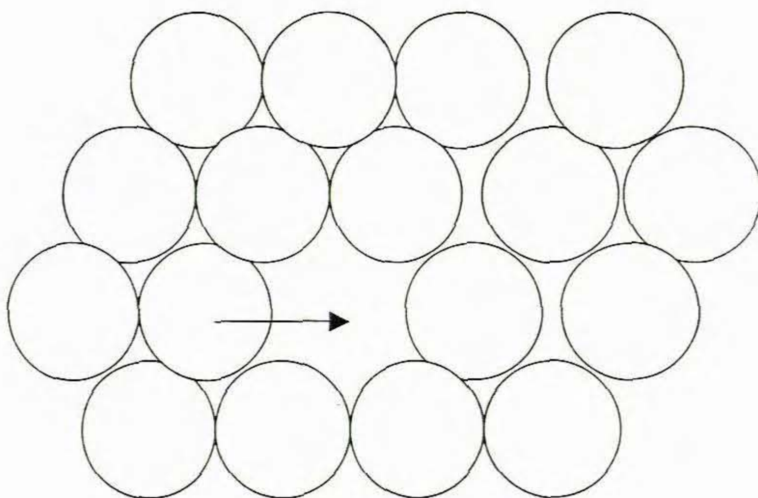

Figure [1.8]. *Vacancy diffusion mechanism. The movement of the atom is indicated by the arrow.(From Schmalzried, 1981:68)*

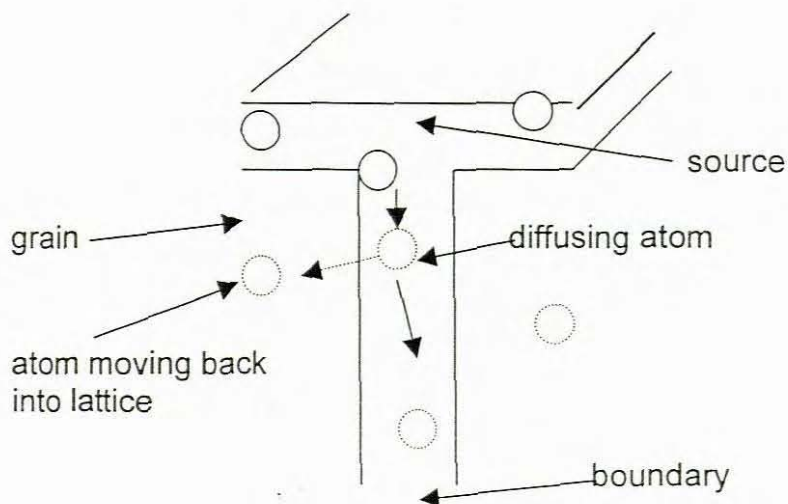

Figure [1.9] *This figure depicts the grain boundary mechanism. The atoms can move from the matrix to the boundary and back.(From Schmalzried, 1981:86)*

Figure [1.10] gives an illustration of A and B deposited on the substrate. Many possible reactions can occur. Firstly, A may react with B to form the compound A_xB. The atoms of A move to the interface with B to form the compound. Secondly, A may react with the

substrate to form A_xSi and no further reaction may occur at the specific temperature. However, if the temperature is increased, A_xSi may dissociate into A and Si and A then react with B to form a new compound. Thirdly, B may diffuse to the interface with A to form A_xB and no further reaction may happen. The atoms of the substrate can diffuse through A and react with B to form a compound of B and Si. It can be concluded from these mechanisms that the mobility of atoms through a compound at a temperature plays an important role in the mechanisms just explained. Of equal importance is the structure of the compound through which the diffusion occurs. An open structure will greatly enhance the mobility of the diffusing atom whereas a close structure will impair the mobility.

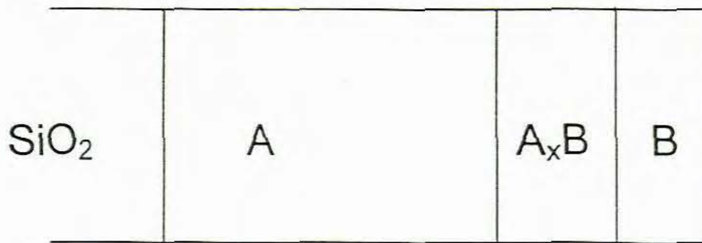

Figure [1.10] ***Diagram of the diffusion of A to the interface with B to form A_xB***

1.5.5 Marker studies

The purpose of inserting a marker into a thin film structure is to identify the diffusing species. Several marker experiments (Tu, Mayer & Feldman, 1992:285; Hong, Comrie, Russell & Mayer, 1991:3655; Lien, Nicolet & Pai, 1985:224; Farmer, Wandt & Pretorius, 1990:1643; Ho, Lien, Shreter & Nicolet, 1985:227) have been developed to obtain information about the motion of atoms. Criteria for the characteristics of a marker can be established.

- The marker should be inert to the reacting chemical system of which it will form part that is, the marker should not react at the temperature of the experiment.

- The marker should be traceable during the experiment.
- The marker should not impair or enhance the reaction rate of the experiment.

Many types of markers (Farmer et al, 1990:1643; Ho et al, 1985:227; Pretorius, Olowolafe & Mayer, 1978:327) can be used to determine the diffusing species. Firstly, atoms of an element can be used to gain information. This can be achieved by substituting a radioactive isotope for the stable atom. The isotope cannot be distinguished form the stable atom, but its net movement can be monitored through radio-emission. Secondly, a heavier element can be inserted in the system. This element should preferably fall in the same chemical group or sub-group to minimise any chemical interference between the marker and the diffusing species. Inert gases such as xenon have been used to establish the diffusing species.

In this investigation Ta (tantalum) was inserted in the Pd_2Si layer of the Si<>|Pd|Cr system. The thickness of the Ta marker was varied to determine whether it influences the rate of the reaction.

1.6 Formation of $CrSi_2$ on Pd_2Si

In this section previous investigations concerning the formation of Pd_2Si and $CrSi_2$ will be evaluated in order to establish a model for the Si< >|Pd|Cr system.

1.6.1 Pd_2Si formation

The information necessary for the formation of Pd_2Si can be summarised as:

(i) The temperature range for the complete formation of Pd_2Si.

(ii) The structure of Pd_2Si when it forms on silicon Si<100> and silicon Si<111>.

(iii) When does the structure form, after or during growth.

(iv) What is the mobility of Pd and Si through the types of Pd_2Si that form.

(v) Are the temperature ranges of formation well defined.

(vi) What occurs in-between these temperature ranges and how will it possibly affect the formation of $CrSi_2$.

(vii) If Pd_2Si contributes to the formation of $CrSi_2$ (Pd is the diffusing species), how does it dissociate.

On Si<111>, Pd_2Si grows epitaxially (Comrie, Egan, Liu & Mayer, 1988:688) and the formation occurs at temperatures as low as 200 $^{\circ}$C. The mobility of the atoms is low at this temperature (Zingu, Mayer, Comrie & Pretorius, 1984:5920). The epitaxial structure is produced during the formation of Pd_2Si and not after the formation is completed and non-epitaxial Pd_2Si reorders itself on epitaxial Pd_2Si (Comrie, Liu, Hung & Mayer, 1988:2402). During growth, vacancies are generated. These vacancies enhance the mobility of the atoms. Silicon is the dominant diffusing species during the epitaxial growth of Pd_2Si on Si<111> (Comrie et al, 1988:689). An activation energy of 1.0 eV (Zingu et al, 1984:5920) was obtained for the formation of Pd_2Si. This indicates that Pd diffusion also occurs during Pd_2Si growth. In Pd_2Si growth on polycrystalline Si<100>, (Wei, Van Der Spiegel & Santiago, 1988:446) formation of Pd_2Si was found to start at 320 ^{0}C. However, when Pd_2Si formation was investigated using a structured marker (Lien, Nicolet and Pai, 1985:225) the formation began at 275 $^{\circ}$C. Silicon is the dominant diffusing species for the non-epitaxial formation of Pd_2Si on Si<100> (Comrie & Egan, 1988:1177). The temperature of 320 ^{0}C does not concur with previous investigations. It can now be concluded that Pd_2Si forms epitaxially on amorphous silicon Si<111> and that during its formation silicon is the dominant diffusing species. The epitaxial structure of Pd_2Si develops during the growth period. On Si<100>, Pd_2Si forms non-epitaxially and silicon is the dominant diffusing species during the growth period. The temperature range for the formation is from ~200 $^{\circ}$C to ~275 $^{\circ}$C.

1.6.2 $CrSi_2$ formation

When the chemical system Si<>|Pd|Cr was heated at 380 °C for 30 minutes (Zingu, Comrie & Pretorius, 1982:2392) no $CrSi_2$ formation was observed in the RBS spectrum. The growth rate of $CrSi_2$ on Si<100> (Natan & Duncan, 1985:80) ~7 $Å.min^{-1}$ at 400 °C and $CrSi_2$ forms epitaxially on epitaxial Pd_2Si. The onset of formation of $CrSi_2$ is thus at ~400 °C. When the chemical system Si<100>|Cr was subjected to a heating process (Botha, Pretorius and Kritzinger, 1981:412) $CrSi_2$ started to form at 400 °C. During the formation of $CrSi_2$, Si was the dominant diffusing species and diffusion occurred by a vacancy mechanism. It was also found that $CrSi_2$ grows epitaxially on Si<111>. It can therefore be assumed that $CrSi_2$ will form non-epitaxially on Si<100>. The thickness of the interposed layer has a definite effect on the growth rate of $CrSi_2$ (Zingu et al [1], 1984:2394). The growth rate of $CrSi_2$ is inversely proportional to the thickness of Pd_2Si. In this investigation, the thickness of Pd_2Si deposited will vary from 100 to 1000 x 10^{-10} m. An activation energy of 1.60±0.2 eV was calculated.

1.6.3 Si< >|Pd|Cr system

Deductions from section [1.6.2] can therefore readily be made. The chemical system Si<>|Pd |Cr when heated to ~300 °C forms the new system

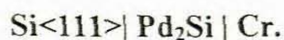

For the Si<111>| Pd_2Si | Cr system, $CrSi_2$ will form epitaxially on Pd_2Si .The dominant diffusing species will be Si and the diffusion will occur by a vacancy mechanism. The formation kinetics will be linear and the activation energy will be in the range of 1.40 to 1.80 eV. For the Si<100> | Pd_2Si |Cr system, $CrSi_2$ will grow non-epitaxially. Silicon will be the dominant diffusing species. The formation kinetics will be linear and activation energy for growth will be 1.60 ± 0.2 eV.

The information necessary for the formation of Pd_2Si and $CrSi_2$ (section 1.6.1) can now be stated as follows:

(i) The formation of Pd_2Si occurs in the temperature range of 200 to 250°C

(ii) The structure of Pd_2Si on Si<100> is non-epitaxial and the structure is epitaxial on Si<111>.

(iii) The structure forms during the growth of Pd_2Si.

(iv) Through epitaxial Pd_2Si the mobility of Si is greater than the mobility of Pd.

(v) The temperature for the onset of $CrSi_2$ formation is at approximately 400°C. The temperature ranges for the formation of Pd_2Si and $CrSi_2$ are thus well defined.

(vi) The dissociation of Pd_2Si into Pd and Si occurs at the interface of Cr and Pd_2Si. Pd diffuses to the interface of the substrate and Pd_2Si to reform Pd_2Si and Si reacts with Cr to form $CrSi_2$.

1.7 Scope of the Investigation

This study analyses the formation of $CrSi_2$ on top of Pd_2Si, starting with samples of Si< >|Pd|Cr. Thin Ta was inserted as a marker in the Pd_2Si layer so the system should actually be represented as Si< >| Pd | Ta | Cr. In the first chapter, previous investigations into the chemical system (but without Ta) were evaluated. The information obtained was used to form a model for the system when subjected to the heating process. Chapter 2 discusses in detail the experimental procedures and precautions taken during this study. Rutherford Backscattering Spectrometry (RBS) which was used for sample characterisation in this investigation, can be readily simulated using the computer program RUMP. In chapter 3 RUMP is used to simulate RBS spectra in order to optimise the thicknesses of the thin film structures used in this investigation. The mechanism of $CrSi_2$ formation on Pd_2Si is studied in detail in chapter 4, by using a Ta marker. Atomic diffusion in the Pd_2Si and $CrSi_2$ layers

is determined by placing thin (~5Å) Ta markers in these layers and observing their movement. A comparison is also made between $CrSi_2$ growth on epitaxial and non-epitaxial Pd_2Si. The interface roughness will be evaluated continuously. The data obtained from different temperatures, on each substrate will be used to generate Arrhenius plots and so determine the activation energy for the formation of $CrSi_2$ on the particular substrate.

CHAPTER 2

EXPERIMENTAL PROCEDURES

2.1 Sample Preparation

2.1.1 Wafer preparation

Single crystal silicon substrates were used in this investigation. The wafers were cut into $1cm^2$ slivers and these were marked for identification. The surface may be contaminated with grease and oxides. The grease was removed by washing with organic solvents. The solvents were used in the sequence; methanol, acetone, trichloroethane, acetone and methanol. The excess methanol was rinsed off with deionized water. Any surface oxides present were removed by submerging the substrates in an aqueous solution of 20% hydrofluoric acid. The slivers were then dried and mounted securely on an aluminium sample holder.

2.1.2 Vacuum deposition

The ultra-high vacuum (UHV) deposition chamber consists of an electron-beam evaporation system utility with three water-cooled hearths. The elements of the chemical system, Pd, Cr and Ta were placed in the hearths. The aluminium sample holders were then placed in the rotating carousel system of the UHV system. **Figure [2.1]** is a schematic diagram of the UVH system. It is necessary to maintain a vacuum of 1.33×10^{-4} Pa to 1.33×10^{-5} Pa during evaporation. This eliminates the external factors that may influence the film growth. These factors, such as the presence of residual gases and chemical reactions that can take place between the substrate and atoms during the deposition, were discussed in section [1.3.1].

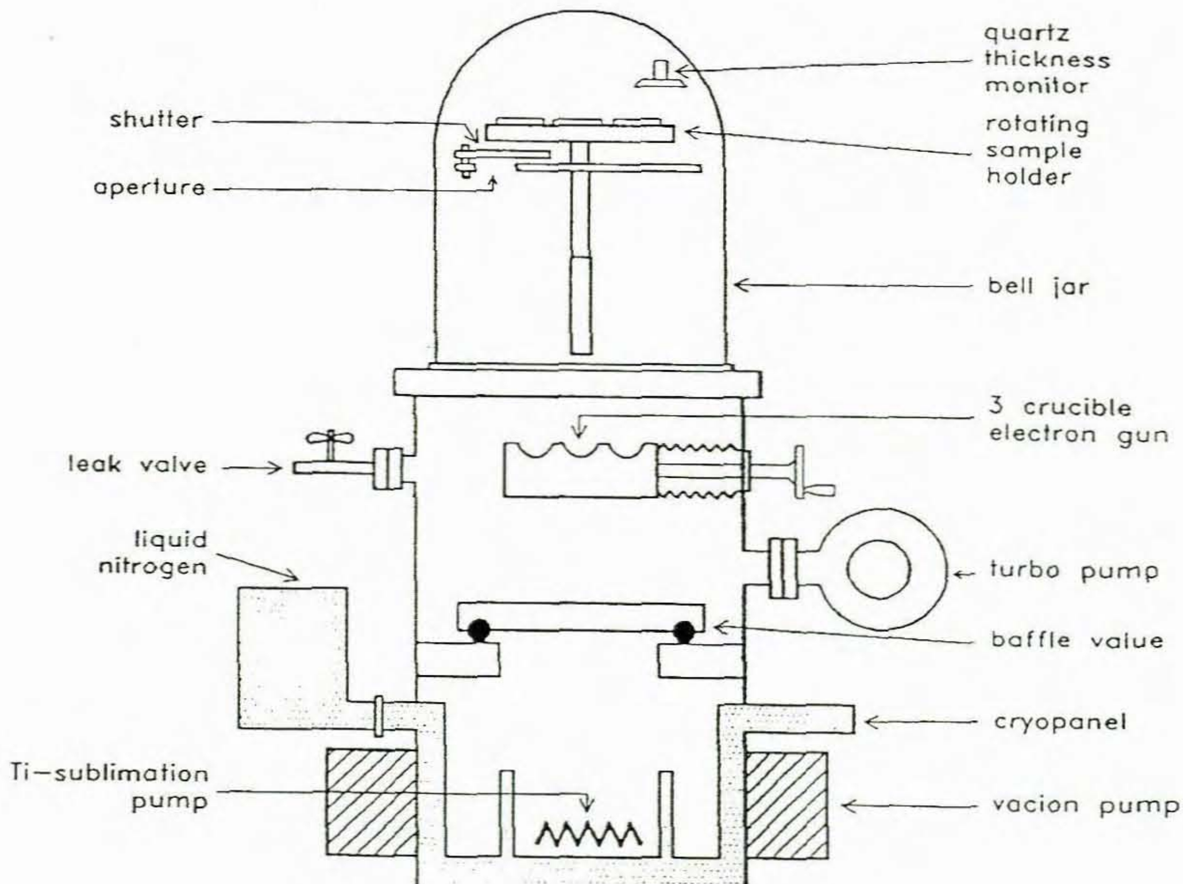

Figure [2.1] ***Schematic representation of Ultra High Vacuum evaporation system.***

The vacuum of 1.33×10^{-5} Pa is obtained by systematically using different types of pumps.

- A mechanical rotary pump pressure 1.33×10^{-1} Pa
- Turbo pump pressure 1.33×10^{-3} Pa
- Ion pumping pressure 1.33×10^{-4} Pa
- Titanium sublimation pumps pressure 1.33×10^{-5} Pa

Ion pumping causes the ionisation of gas molecules and the gettering of ions at the electrodes. The material to be evaporated was firstly preheated and the titanium pump outgassed. A vacuum of 1.33×10^{-5} Pa was maintained during evaporation.

Thin films of Pd and Cr, ranging in thickness of 100 to 2000 Å, of each material, were evaporated onto the substrate. The thickness of Ta ranged from 1 to 10 Å. During the evaporation, the film thickness was continuously monitored with a quartz crystal monitor. The thickness is determined as a function of the change in frequency of the vibrating quartz crystal. The change in frequency is proportional to the accumulation of the deposited material. The microprocessor then calculated the rate of deposition and the accumulated thickness.

2.2 Sample Characterisation

2.2.1 Normal Rutherford backscattering Spectrometry

This section deals with the fundamental principles of backscattering spectrometry and the underlying physical processes. These processes are briefly discussed and then related, by means of equations, to the physical properties of the target (sample) and the projectile.

In the analytical technique of backscattering spectrometry, a beam of mono-energetic alpha particles is impinged on the sample. The energy of this beam of particles is approximately 2 MeV. **Figure [2.2]** illustrates the conceptual layout and the principle of backscattering spectrometry. The charged particles are generated in the ion-source. The energy of these particles is then increased to approximately 2 MeV by the accelerator. The collimator focuses the beam and the analysing magnet filters it for the selected type of particle and energy. Some of the backscattered particles are detected by a surface barrier detector, where an electric signal is generated. The signal is amplified and processed by analogue and digital electronics. The strength of Backscattering spectrometry is thus the speed of the technique, its ability to perceive depth distributions of the atomic species below the surface of the sample and the quantitative nature of the results. These are derived from:

1. The kinematic factor that provides the mass analysis
2. The differential scattering cross-section that provides quantitative analysis
3. The energy loss of a particle that provides the depth analysis

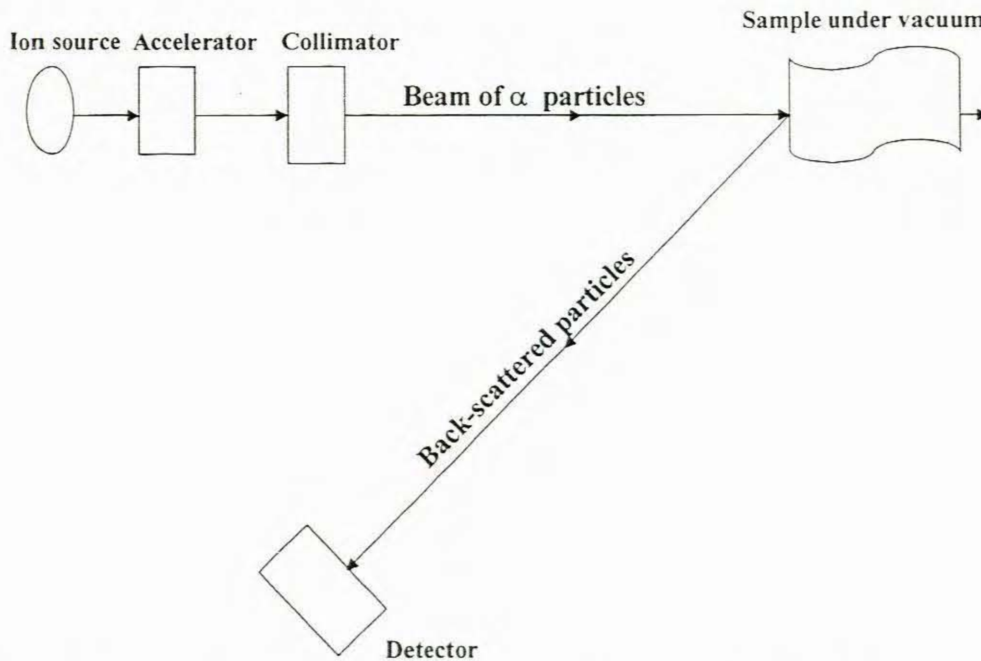

Figure [2.2] *Schematic diagram of the conceptual layout of backscattering spectrometry*

(i) Kinematic factor

In Backscattering spectrometry a moving particle, the projectile collides elastically with the stationary particle, the target. Since the collision is elastic, the conservation of energy and momentum can be applied to the system. The kinetic energy of the projectile before collision is equal to the sum of the kinetic energies of the projectile and the target after the collision. Equation [2.1] expresses the conservation of energy,

$$E_0 = E_1 + E_2 \quad \Rightarrow$$

$$\tfrac{1}{2}m_1v_0^2 = \tfrac{1}{2}m_1v_1^2 + \tfrac{1}{2}m_2v_2^2 \qquad 2.1$$

where m_1 is the mass of the projectile, m_2 is the mass of the target, v_o is the velocity of the target before collision, v_1 is the velocity of the projectile after collision and v_2 the velocity of the target after collision. The momentum, p, parallel and perpendicular to the direction of motion are given by

$$m_1 v_0 = m_1 v_1 \cos\theta + m_2 v_2 \cos\phi \quad \text{.......... 2.2}$$

$$m_1 v_1 \sin\theta - m_2 v_2 \sin\phi = 0 \quad \text{.......... 2.3}$$

The masses of the projectile and the target remain constant after the collision. The ratio of the projectile velocity after collision to the initial velocity of the projectile is called the kinematic factor, K, and is given by

$$K = \frac{E_1}{E_0} = 1 - \left[\frac{2m_1 m_2}{(m_1 + m_2)^2}\right](1 - \cos\theta) \quad \text{.......... 2.4}$$

and θ is measured with respect to the laboratory frame of reference. Equation [2.4] shows that the kinematic factor depends only on the ratio of the masses of the projectile and the target and the scattering angle. The kinematic factor for the elements are given in Appendix A.

(ii) Scattering cross-section

Collisions between the target and the projectile do not happen frequently and not all collisions result in a measurable event. The frequency that a collision will occur and the

probability that a measurable event will take place depends on the number of particles that hit the target and the number of backscattering events that were detected by the detector. If Q is the number of particles that hit the target and dQ the number of collisions measured a the scattering angle $d\Omega$, then the scattering cross-section is defined as

$$\frac{d\sigma}{d\Omega} = \frac{}{l\rho_v}\left[\frac{dQ/d\Omega}{Q}\right] \qquad 2.5$$

where l is the thickness and ρ_v the volume density of the layer. The average differential scattering cross-section σ, is thus given by

$$\sigma \equiv \frac{1}{\Omega}\int_{\Omega}\left(\frac{d\sigma}{d\Omega}\right)d\Omega \qquad 2.6$$

The force that acts during the collision is comparable to the coulombic repulsion between the two nuclei. This comparison is only valid when the distance of closest approach is large in terms of nuclear dimensions, but small in terms of the Bohr radius, $(a_0 = \hbar / m_e e)$. Let the energy immediately before scattering of the projectile be denoted by E. The scattering cross-section is defined in terms of the scattering angle and Z, the atomic number, by

$$\frac{d\sigma}{d\Omega} = \left(\frac{Z_1 Z_2 e^2}{4E}\right)^2 \cdot \frac{4}{\sin^4\theta} \cdot \frac{\left(\sqrt{1-\left(\frac{m_1}{m_2}\sin\theta\right)^2} + \cos\theta\right)^2}{\sqrt{1-\left(\frac{m_1}{m_2}\sin\theta\right)^2}} \qquad 2.7$$

This equation shows for a given projectile and scattering geometry that the scattering cross-section is directly proportional to the square of the atomic number the target and inversely proportional to the square of the energy of the projectile.

(iii) Energy Loss factor

The particle looses energy as it penetrates the different layers of the target. The amount of energy lost depends on the thickness, the composition of and the density of the layer. If l is the thickness of the layer then the energy loss is defined as

$$E(l) = E_0 - \int_0^d \frac{dE}{dl} dl \quad \text{.......... 2.8}$$

E_0 is the energy of the particle just before it hit the target and $E(l)$ is the energy after the particle has penetrated the target to a depth l. Hence if the mean energy is defined by $E_0 - E = \overline{E}$ then

$$l = (E_0 - E) \cdot \left(\frac{dE}{dx}\right)^{-1} \Big|_{E_0} \quad \text{.......... 2.9}$$

Equation [2.9] shows that the thickness is linearly dependent on the mean energy.

(iv) Stopping cross-section

The stopping cross-section (ε) for an element is defined in terms of the projectile and the target properties by

$$\varepsilon = \frac{2Z_1Z_2e^2}{m_2v_1^2} \cdot 2\pi \frac{dx}{x} \cdot \Delta l \quad \text{.......... 2.10}$$

When two elements react to form a compound, for example $xA+yB \rightarrow A_xB_y$, then the beam encounters both atoms of A and B. Hence, if A_xB_y is homogeneous, then the beam will hit x atoms of A and y atoms of B when travelling through the compound. This means that each of x atoms of A and each of y atoms of B will contribute to the stopping cross-section of the compound. This principle is termed the linear additivity. If the volume density of the compound is $\rho_v^{A_xB_y}$ and l the thickness of the layer, then stopping cross-section of the compound will therefore be

$$\frac{d\varepsilon^{A_xB_y}}{dl} = \rho_v^{A_xB_y}\left(x\varepsilon^A + y\varepsilon^B\right) \qquad 2.11$$

Thicknesses of elements that would react to form are given in Appendix B.

In this section, the principles of Backscattering spectrometry and the underlying physical processes were discussed. Each physical process was expressed in terms of the properties of the target and the projectile by means of equations. These equations form the basis of the software used in analysing the raw data obtained from the detector.

2.2.2 *In situ*, real time Rutherford Backscattering Spectrometry

In the previous section, the experiment is performed under conditions of low pressure (1.33×10^{-5} Pa) and constant temperature. During *in situ*, real time Backscattering spectrometry, the target is heated to a specific temperature and the reaction occurring is then monitored in real time. **Figure [2.3]** is a schematic diagram of *In situ*, real time backscattering instrumentation. The samples will be heated to temperatures of 400, 425, 450, 475, 500 and 550°C.

2.2.3 Measurement and data manipulation

All spectra will be expressed as the normalised yield per channel. The time duration for an analysis is approximately 2½ hours. During this time interval, the sample will be heated to the desired temperature and the kinetics monitored. The data derived from the measurements and to be used for presentation will be expressed in terms of the time taken and thickness (Å) of $CrSi_2$ formed. Only the growth kinetics of $CrSi_2$ will be subjected to statistical evaluation to determine whether the growth kinetics is linear of quadratic. In this instance, the correlation coefficient will be used for evaluation. An electronic pulser was used to indicate whether any drift in electronics occurred. The position of this pulse will be approximately at channel 500. This is outside the data region of the spectrum. All data will be accumulated at the end of a one-minute period and all mass or movement during the interval will be expressed as having occurred after the elapse of the minute.

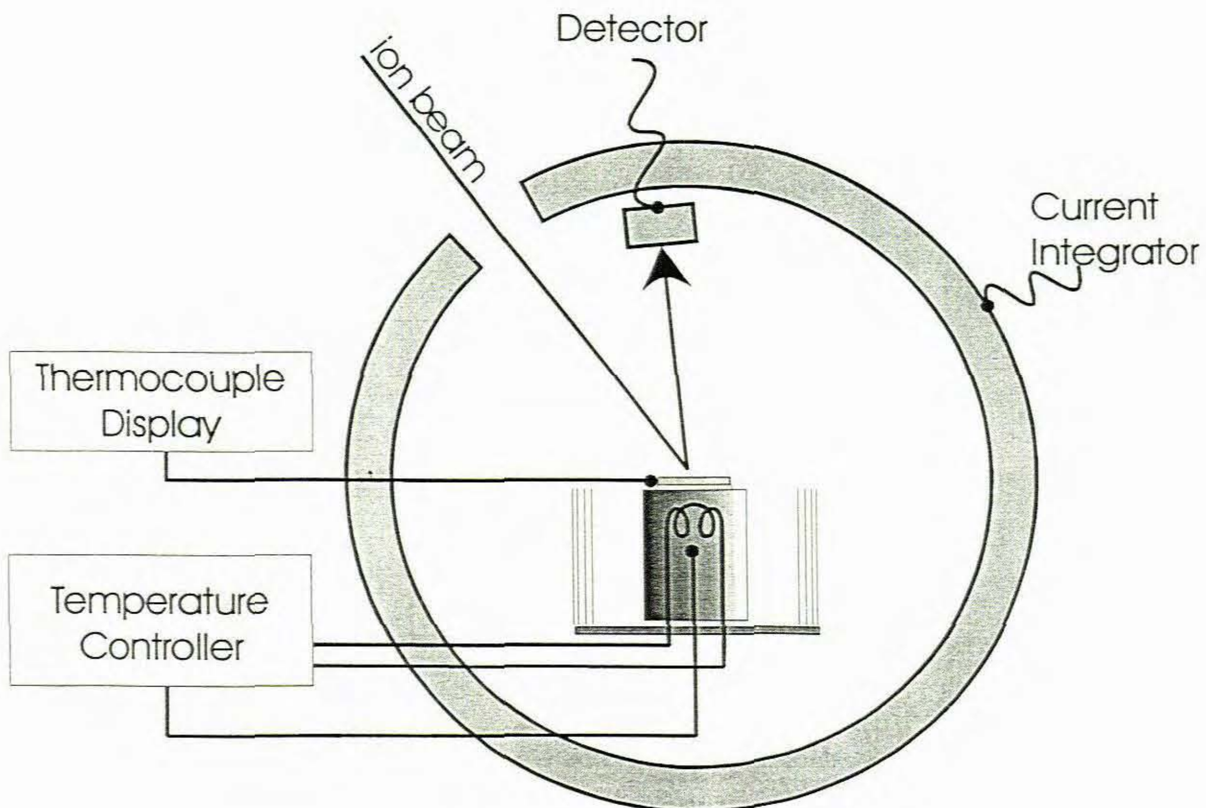

Figure [2.3] ***Layout of a dynamic backscattering system. The layout enables the control of the temperature to which the sample is heated.***

CHAPTER 3

COMPUTER SIMULATIONS

3.1 Introduction

The main technique for characterising samples in this investigation is Rutherford Backscattering Spectrometry (RBS) with accelerated alpha particles. The RBS technique is described in detail in section [2.2]. Because the stopping powers and scattering cross-sections for charged nuclear particles is so well known, it has become possible to simulate RBS spectra very accurately. The best-known and most widely used RBS computer simulation programme is RUMP. In this chapter, the RUMP simulation programme is used for optimising the various parameters, which are important in this investigation. It is also shown how RUMP can be used to analyse measured spectra. RUMP simulation is also applied to predict marker movement for the different mechanisms of $CrSi_2$ growth on Pd_2Si.

3.2 RUMP Simulation Software

The equations, for analysis and simulation of Rutherford Backscattering Spectroscopy spectra that form the basis of RUMP, were discussed in section [2.2.1]. The purpose of this section is to discuss the equations that are not included in section [2.2.1] but do influence the analysis of data. *The symbols used in this chapter were defined in Chapter 2 and any additional definitions will be given in the text.*

RUMP includes the modules simulation (sim) and perturbation (pert). The simulation module is used for theoretically constructing a RBS spectrum of a sample that consists of one or more layers. When analysing the actual data, the thickness of each layer is varied until the theoretical spectrum coincides with the actual data. The pert module is based on a

semi-automated algorithm, which optimises the characteristics such as the thickness of the layers. The backscattering spectrometric data obtained from the multi-channel analyser is referred to as raw data and can be plotted as counts per channel, that is, exactly as recorded. The data can however also be normalised and the yield expressed by

$$\text{Yield} = \frac{count * corr}{Q * \partial\Omega * \Delta E_{channel}} \qquad 3.1$$

Corr is the correction factor applied and allows for the optimisation of the beam charge to compensate for inaccuracies during the charge integration. Accurate integration is achieved by secondary electron suppression. When the beam is passed through the sample layer, the number of scattering centres (atoms) is directly proportional to the beam current and the detector solid angle. The relation is given by

$$\text{Y} \approx \frac{\partial\sigma}{\partial\Omega} * \partial\Omega * Q * \frac{\rho_a}{\cos\theta} \qquad 3.2$$

Where Y is the total number of scattering centres. Thus, when the thickness is determined by the number of counts between two set points, that is the integration of the peak, the quantities are assumed exact. When the particle is scattered, its energy is estimated from the detected energy. The energy loss on the ingoing path is assumed to be a constant fraction of the total energy and can thus be obtained from the overall energy loss and is defined in terms of the stopping powers by equation [3.3].

$$E_{scat} = E_0 - \frac{\left(\partial E/\partial l\right)_0}{\cos\theta} * \frac{\Delta E}{K\frac{\left(\partial E/\partial l\right)_{E_0}}{\cos\theta} + \frac{\left(\partial E/\partial l\right)_{KE_0}}{\cos\theta}} \qquad 3.3$$

3.3 Phase Identification

The denser an element or compound is, the more atoms it contains and hence the more scattering centres. This relation was defined by equation [2.7] in terms of the stopping cross-section and the atomic number, that is $\varepsilon \propto (Z_1 Z_2)^2$. Considering the example in section [1.5.2], where A and B react to form the compound A_xB. In this instance, A is denser than B. Hence, the density of the compound decreases as the percentage composition of B, the less dense compound, increases. Since the stopping cross-section is directly proportional to the product of the atomic masses of the elements, the stopping cross-section of the compound decreases. Consequently, the peak height decreases.

3.3.1 Palladium silicide phases

For the phases of the Pd – Si binary system, discussed in section [1.4.1], the RBS peak height of pure (100%) palladium will be greater than the peak height of Pd in for instance PdSi. In the same manner, the peak height of Pd in Pd_9Si_2 will be greater than the peak height of Pd in Pd_2Si. It is thus evident that the percentage composition of silicon in the silicon phase will increase with the decrease in Pd and the peak height of the silicon in the phase will therefore increase. A simulated backscattering spectrum of the silicide phases for the Pd – Si binary system is illustrated in **figure [3.1]**. Since the peak height of a phase varies with the percentage composition of palladium, the ratio of the Pd signal to that of pure palladium or another peak can be used to identify the phase.

3.3.2 Chromium silicides phases

Similarly, the peak heights of Cr in the phases of the Cr – Si binary system will differ. For pure chromium, the Cr signal height will be the greatest, decreasing with increasing concentration of silicon in the chromium silicide phases. In this case, the percentage silicon will also increase and so the height of the silicon signals. Since the peak height for.

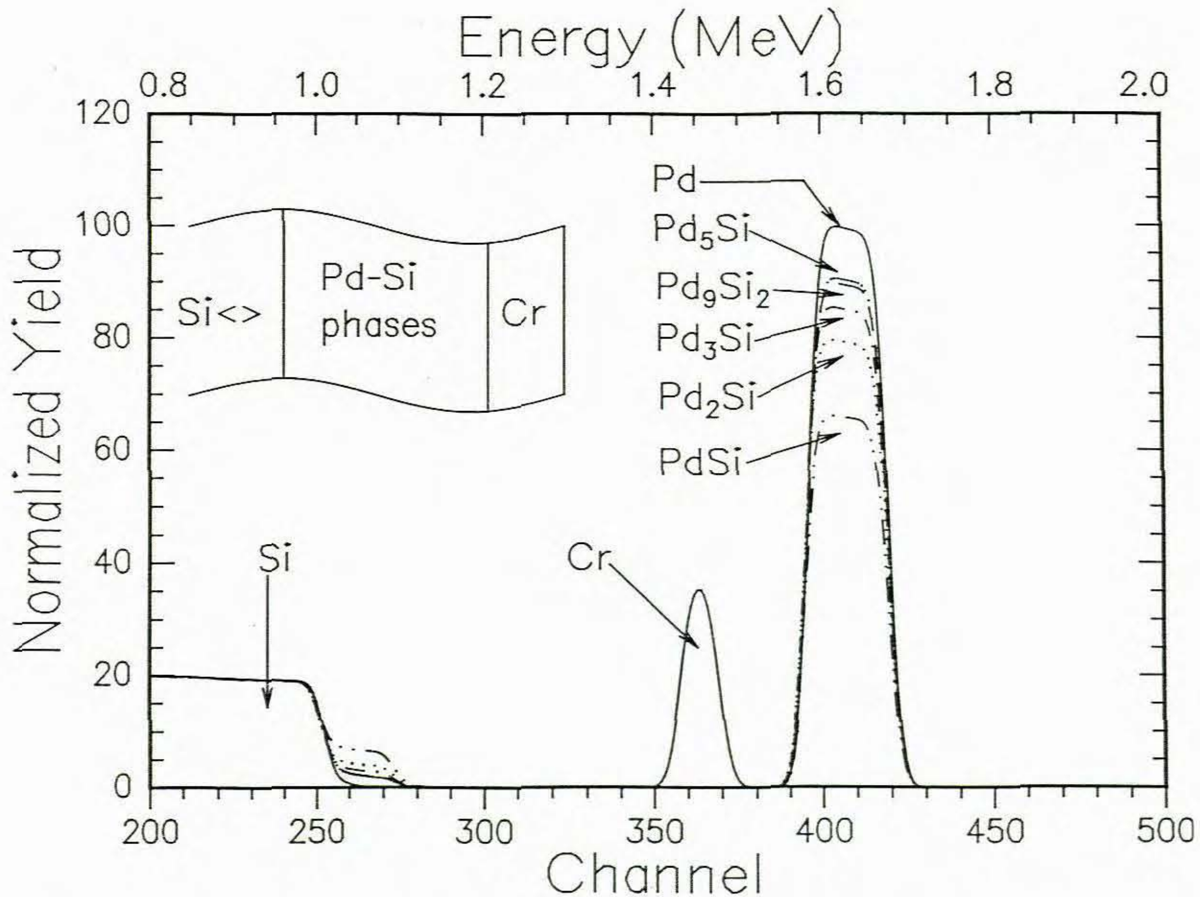

Figure [3.1] ***A simulated backscattering spectrum of the silicide phases for the Pd – Si binary system. The thickness of the Pd_2Si layer was 650 Å and the thickness of the $CrSi_2$ was arbitrarily chosen.***

the phases of the Cr – Si system varies in a similar manner as the phases of the Pd – Si binary system, the ratio of the peak heights can be used to identity the specific phase. A simulated backscattering spectrum of the chromium silicide phases is illustrated in **figure [3.2]**.

3.4 Mechanism and Diffusing Species

It was established that, in Si < >| Pd | Cr structures, Pd_2Si forms first and that $CrSi_2$. then forms on top of Pd_2Si. The formation of Pd_2Si is complete at the temperature of 300^0C and the formation of $CrSi_2$ begins at 400^0C. There is no diffusion of Cr into Pd_2Si, nor do

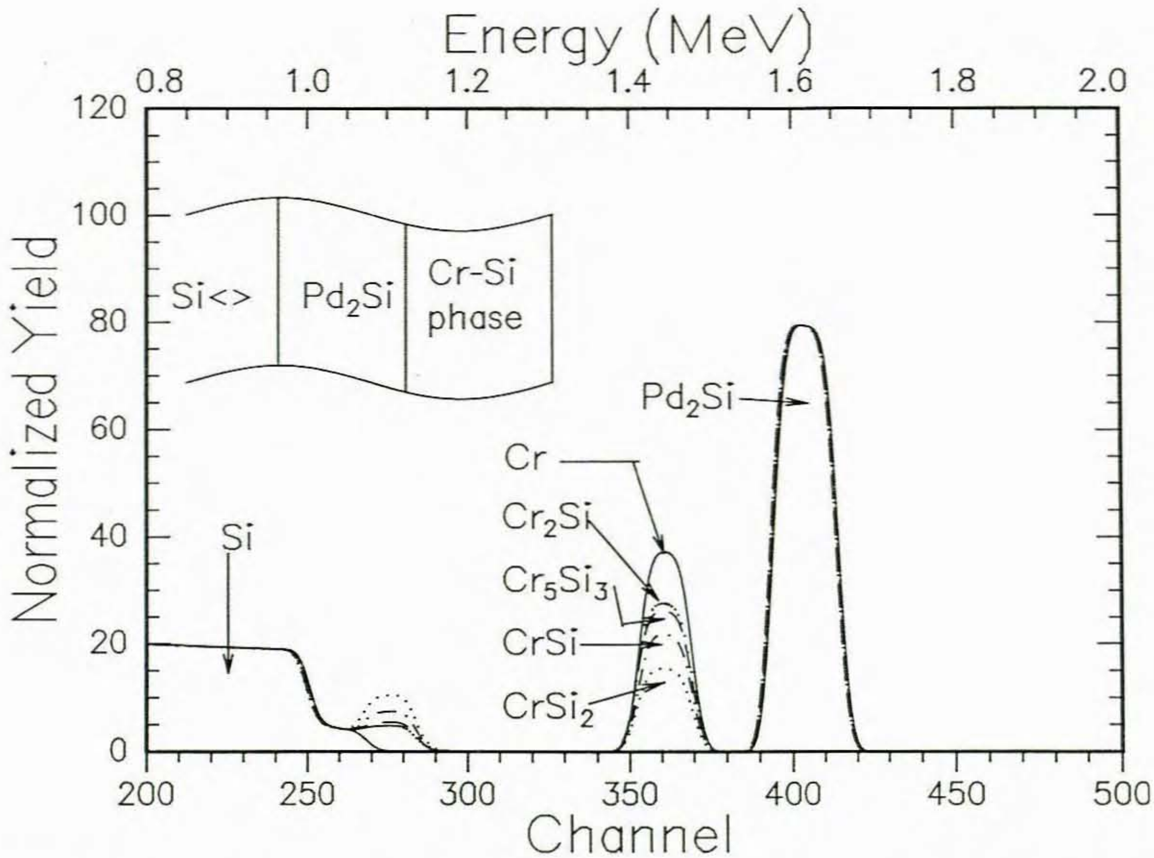

Figure [3.2] ***A simulated backscattering spectrum of the silicide phases for the Cr – Si binary system. The thickness Pd_2Si layer is 650 Å and the thickness of Cr was arbitrarily chosen.***

any other reactions occur in the temperature range between 300 to 400°C. The formation of $CrSi_2$ can occur by three possible mechanisms. Firstly, the silicon necessary for the formation can be derived directly from the substrate, Si< >. In this instance, the silicon diffuses through the Pd_2Si to the $CrSi_2$ | Cr interface to form $CrSi_2$ (equation [3.4]). This mechanism will be referred to as the silicon-diffusion mechanism.

$$2Si + Cr \rightarrow CrSi_2 \quad \ldots\ldots 3.4$$

Secondly, the Pd_2Si may dissociate at the Pd_2Si | $CrSi_2$ interface (see figure [3.3]) into palladium and silicon

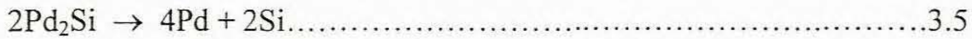

$$2Pd_2Si \rightarrow 4Pd + 2Si \quad \text{......} \quad 3.5$$

The silicon then diffuses to the interface between $CrSi_2$ and Cr and reacts with Cr to form $CrSi_2$ (equation [3.4]), while the palladium diffuses through the Pd_2Si layer to the interface of Pd_2Si and the substrate, Si<>, to reform Pd_2Si.

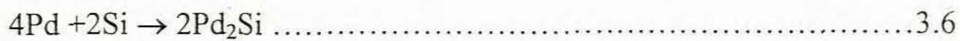

$$4Pd + 2Si \rightarrow 2Pd_2Si \quad \text{......} \quad 3.6$$

This mechanism will be referred to as the palladium-diffusion mechanism. Schematic representation of these two mechanisms is given in **figure [3.3]** to illustrate the position of the marker after each of the reactions took place. In the third instance, a combination of these mechanisms may occur. This means that the amount of $CrSi_2$ formed may be due to the dissociation of Pd_2Si as well as the direct diffusion of silicon from the substrate. The contribution of each of these mechanisms can be expressed as the percentage of the total possible amount of $CrSi_2$ that formed. In this instance, the final position of the marker will differ from the positions indicated in **figure [3.3]**.

3.5 Simulation of Marker Movement

During the silicon-diffusion mechanism, there is no movement of the Ta marker relative to the Pd_2Si layer. However, as the $CrSi_2$ is formed, the mass in front of the marker increases. Hence, the path of the beam before it reaches the marker layer increases and the marker moves deeper into the sample. This is illustrated in **figure [3.4]**. In the palladium-diffusion mechanism, there is a net movement of the marker. The thickness of the Pd_2Si layer is irrelevant since the silicon is derived from the substrate. When the Pd_2Si dissociates, the

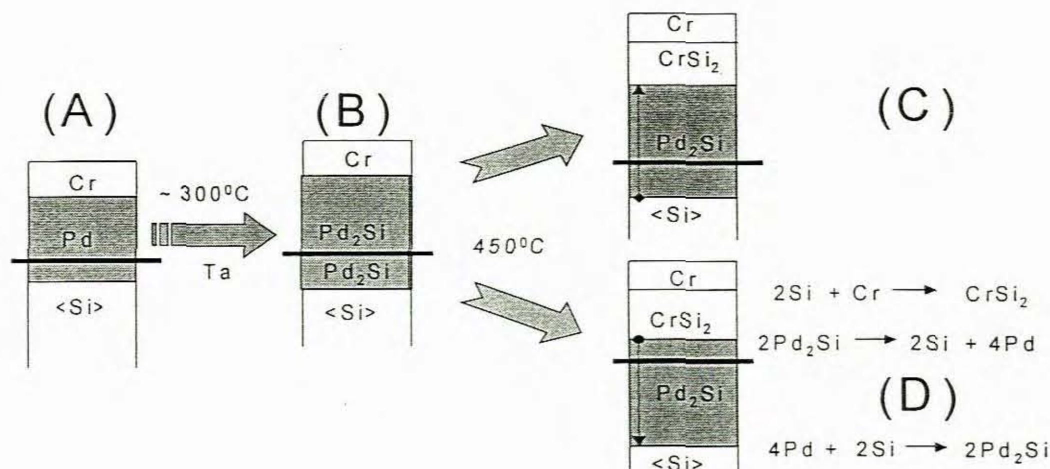

Figure [3.3]. *Schematic illustration of Ta marker movement for the two possible mechanisms during formation of $CrSi_2$ on Pd_2Si. The as-deposited sample is represented by (A). The complete formation of Pd_2Si at 300°C is given by (B). The formation of $CrSi_2$ by the Si-diffusion mechanism is given by (C) and the Pd-diffusion mechanism, in which the marker moves to the interface of Pd_2Si and $CrSi_2$ is illustrated by (D).*

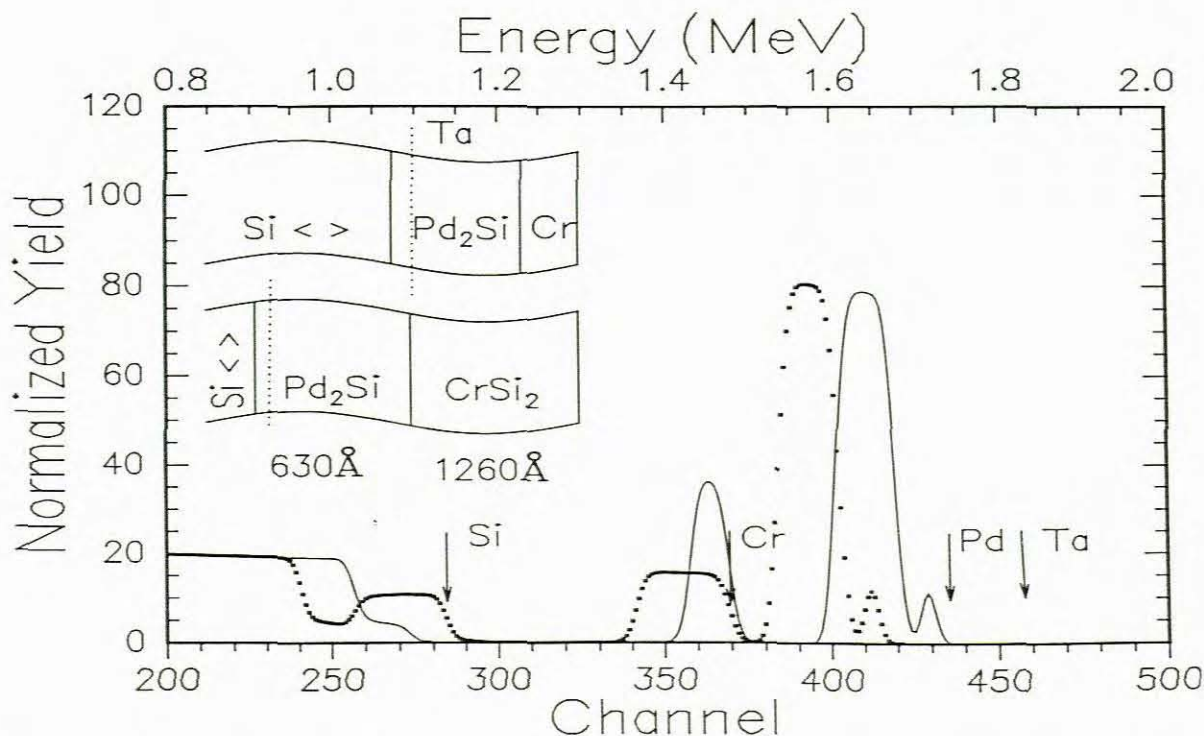

Figure [3.4]. *Movement of the Ta marker (discontinuous line in the Pd_2Si layer) during the Si-diffusion mechanism. The spectrum illustrated by the continuous line is that of the sample when Pd_2Si has completely formed. The dotted line represents the completely formed $CrSi_2$. The marker does not move with respect to the Pd_2Si layer, but to the surface, moves inwardly. The arrows indicate the energy of alpha particles scattered from a particular element when located on the surface of a sample.*

palladium moves to the interface of the substrate and Pd_2Si and Pd_2Si is reformed, hence, the marker will move outwardly with respect to the Pd_2Si layer and this is illustrated in **figure [3.5]**. As the marker moves, more $CrSi_2$ is formed at the interface of Pd_2Si and $CrSi_2$. For each two moles of Pd_2Si that dissociated one mole of $CrSi_2$ formed.

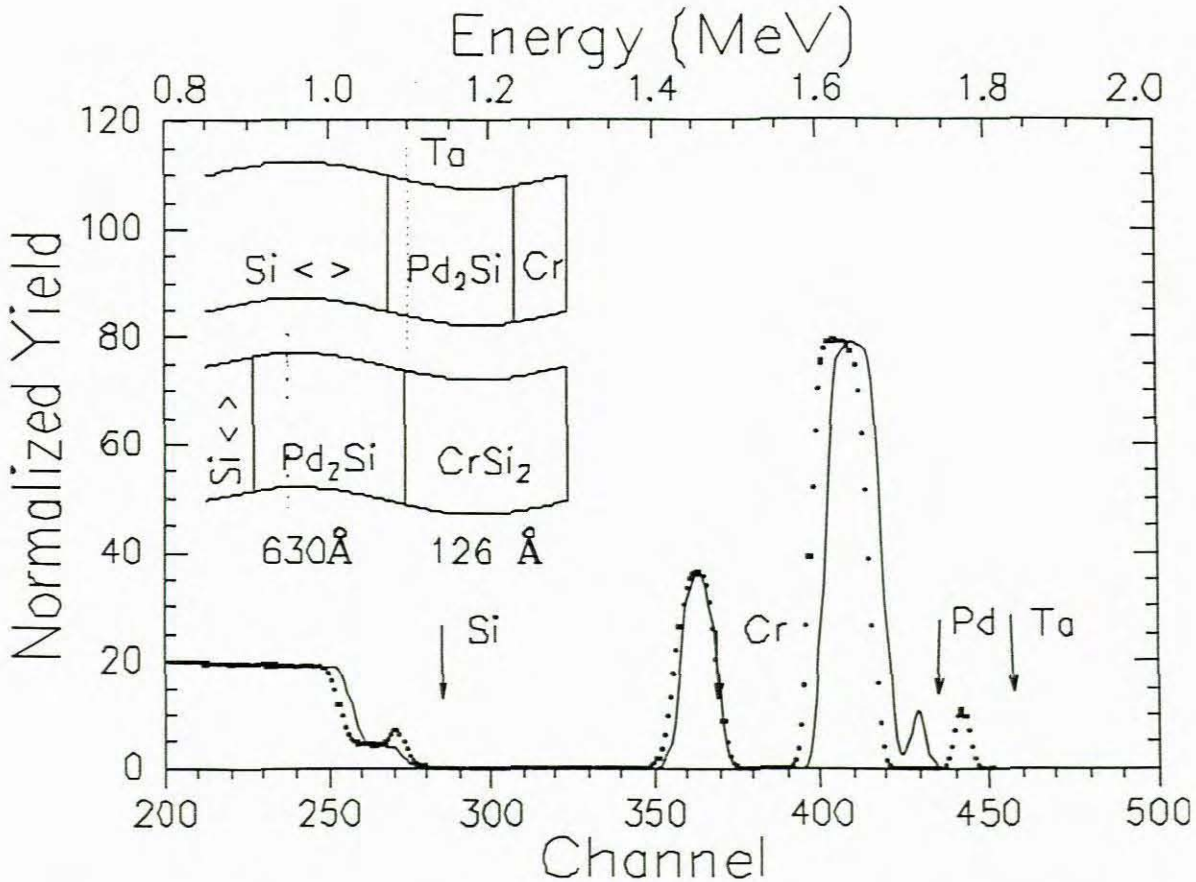

Figure [3.5]. *Movement of the Ta marker, represented by the discontinuous line in the Pd_2Si layer, during the Pd-diffusion mechanism. The spectrum illustrated by the continuous line is the as-deposited sample and the dotted line is the spectrum of the completely formed $CrSi_2$. The marker moves relative to the Pd_2Si layer. With respect to the surface, the marker moves outwards.* **Note that if the stoichiometric amount of Pd_2Si necessary for complete formation of $CrSi_2$ is simulated than the marker will not be ideally resolved.** *It can be seen that the number of channels moved by the marker for the relatively small amount of $CrSi_2$ formed is comparatively larger than in the case of the silicon diffusion mechanism. The arrows indicate the surface energies of the elements.*

Since Pd is denser than Cr (*cf.* Section [3.2]) and hence Pd_2Si is denser than $CrSi_2$, the marker will move outwardly with respect to the surface. The marker thus moves in different direction with respect to the surface. The relative change in position of the marker can

be expressed as channels per thickness (Å) of $CrSi_2$ formed. These points will represent the extreme instances. Any movement or change in position in between these two extremes will indicate that both the mechanisms contribute to the formation of $CrSi_2$. A theoretical simulation of the two mechanisms is depicted in **figure [3.6]**.

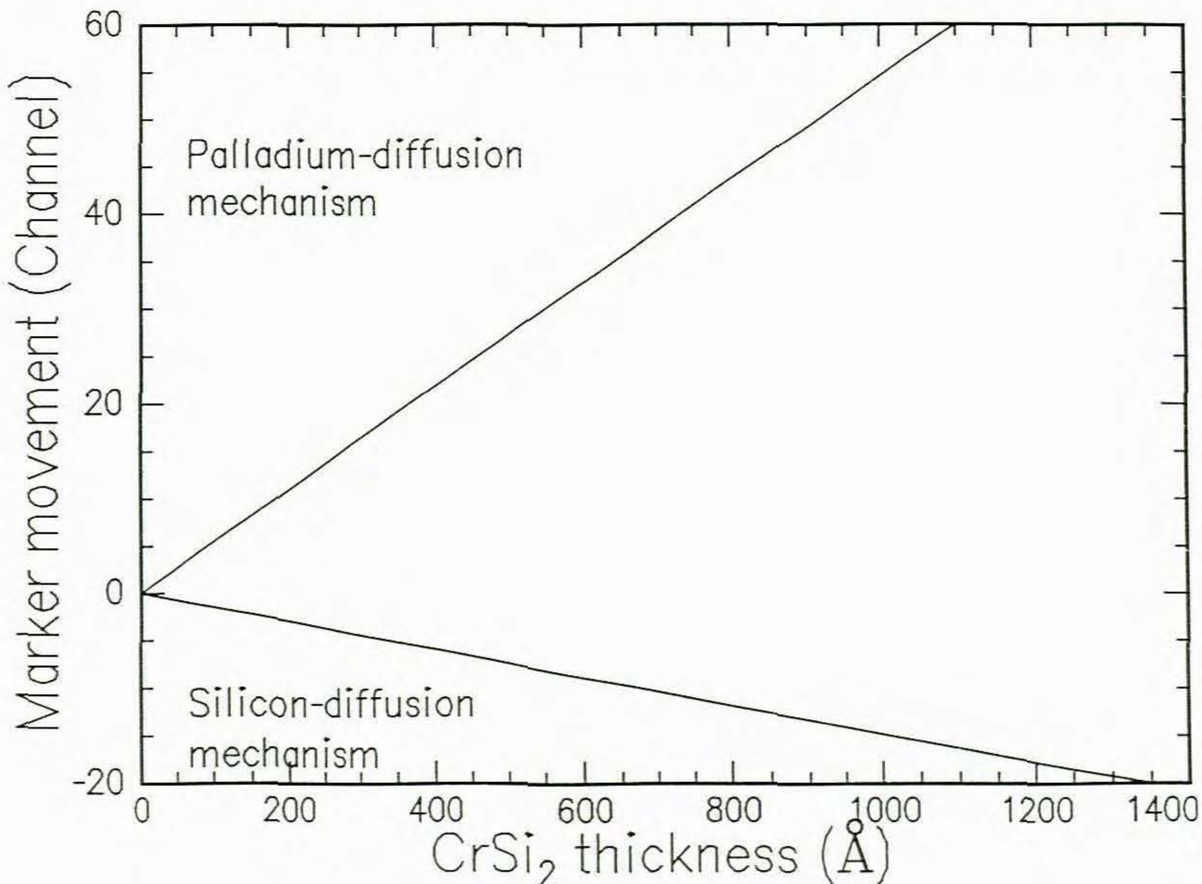

Figure [3.6]. ***Plot of the theoretical simulation of the movement of the marker for both the Pd and Si-diffusion mechanisms. Any movement of the marker within these two extremes would indicate that both mechanisms play a role in the formation of $CrSi_2$.***

3.6 Optimisation of Experimental Parameters

The aim of the optimisation of experimental procedures is to establish the thickness of the layers that should be deposited in order to obtain a backscattering spectrum that is ideally resolved. The optimisation should therefore be based on the physical properties of the elements to be deposited and the compounds these elements may form. The physical properties were discussed in section [2.2]. Since the mass of the projectile and the elements

remain constant throughout the experiment, these properties can be used to sketch a spectrum of near ideal resolution. Considering the kinematic factor (section [2.2.1]), of the elements Cr, Pd, and Ta, Ta is the heaviest. Hence, the peak of tantalum will appear at the highest energy, that is, furthest from the substrate, Si<>. The lightest, Cr, will appear nearest to the substrate and at the surface position since it is the top layer. **Figure [3.7]** illustrates the relative positions of the elements and the thickness of the layers. From this

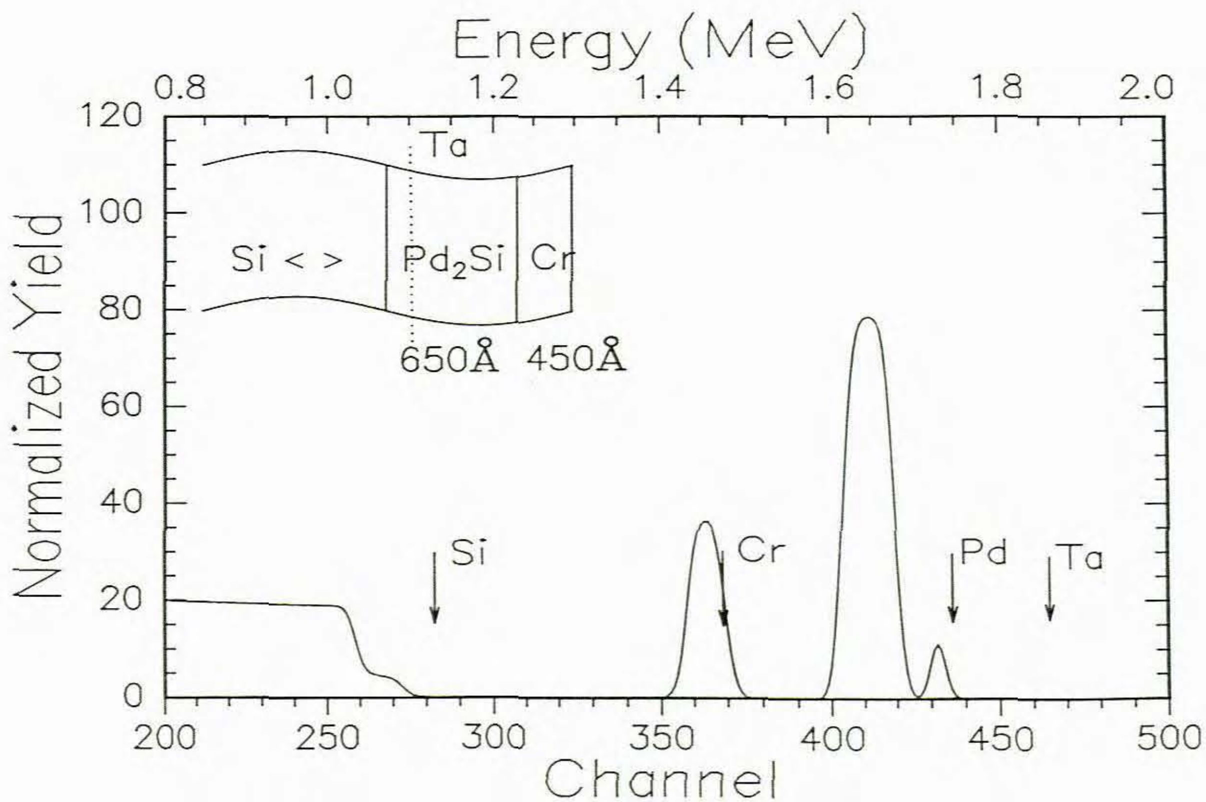

Figure [3.7]. ***Determining the relative positions of the elements by RBS computer simulation. The arrows indicate the energy of the alpha particles scattered from a particular element when located on the surface of the sample.***

figure, it can be seen that, the small peak of the Ta marker is nearly 40 channels below its surface position. The thickness of Ta varies from 5 to 10 Å and will thus not significantly influence the Gaussian distribution of the depth profile.

3.6.1 Pd thickness

From figure [3.7], it is evident that the thickness of Pd and Cr should be optimised. **Figure [3.8]** illustrates the optimisation of the Pd layer, keeping the thickness of the Cr layer constant, in order to achieve an ideal resolution for the Ta peak and thus able to follow it's movement.

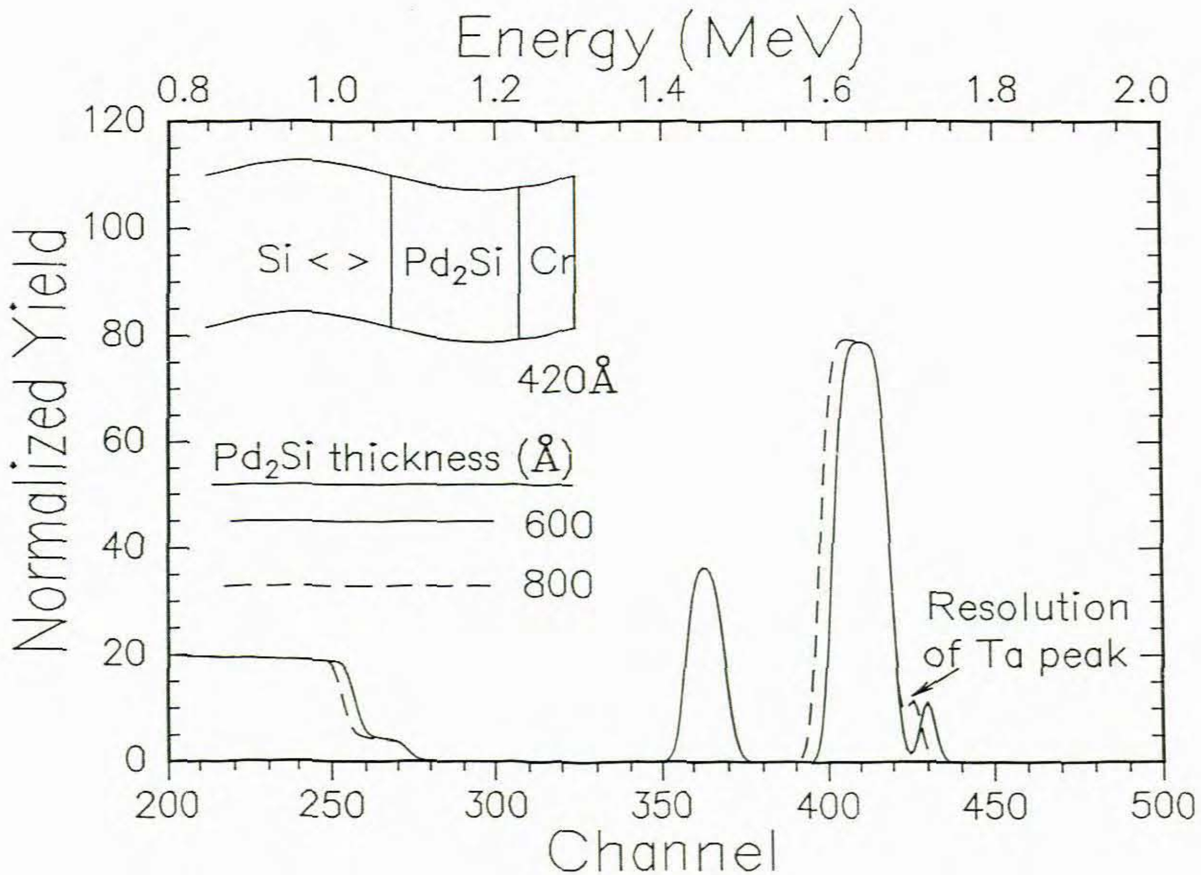

Figure [3.8]. ***Optimisation of the thickness of the Pd_2Si layer to obtain a good resolution for the Ta peak. The thickness of the Cr layer was arbitrarily chosen as 420Å and the maximum thickness of the Pd_2Si layer, obtained from the simulations, was 650Å. It is evident that an increase in Pd_2Si thickness adversely influences the resolution of the marker.***

It should be considered that Pd_2Si forms from the interaction of Pd and Si and the thickness of Pd_2Si should be optimised instead of the thickness of Pd. The resolution of the Ta peak also depends on the position of the marker within the Pd_2Si layer. **Figure [3.9]** shows the position of the Ta marker with respect to the high energy edge of the Pd signal. It is

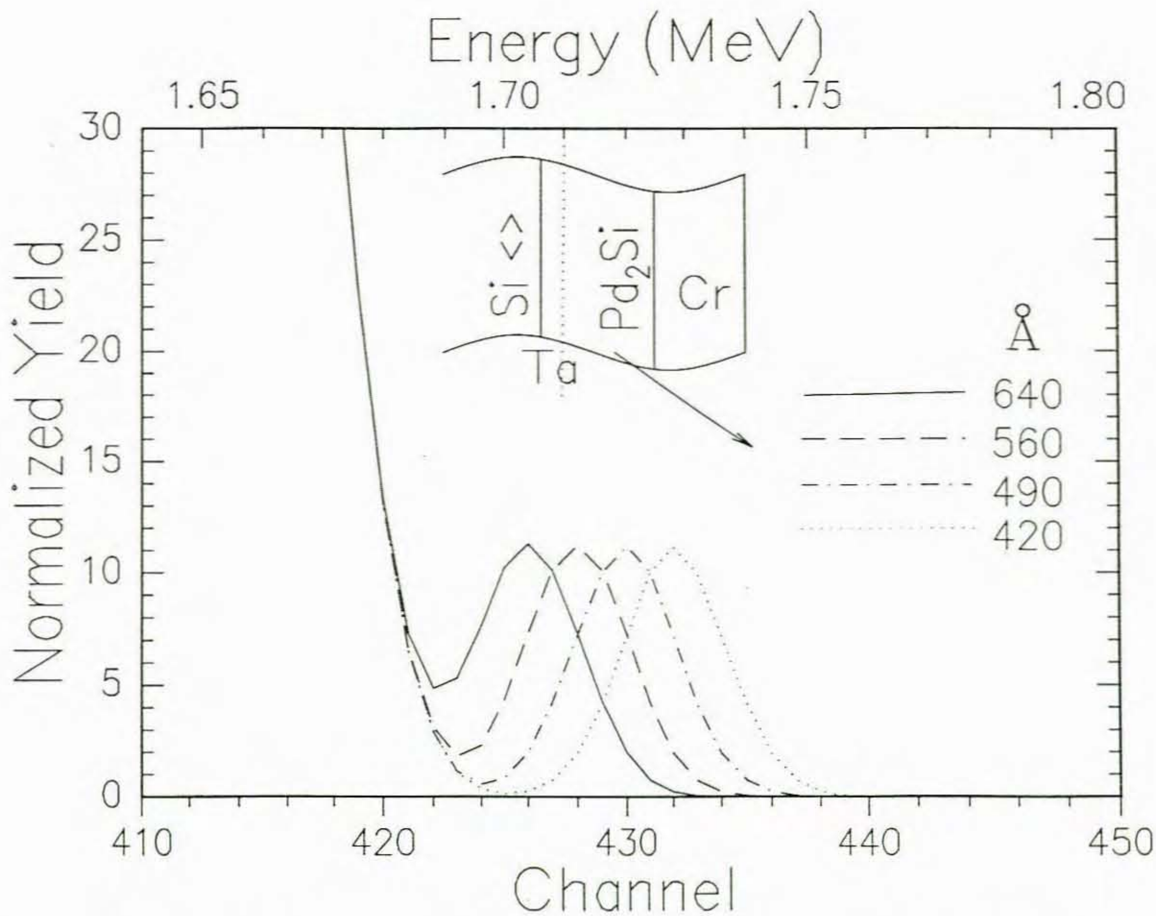

Figure [3.9]. ***Optimisation of the position of the Ta marker in the Pd_2Si layer. The optimum thickness of the Pd_2Si layer was ~630Å. At a front layer thickness of about 560Å the resolution is ideal, since inward and outward movement of the marker is allowed. However, this ideal thickness does not allow the palladium-diffusion mechanism to go to completion, since a thickness of ~1700Å is required to react with 420Å of Cr.***

evident that at a marker position of about 425 serious overlapping with the Pd signal occurs. **Figure [3.10]** depicts a plot of the thickness (Å) of the front Pd_2Si layer and the marker position. The ideal thickness of the Pd_2Si layer is thus approximately 630Å and the front layer thickness should be 600Å thick. This will allow for ideal resolution of the Ta marker in the Pd_2Si layer should the palladium diffusion mechanism occur, that is, the net movement of the marker is inwards.

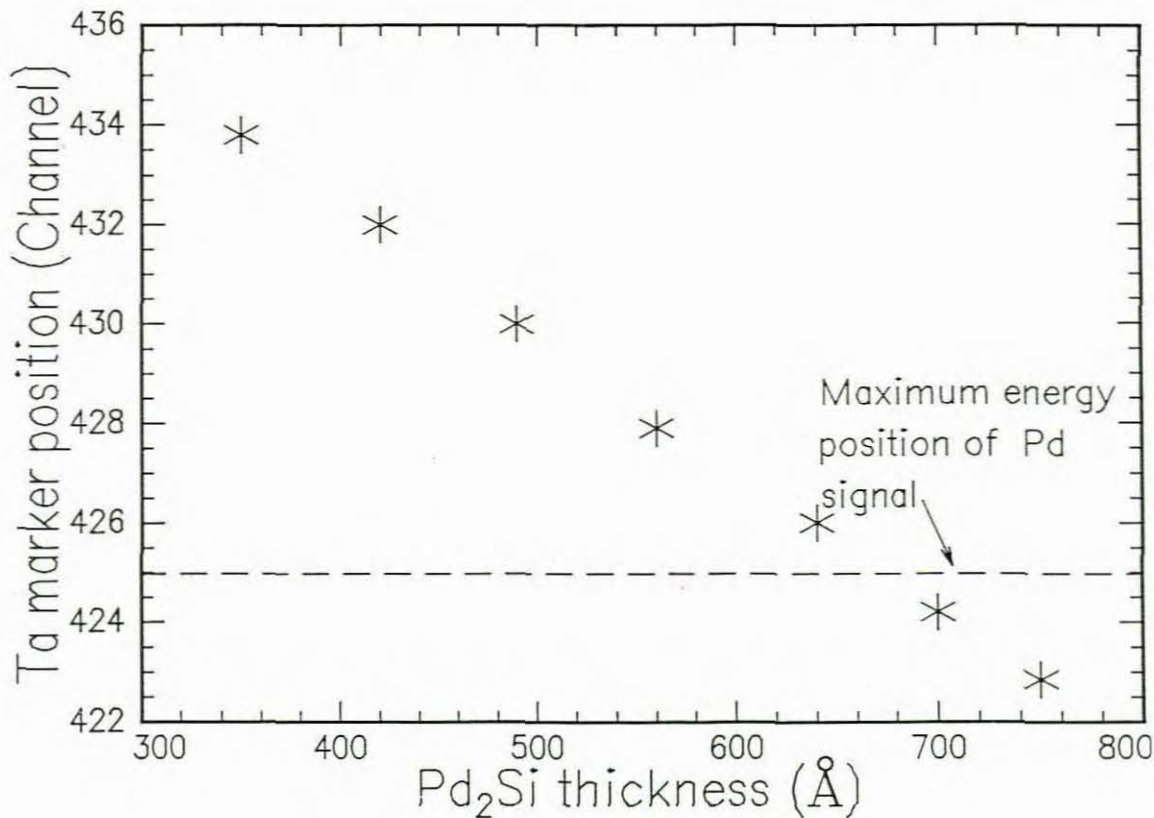

Figure [3.10]. ***Illustration of the change in marker position with increasing thickness of the front Pd_2Si layer. The thickness of the Cr layer is 400Å. At a marker position of channel 425 serious overlapping with the Pd signal starts to occur. The ideal maximum thickness of the front Pd_2Si layer should be 630Å. However, in this instance the marker will be located at the interface of the substrate and the front Pd_2Si layer. For this reason the thickness of the back Pd_2Si layer was chosen to be 50Å.***

3.6.2 Cr thickness

The optimisation of the Cr layer thickness is based on the thickness of the Pd_2Si layer and the position of the Ta marker in the Pd_2Si layer, as determined in the previous section. With the formation of $CrSi_2$, approximately 3Å of $CrSi_2$ is formed for every Å of Cr, the distance the beam traverses is drastically increased and thus affects the resolution of the Cr and Pd peaks. In the instance of the silicon diffusion mechanism, both the Pd and Ta peaks will move inwards. In the case of palladium diffusion mechanism, both peaks will move inward, but the Pd peak to a greater extent than the Ta peak. The method for determining the resolution of the Cr and Pd peaks is illustrated in **figure [3.11]**. Since the

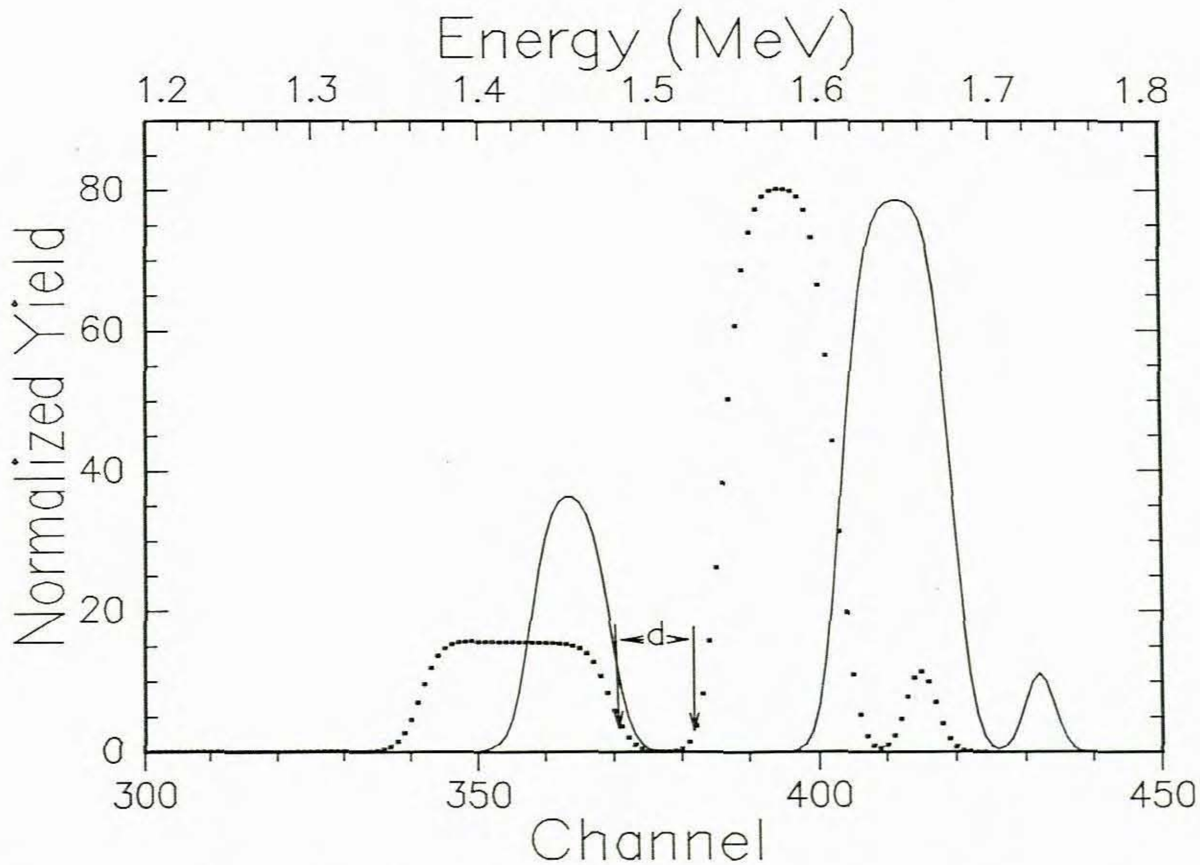

Figure [3.11]. ***Determining the resolution of the Cr and Pd peak to optimise the thickness of the Cr layer for forming $CrSi_2$. The distance, d, is the distance in channels from the base of the Cr in $CrSi_2$ peak and Pd in Pd_2Si peak. This distance is dependent on the thickness of $CrSi_2$ formed, which is 1250Å in this case.***

distance d, in channels, is proportional to the thickness of the $CrSi_2$, a plot of the thickness against d, illustrated in **figure [3.12]**, will indicate the maximum thickness of Cr to obtain a good resolution.

3.7 Marker Movement in $CrSi_2$

In the previous simulations for the formation of $CrSi_2$, it was assumed that the silicon interacts with the chrome at the interface of the Pd_2Si and Cr layer to form the silicide. However, a second mechanism, in which the Cr may diffuse through the $CrSi_2$ to the interface between the $CrSi_2$ and Pd_2Si layers to interact with the Si forming $CrSi_2$, may

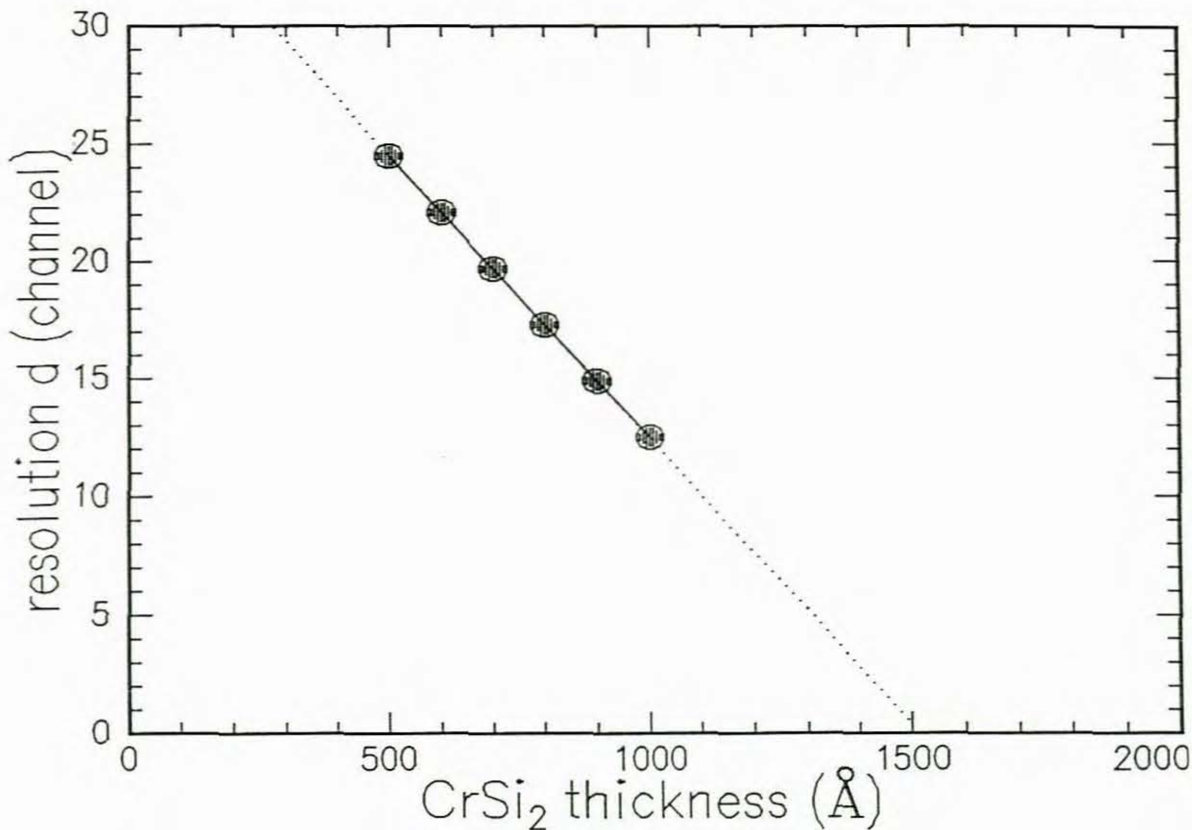

Figure [3.12] ***Plot of the resolution distance d against the thickness of $CrSi_2$. The dotted line is an extrapolation to obtain the maximum thickness (1500Å) of $CrSi_2$ that would yield an ideal resolution. Since 1Å of Cr yield 3Å $CrSi_2$, the maximum thickness of Cr is thus 500Å.***

also occur. These two mechanisms for $CrSi_2$ formation are depicted in **figure [3.13]**. The marker is inserted in the Cr layer at thickness of ~80Å to eliminate any interference that may be caused by the marker movement. As with the Ta in Pd_2Si, these two mechanisms can also be expressed in terms of the channel position of the marker to indicate the two extremes and is illustrated in **figure [3.14]**. Results lying within these two extremes indicate that both chromium- and silicon diffusion contribute to the formation of $CrSi_2$.

3.8 Interface Roughness

The interface between the single crystal Si substrate and the Pd_2Si layer is ideally sharp and planar. The nature of the interface depends on the orientation of the silicon substrate on which it was formed. In many instances the interface is slightly uneven, giving

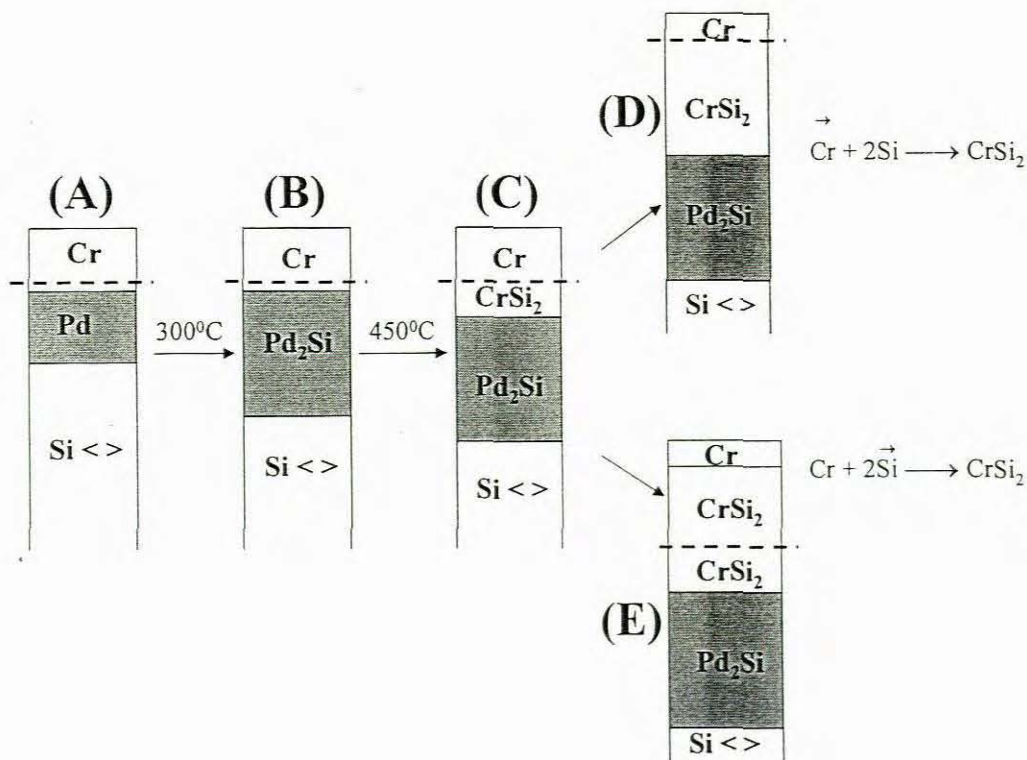

Figure [3.13]. ***Illustration of the mechanisms for the movement of Ta in $CrSi_2$ during the formation of $CrSi_2$. The discontinuous line represents the Ta marker. The as-deposited sample is depicted in (A). (B) represents the formation of Pd_2Si and (C) represents the heated sample just after the layer of Cr has reacted with the Si, forming $CrSi_2$ in front of the marker. Chrome diffusion mechanism is illustrated by (D) and silicon diffusion mechanism by (E). The arrows over the Cr and Si in the corresponding equations signify which species is diffusing.***

rise to the term interface roughness or lateral non-uniformity, the determination of which is given in section [4.1]. The roughness occurs when material is derived from the substrate. As in the instance of silicon derived from the substrate, the silicon is removed in an uneven manner, causing the lateral non-uniformity. The orientation of the substrate influences the degree of roughness to a great extent. Hence, if the Pd_2Si layer is epitaxial, then the degree of roughness will be greater than in the instance of the Pd_2Si layer being polycrystalline. This is because at the epitaxial growth sites preferential crystal growth occurs, causing crystal pitting out from the interface. The non-uniformity is determined by simulating and averaging several values for the sample interface structure. Each sample structure has a

slightly different layer thickness. An illustration of a typical substrate – Pd_2Si interface and the corresponding sample structure is depicted in **figure [3.15]**. The semi-automated algorithm, contained in the module Pert, discussed in section [3.2], interpolates the thickness

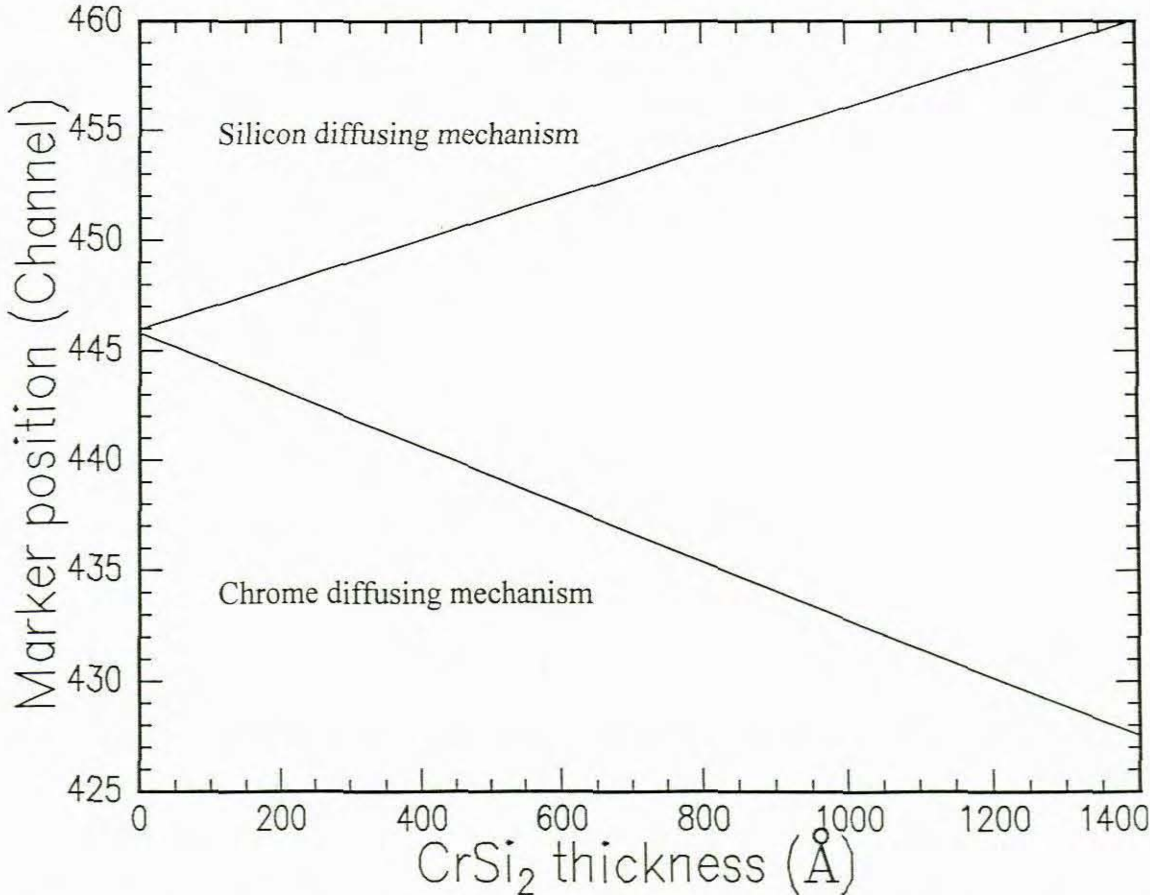

Figure [3.14] ***Illustration of the two mechanisms identifying the diffusing species during the formation of $CrSi_2$. In the Cr diffusion mechanism the Ta marker move outwards toward the sample surface and for the Si diffusion mechanism the marker moves inwards. The $CrSi_2$ thickness is the amount formed after complete formation of the front layer of $CrSi_2$. The initial marker position, which is at channel 446, is independent of the thickness of the front layer of $CrSi_2$.***

values of the sample structures, and the best fit is selected. A sample structure is then constructed and the spectrum drawn. Measured RBS spectra are given in figure [3.16], showing that the Si <111> | Pd_2Si interface is much more rough and non-uniform than the Si <100> | Pd_2Si interface, due to the fact that Pd_2Si forms epitaxially on Si <111> substrates.

In this chapter it was demonstrated how the software programme RUMP can be used to establish the thickness of the various layers of Pd, Ta and Cr, the position of the

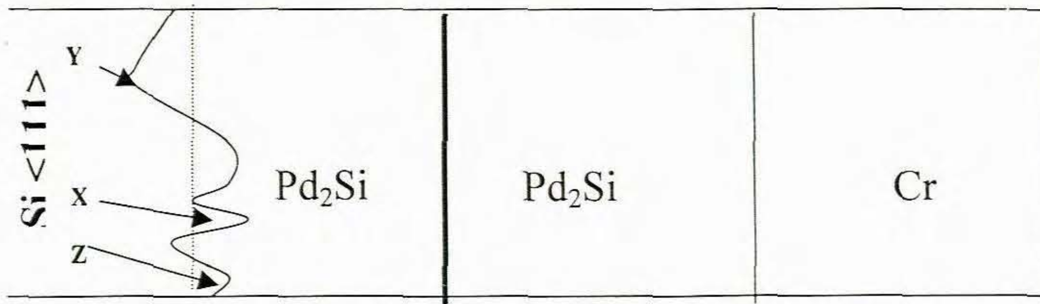

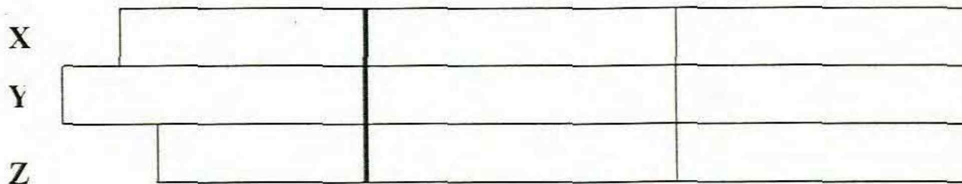

Figure [3.15]. *Illustration of a typical substrate – Pd_2Si interface (A) and the corresponding sample structures (B) for the determination of the degree of interface roughness between these two layers. The dotted line in (A) indicates the averaging of the different sample structures. By specifying the variation in thickness of the back layer of Pd_2Si, (interface width), for example, the layer thickness is 500Å and the variation 50Å, PERT interpolates the best fit to the layer. The thickness of the layers is based on the optimised parameters, determined in section [3.6].*

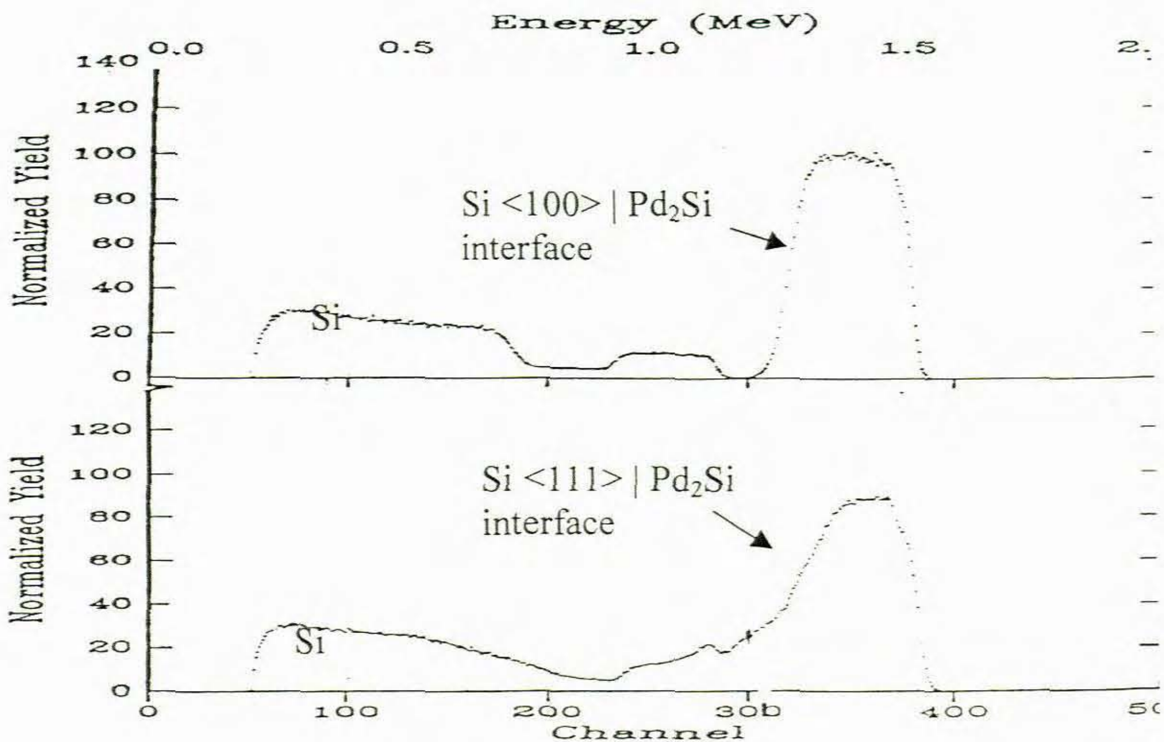

Figure [3.16]. *Spectra illustrating the degree of interface roughness for the growth of $CrSi_2$ on non-epitaxial Pd_2Si (top) and growth on epitaxial Pd_2Si (bottom)*

marker in the Pd layer and how the degree of lateral non-uniformity can be ascertained. These established parameters would be used to prepare the different samples as detailed in Chapter 2. The significance of the analysis of these reacted samples will be discussed in chapter 4.

CHAPTER 4

FORMATION OF $CrSi_2$ ON Pd_2Si

4.1 Introduction

This chapter deals with the experimental data obtained during this study. Sections [4.2] and [4.3] detail the experimental data of $CrSi_2$ formation on non-epitaxial Pd_2Si and epitaxial Pd_2Si using a thin marker. The effect of marker thickness on the formation of epitaxial Pd_2Si using a thin marker is discussed under section [4.4]. The RUMP analysis of the spectra by simulation and perturbation were done after the desired temperature was reached, at which $CrSi_2$ already started to form. The kinetics, either linear or parabolic (*cf.* Section [1.4.2]), was determined by ordinary least square statistics. The percentage silicon diffusion mechanism (%SDM) was calculated as the percentage of the silicon (expressed as a thickness) that passed the marker relative to the silicon (expressed) thickness necessary for the $CrSi_2$ formed, for example;

$$\%\,SDM = \frac{\text{Thickness (Å) of Si passed the marker} * 100}{\text{Thickness (Å) of Si needed for } CrSi_2 \text{ formation}}$$

Hence when 100Å of silicon passed the marker and 400Å of $CrSi_2$ formed, then the % SDM is 100*100/(400/3.33) ~ 83% (see Appendix B for thicknesses that react). Similarly, the interface roughness is expressed as the interface width (variation in thickness as a percentage of the Si <>| Pd_2Si interface) as a percentage of the thickness of the Pd_2Si layer.

$$\%\,\text{Interface Roughness} = \frac{\text{Interface width (Å)} * 100}{\text{Thickness (Å) of back } Pd_2Si \text{ layer}}$$

The marker position at the different temperatures were corrected to correspond with the

position at 400 ^{0}C.

4.2 Non-epitaxial Pd_2Si

4.2.1 Kinetics

The kinetics of $CrSi_2$ formation on Pd_2Si was measured using iso-thermal "in situ" real time RBS measurements. Zero time was chosen where the indicated temperature was reached and therefore indicates prior $CrSi_2$ formation. The plot of the growth in thickness (Å) during formation $CrSi_2$ at the temperatures of 400, 425, 450 and 475^{0}C are depicted in **figure [4.1]**, indicating that the formation kinetics is linear.

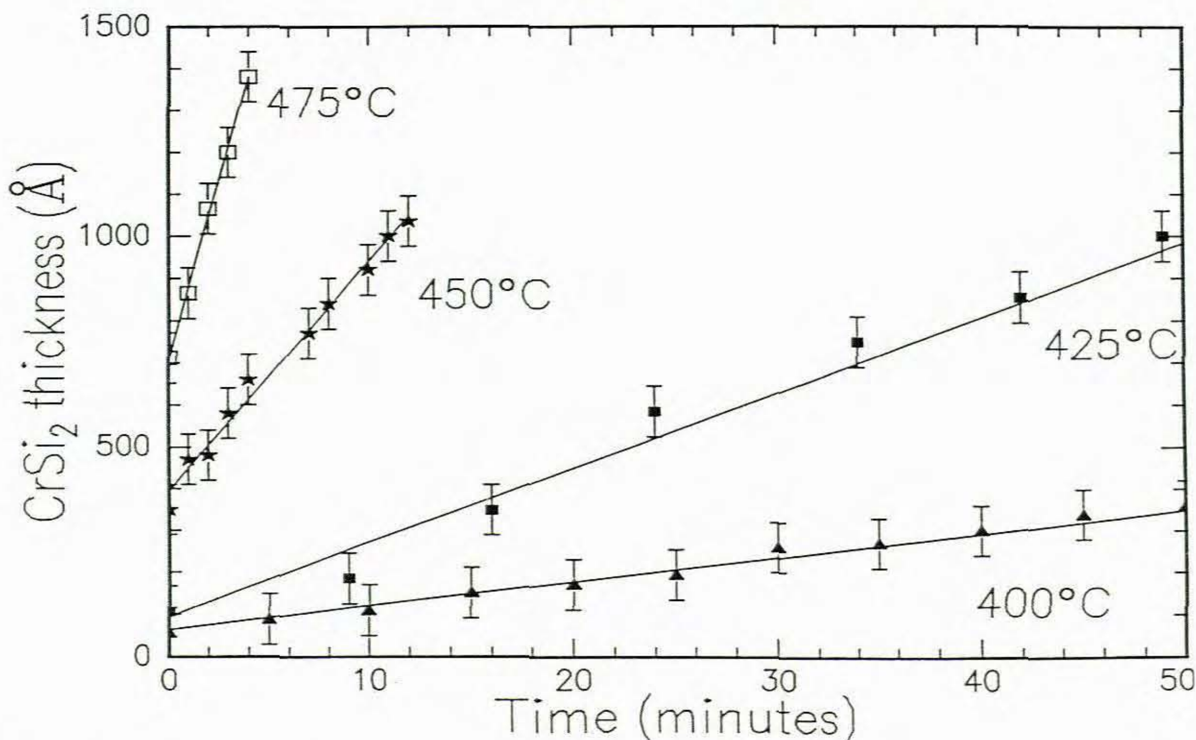

Figure [4.1]. *Graph of the growth in thickness (Å) of $CrSi_2$ on Pd_2Si – Si<100> at various temperatures. The statistical treatment of the data showed a linear dependence of the growth (Å) on the time (minutes) elapsed. Although the times taken for complete $CrSi_2$ formation at 400 ^{0}C was approximately 140 minutes, the scale of 0-50 minutes was chosen to illustrate the growth at 450 and 475 ^{0}C.*

At 500 ^{0}C, the reaction was completed within 60 seconds - not yielding significant or reliable data and the reaction was completed before the temperature of 550 ^{0}C could be

reached. **Table [4.1]** gives the growth rates at the different temperatures and an activation energy of 2.1 eV is found (see **figure [4.2]**). It is evident that the growth rate increase

Table [4.1]. ***The growth rate of $CrSi_2$ on polycrystalline Pd_2Si at various temperatures.***

Temperature (^{0}C)	400	425	450	475
Growth rate (Åmin^{-1})	5.6	17.8	53.8	165.7

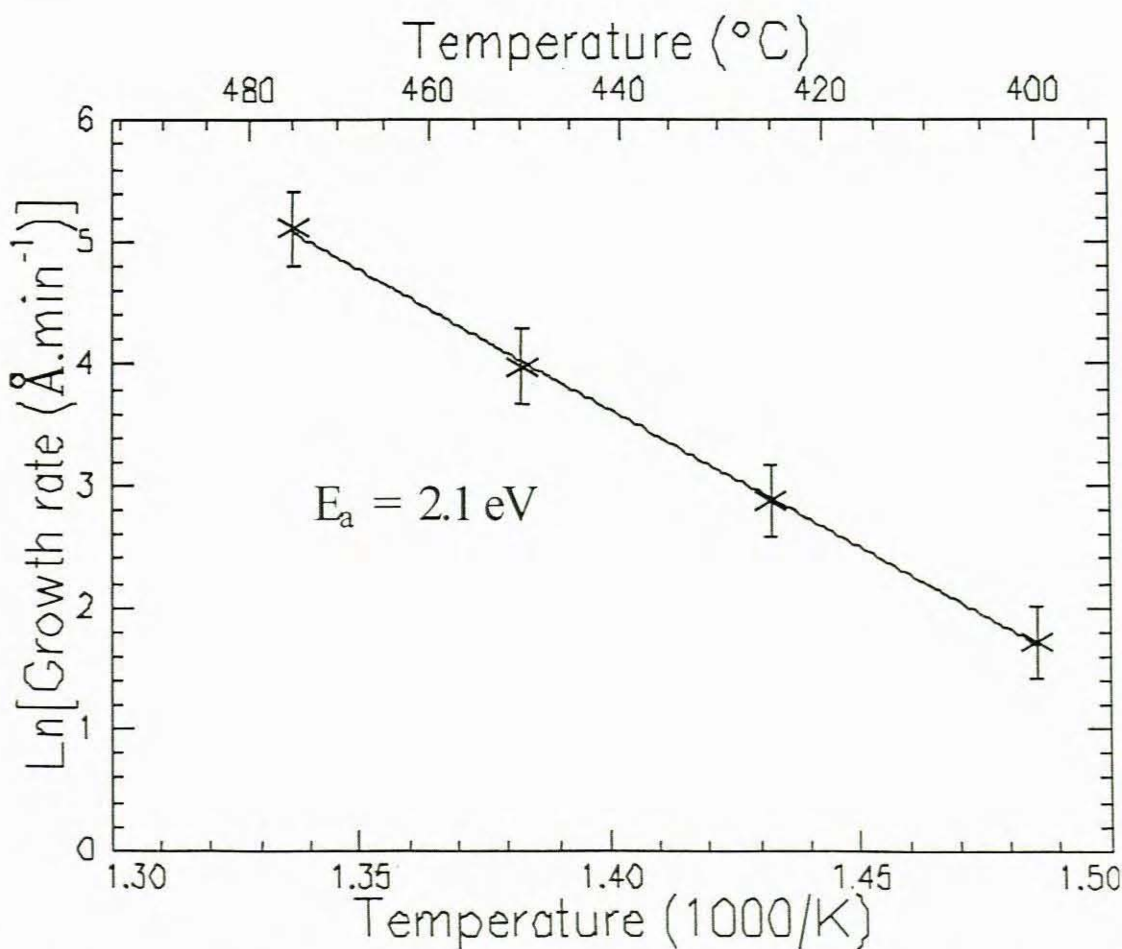

Figure [4.2]. ***Arrhenius plot of the growth rates of $CrSi_2$ on Pd_2Si – Si<100> at the various temperatures.***

three-fold for a temperature increase of 25 ^{0}C. It should be considered that the specimen was at first heated to a few degrees below the set temperature and then to the specific temperature. This overcame the problem of over-shooting, that is, when the temperature increases to above – and then decreases to the set temperature.

4.2.2 Diffusion mechanism

In this section, the experimental data is evaluated to ascertain the diffusion mechanism. **Figure [4.3]** illustrates two RBS spectra before and after $CrSi_2$ formation at 425 ^{0}C.

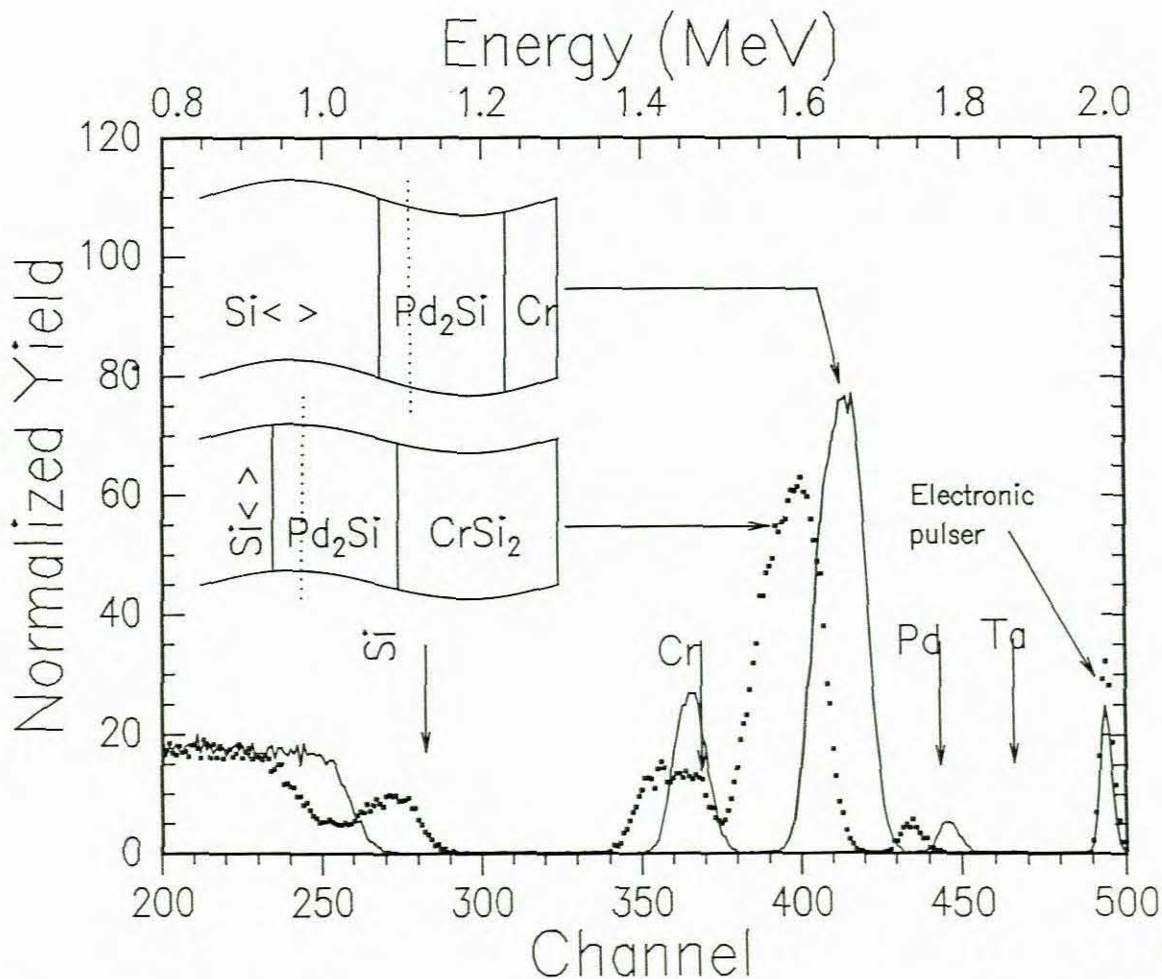

Figure [4.3]. ***Rutherford backscattering spectra, indicating the inward movement of the Ta marker (discontinuous line in Pd_2Si layer) during $CrSi_2$ formation on Pd_2Si – Si<100> at 425 ^{0}C. The continuous line represents as deposited sample and the dotted line the sample when $CrSi_2$ completely formed. The thickness of the Pd_2Si layer is 580Å and the $CrSi_2$ layer 790Å. The arrows indicate the energy of the elements when located at the surface. The pulsar was inserted to verify whether any electronic drift occurs.***

This figure compares excellently with figure [3.4], in which the theoretical simulation of the silicon diffusion mechanism was illustrated. **Figure [4.4]** depicts the *in situ* real time backscattering spectrum of $CrSi_2$ formation at 425 ^{0}C, showing the inward movement of

the marker and hence that the silicon diffusion mechanism is the dominant mechanism.

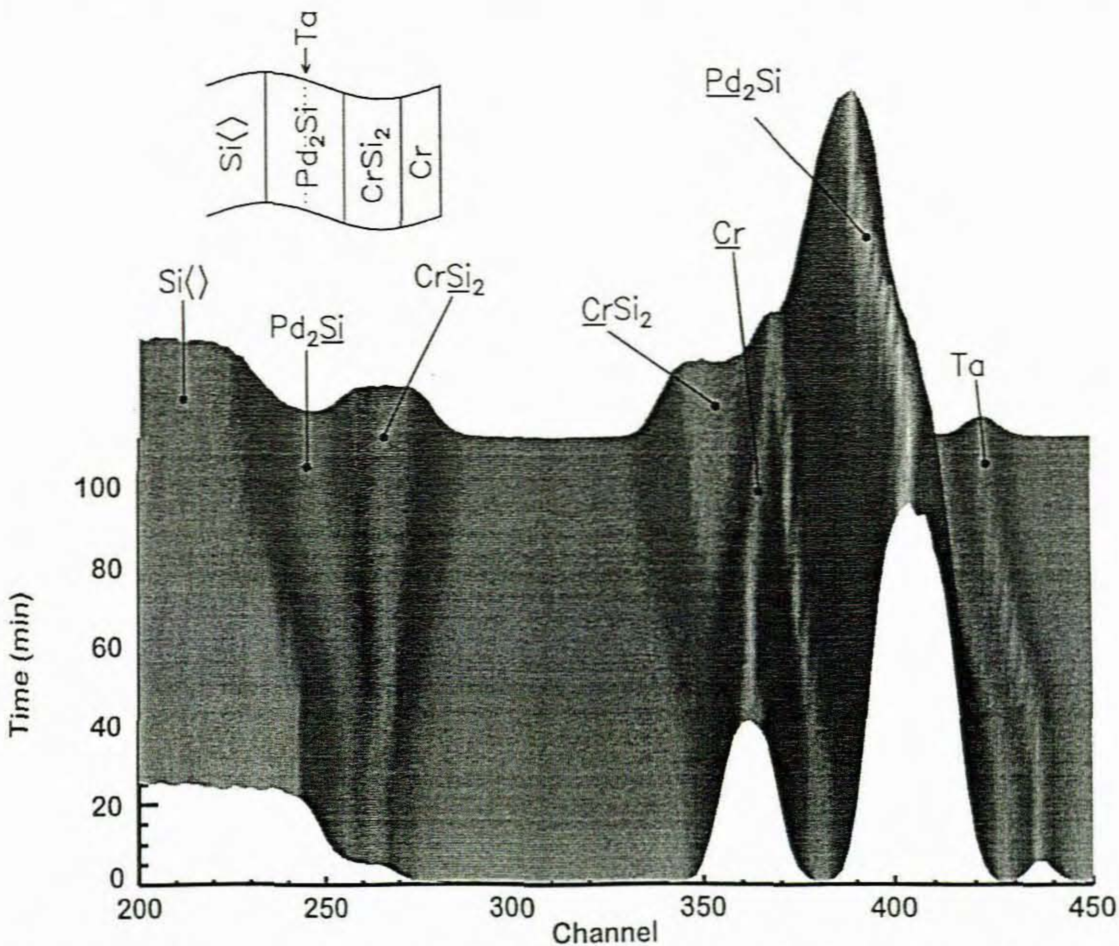

Figure [4.4]. ***Representation of the* in situ *real-time Rutherford Backscattering composite spectra during the formation of $CrSi_2$ on non-epitaxial Pd_2Si at 425 ^0C. It clearly shows the inward movement of the marker with respect to the surface. Hence, the formation is predominantly due to silicon movement from the substrate, i.e. the silicon diffusion mechanism.***

The marker position as a function of $CrSi_2$ thickness at the various temperatures is illustrated in **figure [4.5]**. The slight displacement of the experimental points with respect to the line representing Si diffusion indicates a small amount of Pd diffusion during the initial stages of $CrSi_2$ growth. This slight displacement is only seen at the temperatures of 400 and 425°C. At the higher temperatures of 450 and 475°C, the displacement is however not visible since the palladium dissociation occurred before the temperatures were reached. The hundred percentage silicon diffusion at these temperatures can be seen in the inset of figure [4.5] where all the measurements are given.

Figure [4.6] depicts the percentage silicon diffusion mechanism, calculated as in section [4.1], during the growth of $CrSi_2$. This figure shows that the palladium diffusion mechanism (a maximum of about 10%) occurs in the early stages of the reaction, which is until approximately 350Å of $CrSi_2$ has formed. Afterwards, the silicon diffusion mechanism is the only reaction mechanism. Consequently, the marker position does not coincide with the theoretical simulation and will be displaced slightly above the theoretical line (*cf.* figure [3.12], section [3.5]). Hence, the marker position at the temperatures of 450 and 470 ^{0}C will be slightly lower than the marker position at 400 and 425 ^{0}C, at which the palladium diffusion mechanism could be monitored. At the relatively high temperatures of 450 and 475 ^{0}C, there is no palladium diffusion – the diffusion occurred while the sample was heated to the desired temperature.

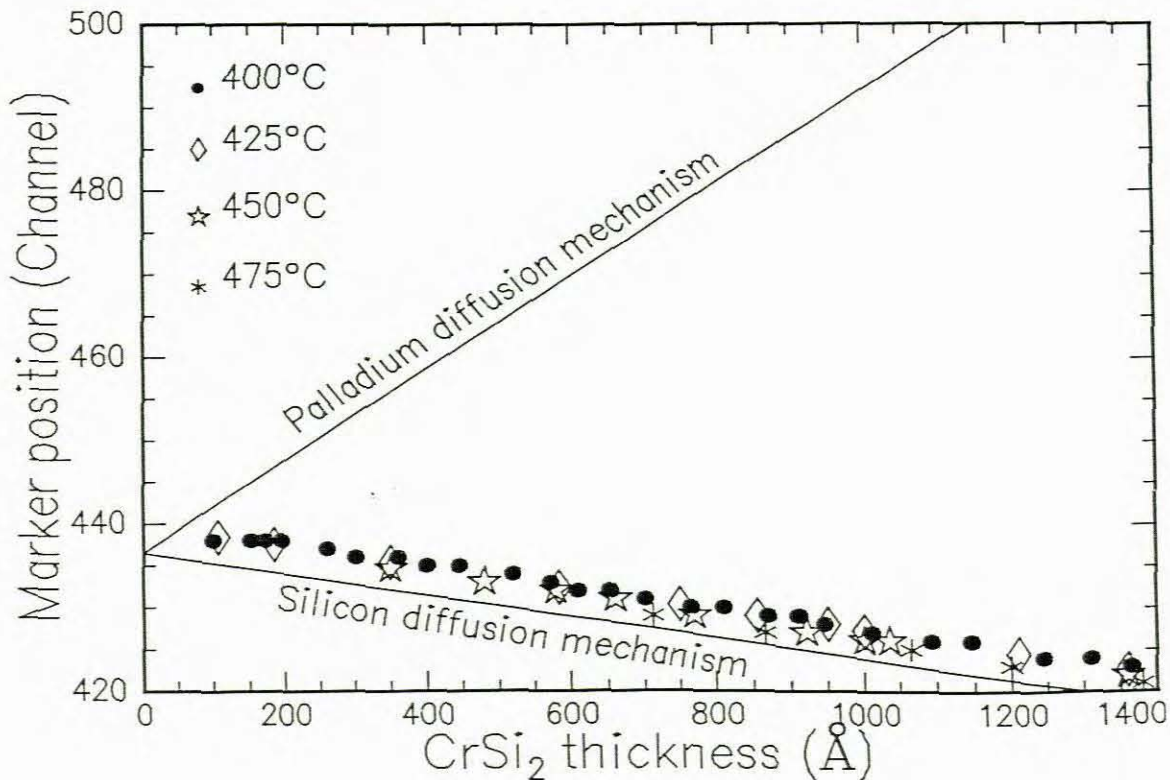

Figure [4.5]. ***Illustration of the marker movement during $CrSi_2$ formation on non-epitaxial Pd_2Si, at the various temperatures. The movement follows the silicon diffusion mechanism, indicating that this mechanism is dominant. The slight displacement of the measured marker position from the theoretical simulation is due to the palladium diffusion, taking place during the early stages of $CrSi_2$ formation.***

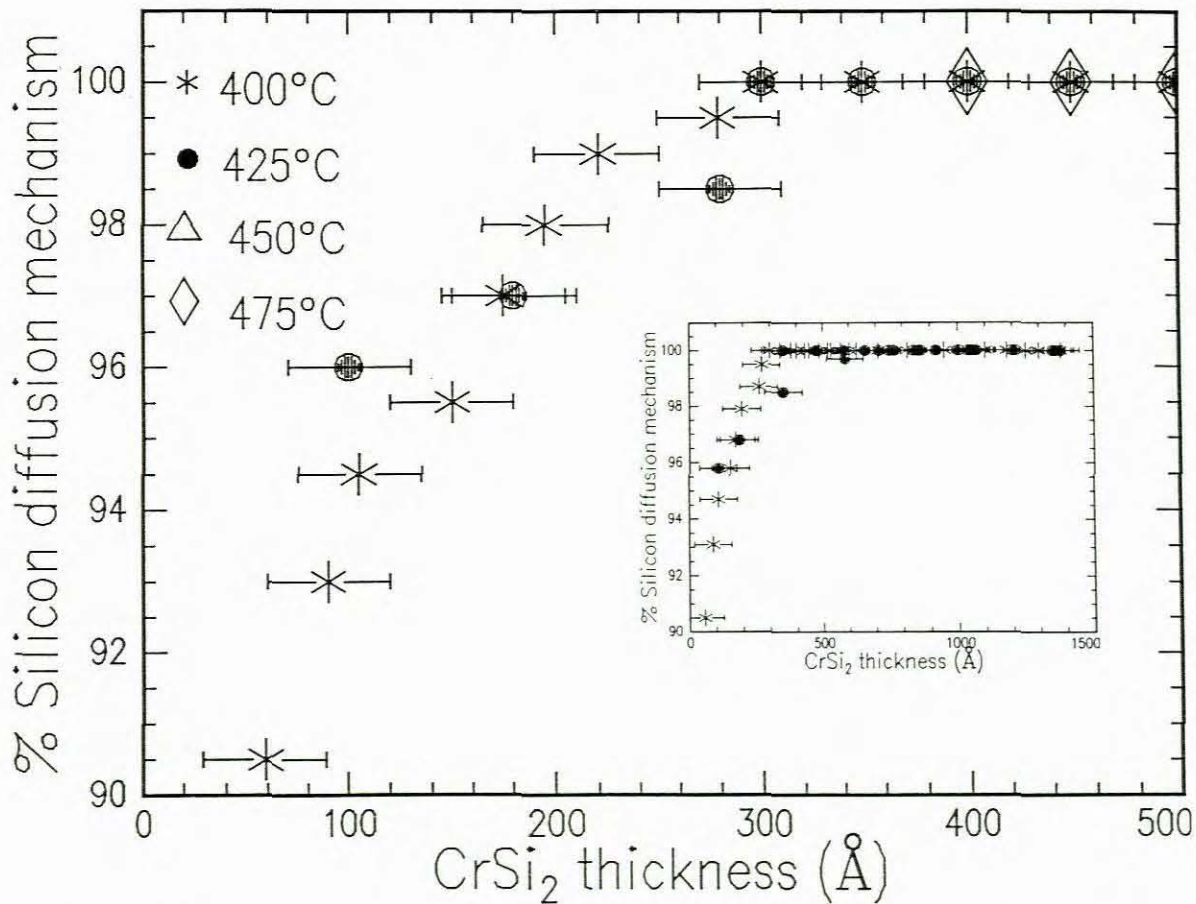

Figure [4.6] ***Illustration (exploded view) of the % silicon diffusion mechanism for the formation of $CrSi_2$, expressed as the percentage of silicon thickness that passed the marker to the total silicon thickness necessary for $CrSi_2$ formation during the reactions. It is evident that, although the silicon diffusion mechanism is dominant mechanism, the palladium diffusion mechanism occurs in the early stages of the reaction. The inset gives all the measurements.***

4.2.3 Interface Roughness

The degree of interface roughness or lateral non-uniformity is depicted in **figure [4.7]**. From this figure, it can be seen that, at the lower temperatures of 400 and 425 ^{0}C the degree of lateral non-uniformity is more prominent compared to the data at 450 and 475 ^{0}C. This is because palladium diffusion already occurred before the higher temperatures could be reached. Furthermore, the maximum degree of lateral non-uniformity or interface roughness increases slightly with the increase in temperature.

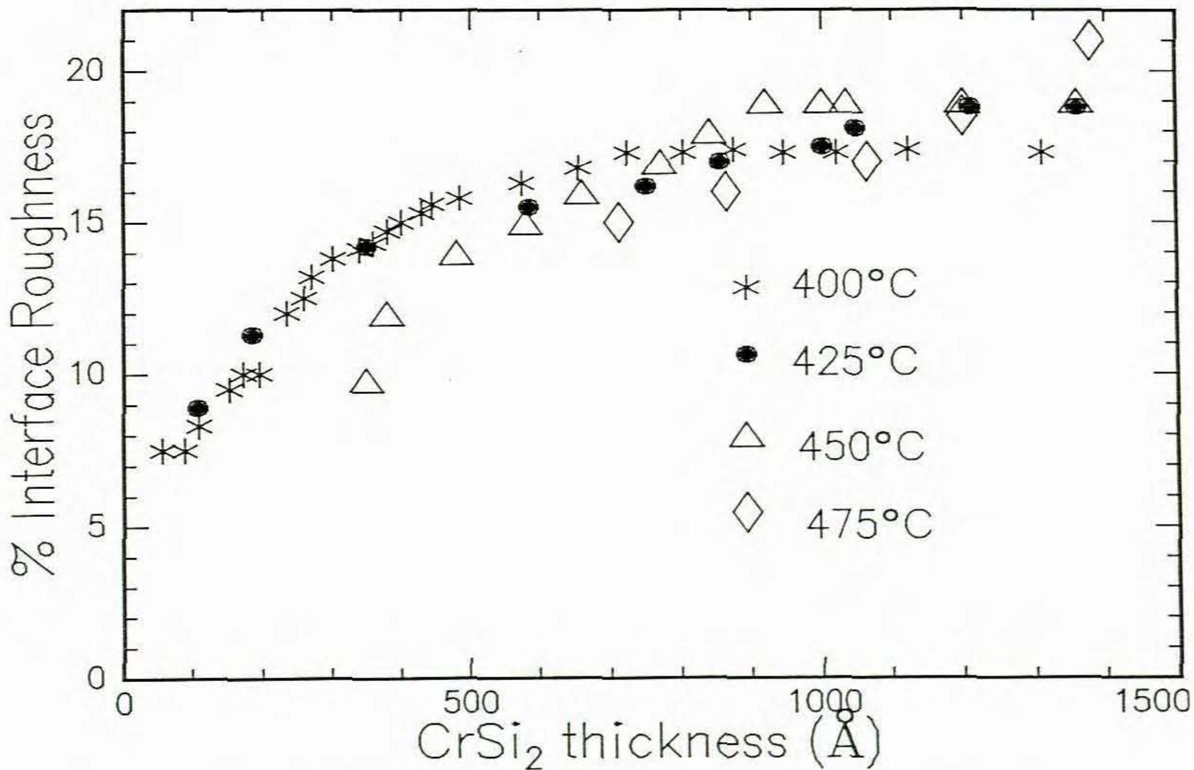

Figure [4.7]. ***Illustration of the degree of Si<100> | Pd_2Si interface roughness or lateral non-uniformity for $CrSi_2$ formation on non-epitaxial Pd_2Si.***

4.3 Epitaxial Pd_2Si

4.3.1 Kinetics

Figure [4.8] shows the plot of the growth rate of $CrSi_2$ on epitaxial Pd_2Si. As in the case of growth of $CrSi_2$ on non-epitaxial Pd_2Si, the plots indicate that the formation kinetics is linear. In addition, the reaction at 500 ^{0}C was completed within one minute and did not yield reliable and significant data. For the growth rate to be monitored at 550 ^{0}C, the reaction was completed before the temperature could be reached. The growth rates at the various temperatures are given in **table [4.2]**. From this table, it can be seen that the growth rates on epitaxial Pd_2Si at the different temperatures are marginally less than the growth rates at the temperatures on non-epitaxial Pd_2Si. The Arrhenius plot of the growth rates on epitaxial Pd_2Si at the different temperatures is illustrated in **figure [4.9]**, giving an

activation energy of 1.9 eV.

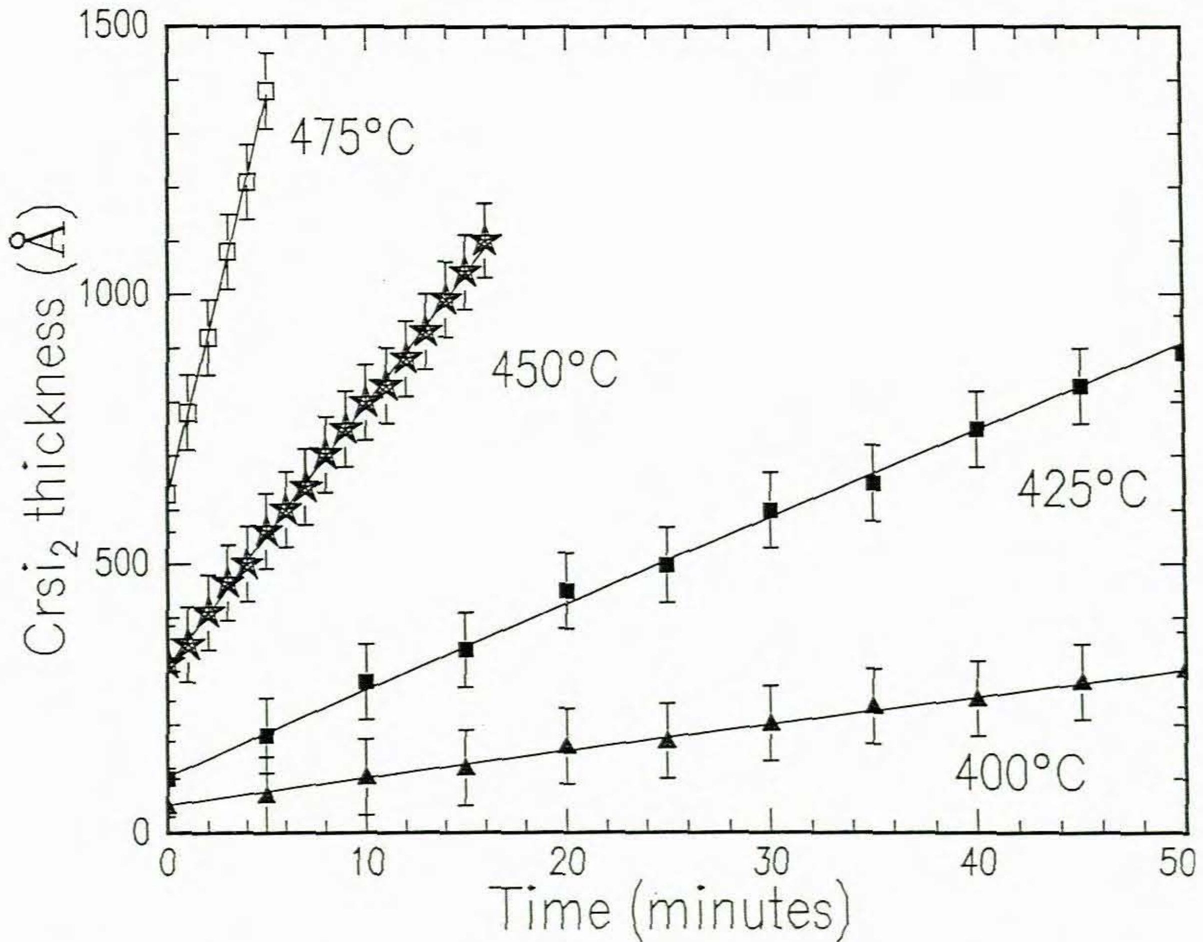

Figure [4.8]. *Plot of the growth rates during the $CrSi_2$formation on Pd_2Si – Si<111>. The growth in thickness (Å) is linearly dependent on the time (minutes) elapsed. The time scale of 0 – 50 minutes was selected to indicate the growth rates of the reaction at 450 and 475 ^{0}C. In this instance, the time for complete $CrSi_2$ formation at 400^{0}C was approximately 170 minutes.*

Table [4.2]. *The growth rate of $CrSi_2$ on epitaxial Pd_2Si at the various temperatures.*

Temperature (^{0}C)	400	425	450	475
Growth rate (Åmin^{-1})	5.0	15.8	47.4	147.8

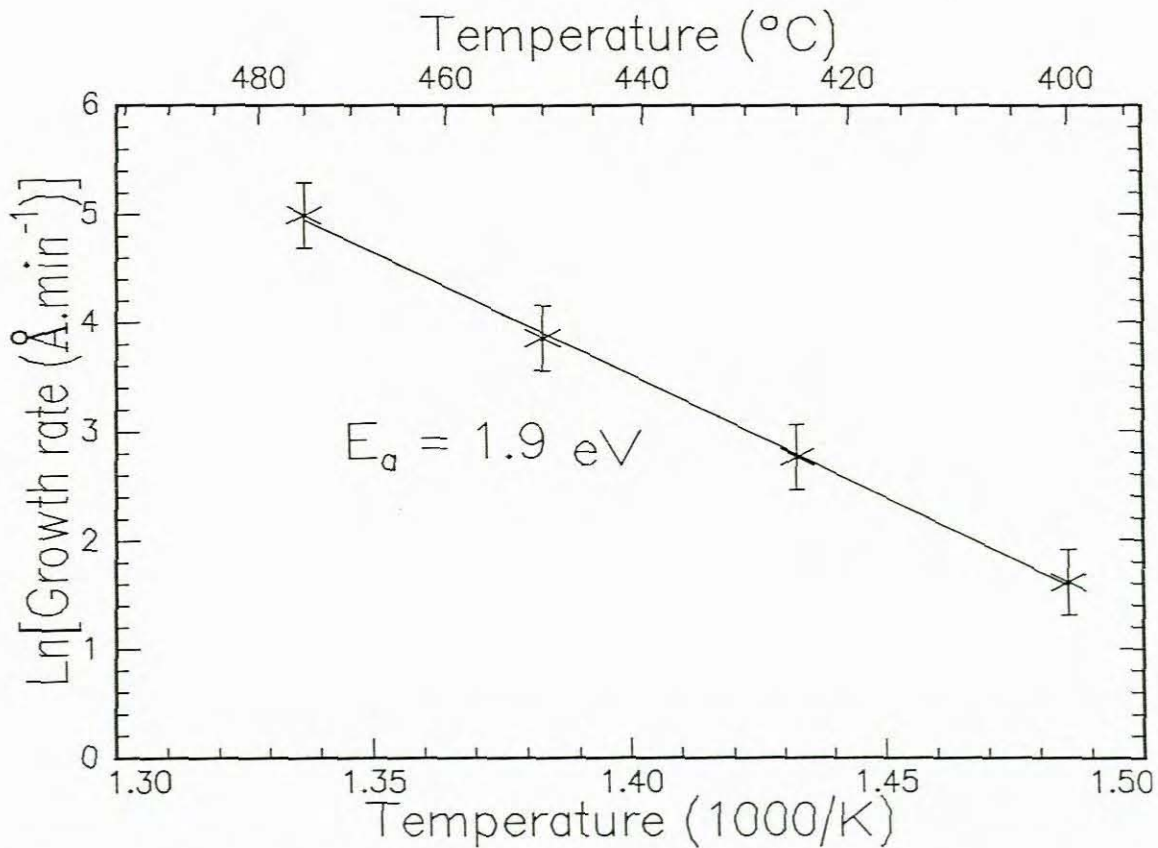

Figure [4.9]. ***The Arrhenius plot of the growth rates of $CrSi_2$ on epitaxial Pd_2Si at the various temperatures.***

4.3.2 Diffusion mechanism

Figure [4.10] shows Rutherford backscattering spectra on epitaxial Pd_2Si of the as deposited sample and the sample after $CrSi_2$ had completely formed. As in the instance of $CrSi_2$ formation on non-epitaxial Pd_2Si, **figure [4.10]** compares well with the theoretical simulation depicted in figure [3.4]. It evident that the inward movement of the marker indicates that the silicon diffusion mechanism occurs during the reaction, that is, silicon is derived directly from the substrate. The *in situ* real time backscattering composite spectrum is depicted in **figure [4.11]**, showing the inward movement of the marker. The marker position as a function of $CrSi_2$ thickness at different temperatures is given in **figure [4.12]**, clearly indicating the slight displacement above the theoretical line representing the silicon diffusion mechanism due to some initial Pd diffusion.

As in the case of $CrSi_2$ formation on non-epitaxial Pd_2Si, there is also palladium diffusion in the early stages of the formation on epitaxial Pd_2Si. This gives rise to the slight displacement of the marker from the theoretical simulation.

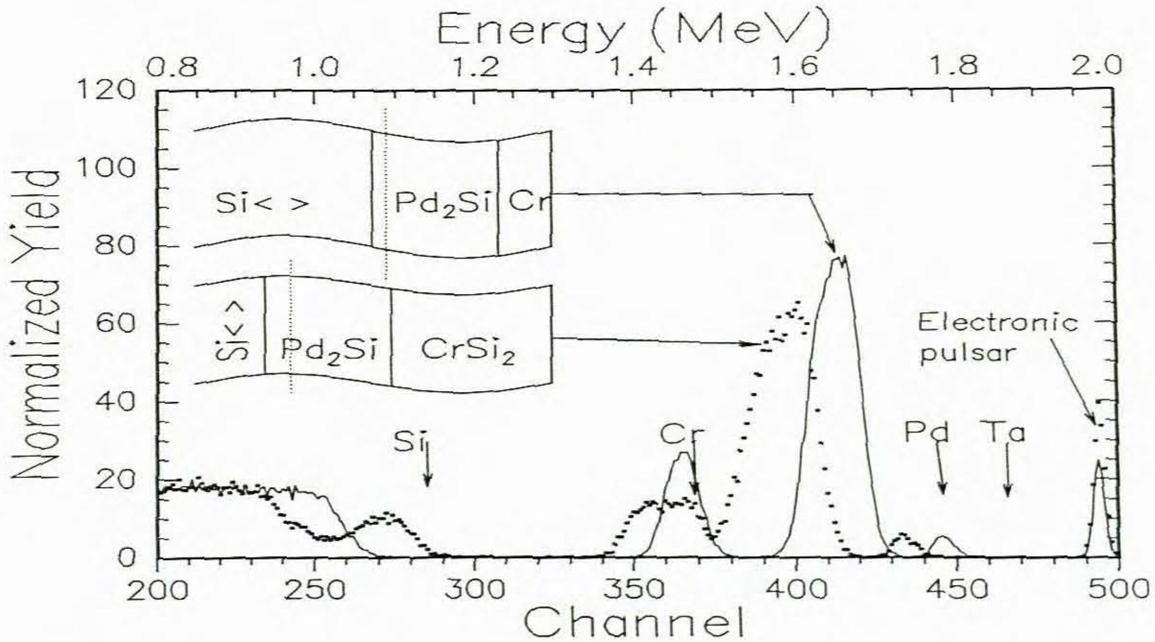

Figure [4.10]. ***Backscattering spectra at 425 ^0C of the sample after the complete formation of Pd_2Si (continuous line) and the sample when $CrSi_2$ layer (950Å) completely formed (dotted line), indicating the inward movement of the marker (continuous line in Pd_2Si layer). Hence, the silicon diffusion mechanism occurs during the reaction.***

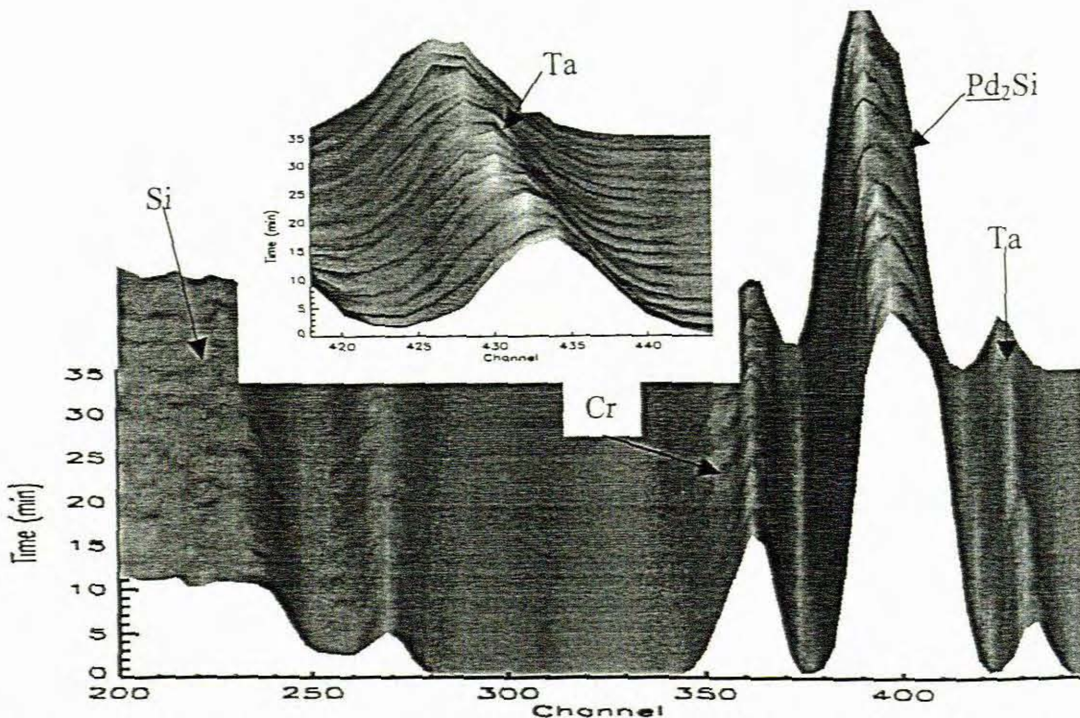

Figure [4.11]. *Illustration of the* in situ *real time RBS spectra of $CrSi_2$ formation on epitaxial Pd_2Si at 425^{0}C. The inset is an exploded view of the marker movement.*

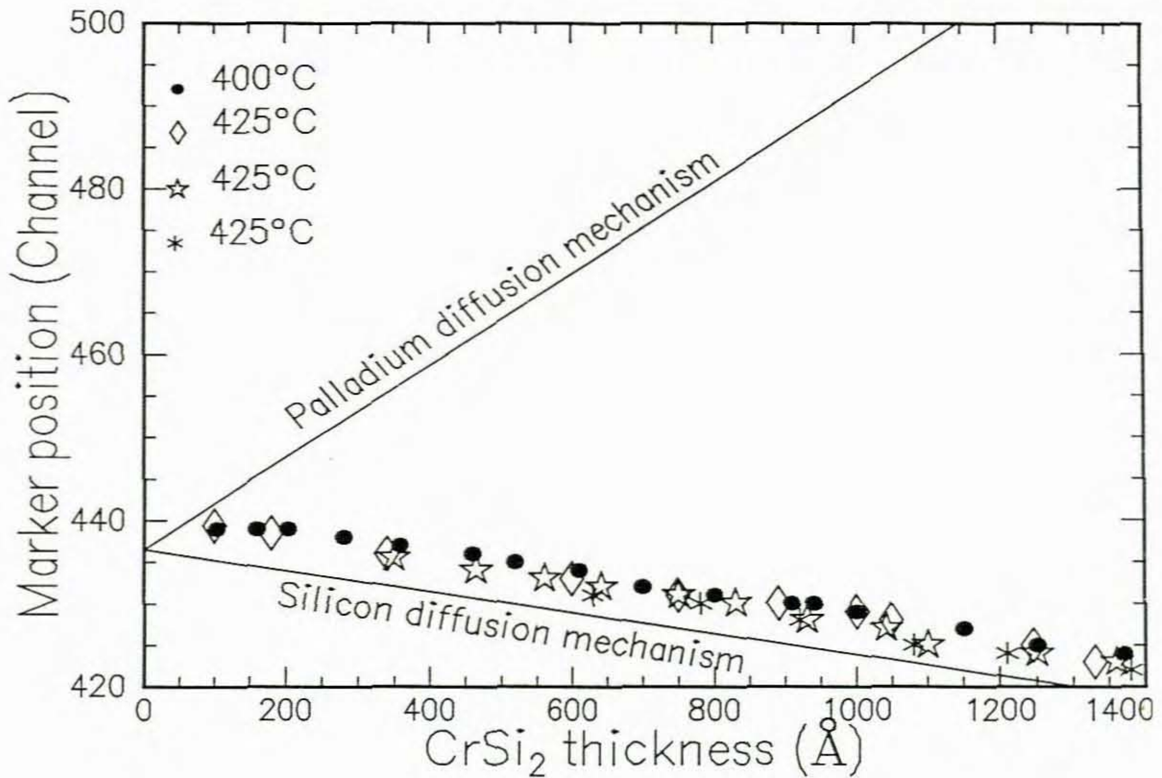

Figure [4.12]. ***Illustration of the marker movement during $CrSi_2$ formation on epitaxial Pd_2Si. The movement follows the silicon diffusion mechanism, showing that this mechanism is dominant. The slight displacement of the marker position from the theoretical simulation is due to palladium diffusion in the early stages of the reaction***

- **Figure [4.13]** shows that more than 10% Pd diffusion occurs during the initial stages of $CrSi_2$ formation which decreases to about zero after formation of about 500Å of $CrSi_2$.

4.3.3 Interface roughness

Since the $CrSi_2$ formation occurs on epitaxial Pd_2Si, the degree of roughness of the Si<111> | Pd_2Si interface is expected to be relatively high, especially as the silicon is derived from the substrate, Si<111> during $CrSi_2$ formation. An illustration of the degree of interface roughness is depicted in **figure [4.14]** as a function of $CrSi_2$ thickness from which

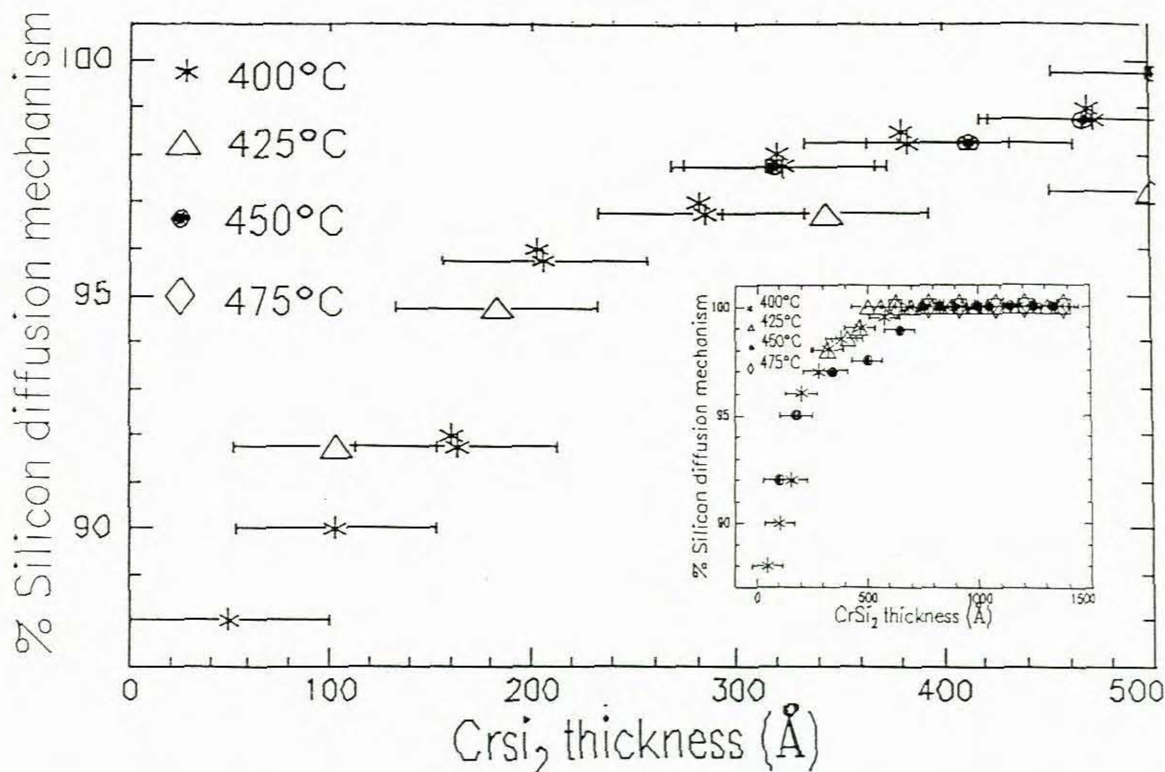

Figure [4.13]. *Illustration (exploded view) of the % silicon diffusion mechanism for the formation of $CrSi_2$ on non-epitaxial Pd_2Si. The silicon diffusion mechanism is the dominant mechanism, although the palladium diffusion mechanism takes place in the early stages of the reaction. The inset gives all the measurements.*

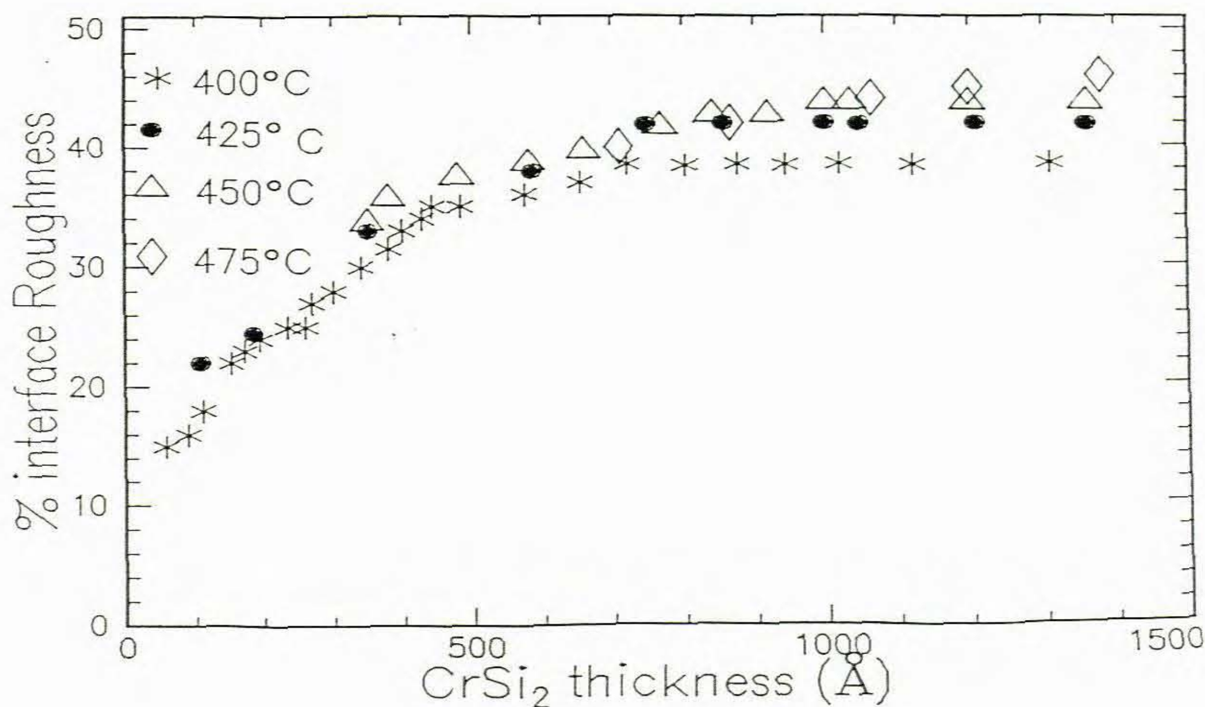

Figure [4.14]. *Illustration of the degree of Si<111> | Pd_2Si interface roughness or lateral non-uniformity for $CrSi_2$ formation on epitaxial Pd_2Si.*

can be seen that the roughness is twice as bad as compared to $CrSi_2$ formation on non-epitaxial Pd_2Si (see figure [4.7]).

4.4 Effect of marker thickness

In the previous sections $CrSi_2$ formation when using a thin (5Å) marker was discussed. In this section, the marker thickness is approximately twice (10Å) that of the thin marker. The experiment was only carried out on non-epitaxial Pd_2Si at a temperature of 425^0C. At the lower temperature of 400 ^{0}C, the reaction did not proceed. The data for the thick marker will be presented with the data at 425 ^{0}C for the thin marker on both non-epitaxial and epitaxial Pd_2Si.

4.4.1 Kinetics

Table [4.3] gives the growth rate at 425 ^{0}C for $CrSi_2$ formation on Pd_2Si – Si< > using a thin and thick marker on different substrate orientations. The growth rate for the formation of $CrSi_2$ on non-epitaxial Pd_2Si at 425 ^{0}C is depicted in **figure [4.15]**. It can be seen that the growth rate in not affected much by the thickness of the Ta marker in the Pd_2Si layer of by the epitaxy of the Pd_2Si layer.

Table [4.3] *Growth rates of $CrSi_2$ formation on Pd_2Si at 425 ^{0}C for thin and thick Ta markers on the two different substrate orientations*

Marker thickness Substrate	Thick (10Å) Si<100>	Thin (5Å) Si<100>	Thin (5Å) Si<111>
Growth rate (Åmin^{-1})	16.7	17.8	15.8

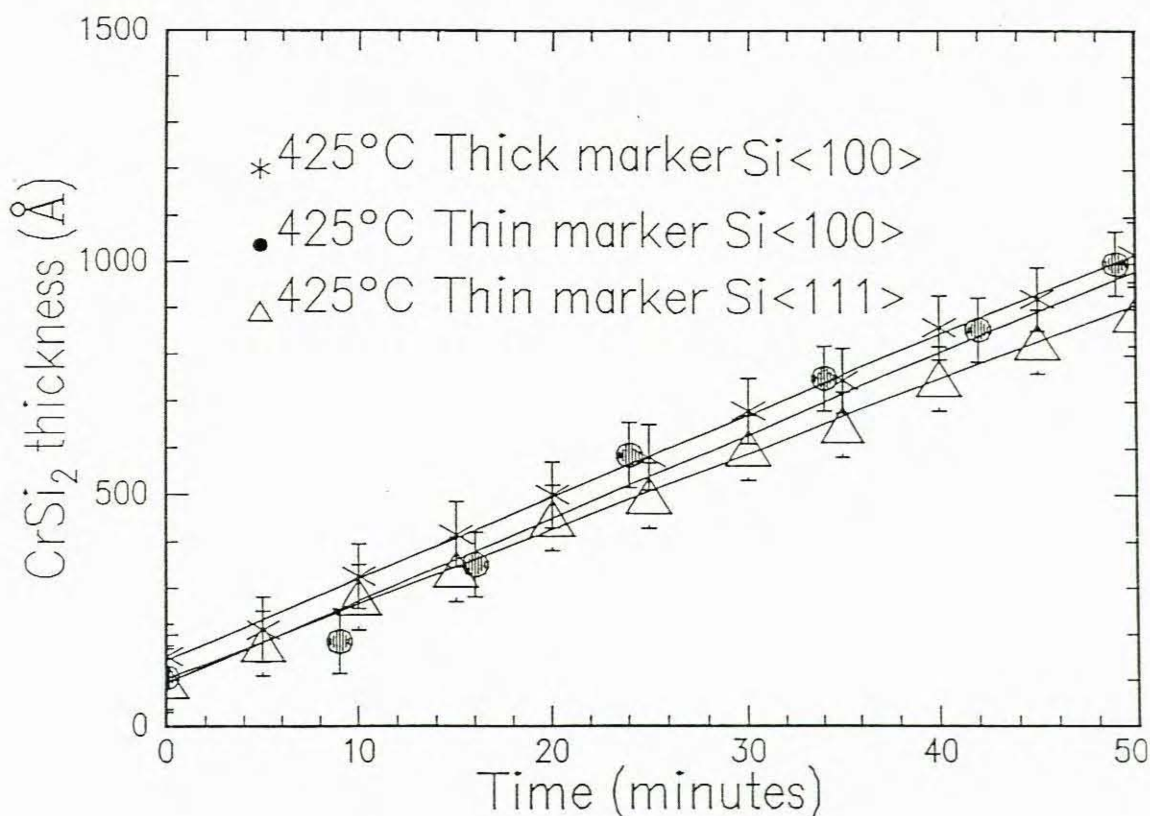

Figure [4.15]. ***Growth of $CrSi_2$ on non-epitaxial Pd_2Si using a thick Ta marker (12Å) compared to the growth on non-epitaxial and epitaxial Pd_2Si using a thin Ta marker (5Å). It can be seen that there is only a marginal difference in the growth rates for the different marker thicknesses and the substrate orientation. The growth rate with a thin (5Å) marker of $CrSi_2$ formation on non-epitaxial Pd_2Si is slightly higher than the growth rate with a thick (10Å) marker on non-epitaxial Pd_2Si.***

4.4.2 Diffusion mechanism

Figure [4.16] illustrates the backscattering spectra of $CrSi_2$ formation using a thick (10Å) marker. The slight inward movement of the marker shows that the silicon diffusion mechanism does occur, but to a lesser extent than in the instance of a thin (5Å) marker. This indicates that the percentage palladium diffusion mechanism is relatively high, but does not indicate when the palladium diffusion occurred, that is in the initial stages of $CrSi_2$ formation or during $CrSi_2$ formation. The *in situ* real time Rutherford Backscattering Spectrometric spectrum of $CrSi_2$ formation at 425 ^{0}C using a thick marker is depicted in **figure [4.17]** . The % silicon diffusion mechanism for the thick marker and for the thin marker,

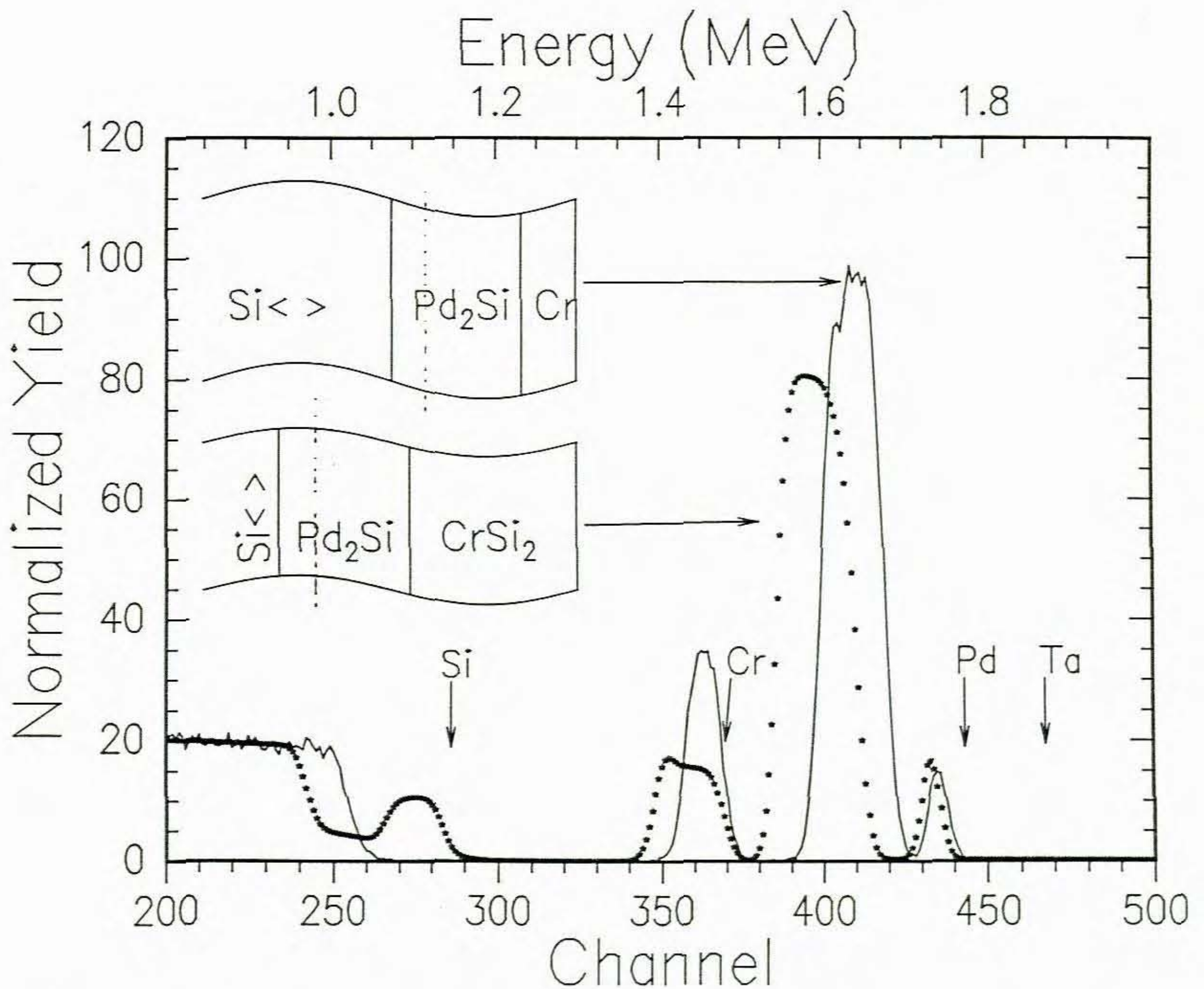

Figure [4.16]. ***Backscattering spectra of $CrSi_2$ formation on non-epitaxial Pd_2Si using a thick (10Å) marker. The continuous line represents the as deposited sample and the dotted line the sample when all the $CrSi_2$ (900Å) formed. The arrows indicate the energy of the elements when located at the surface of the sample. The slight inward movement of the marker is indicative of the silicon diffusion mechanism occurring during $CrSi_2$ formation, but to a lesser extent than during the formation using a thin marker.***

on both non-epitaxial and epitaxial Pd_2Si is illustrated in **figure [4.18]**, showing the marked effect of the Ta thickness on the mechanism. There is relative to the mechanism for the thin marker very little movement, indicating that the mechanisms contribute equally to the formation of $CrSi_2$.

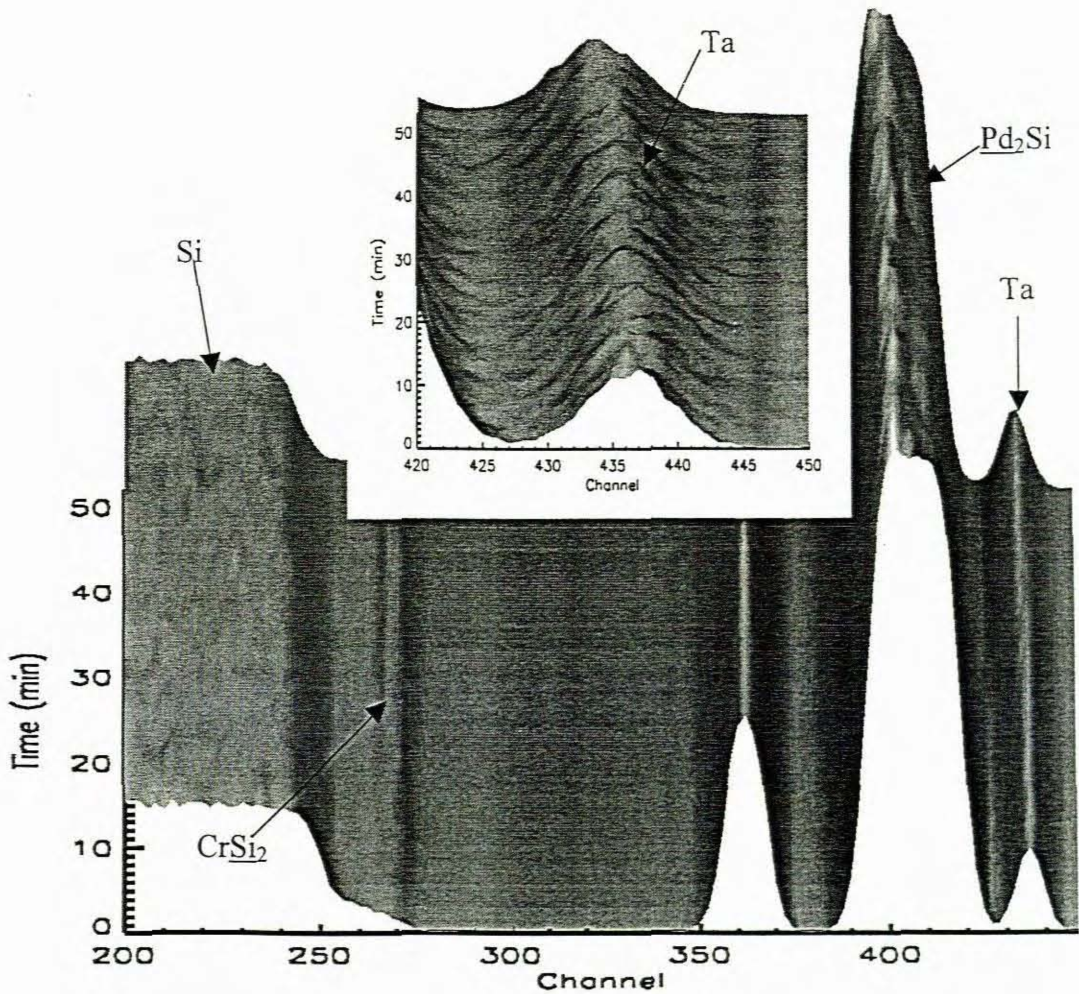

Figure [4.17]. *Illustration of the* in situ *real time RBS spectra of* $CrSi_2$ *formation at* 425^0C *using a thick marker. It can be seen that there is virtually no marker movement during the reaction. The inset is an exploded view of the Ta marker to depict the slight movement.*

The marker movement for the thick marker and the thin marker is depicted in **figure [4.19]**.

4.4.3 Interface Roughness

The use of a thin marker, discussed in the previous sections, had no significant effect on the growth kinetics, the percentage silicon diffusion mechanism or the degree of lateral non-uniformity.

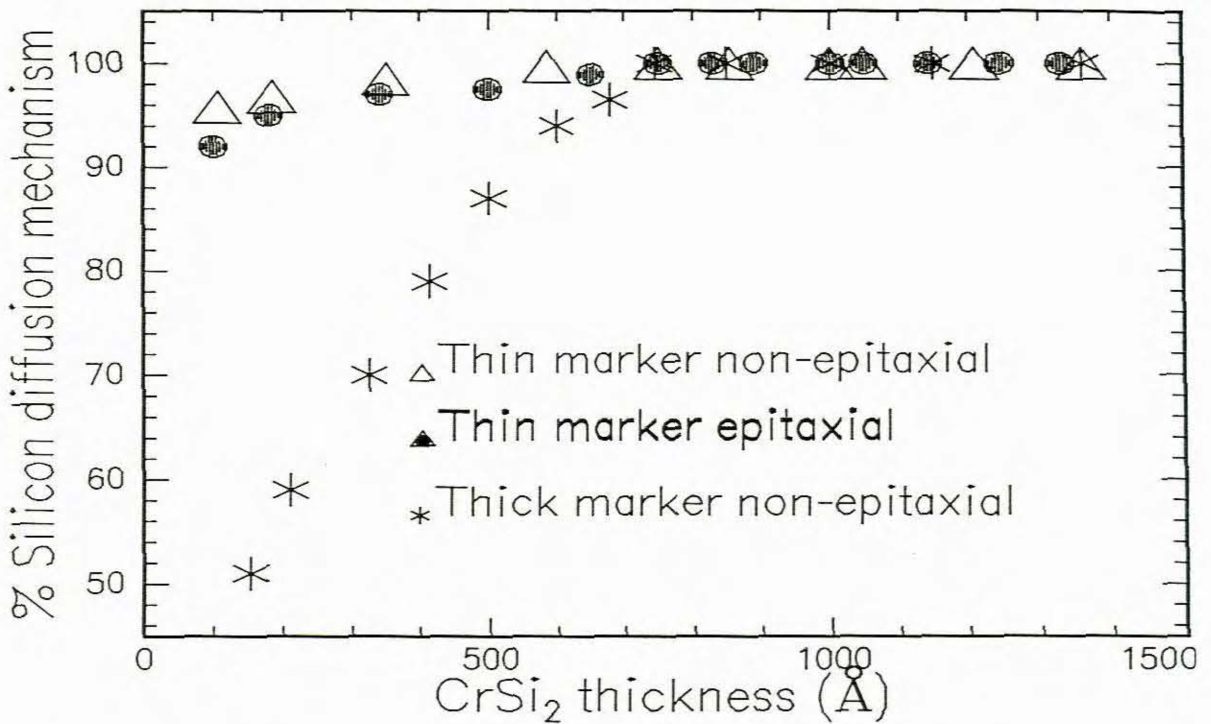

Figure [4.18]. ***Illustration of the % silicon diffusion mechanism for $CrSi_2$ growth, using a thick Ta marker (10Å) and a thin Ta marker (5Å) on both epitaxial and non-epitaxial Pd_2Si.***

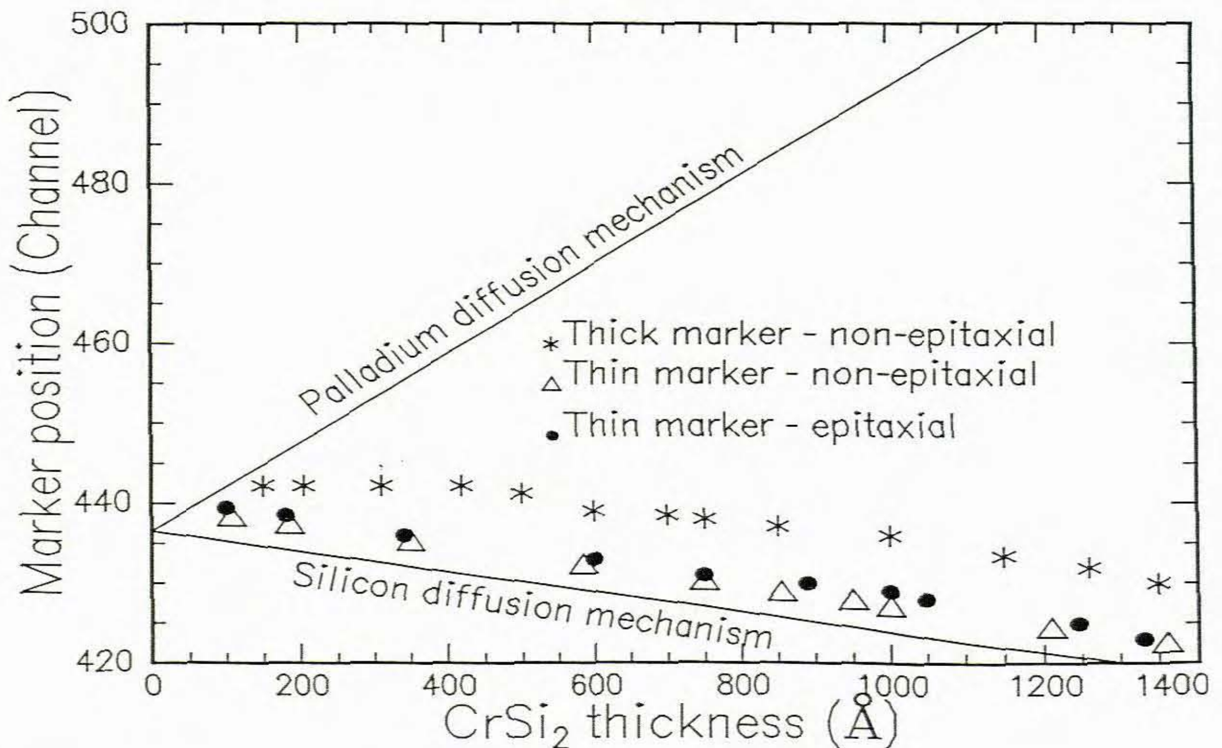

Figure [4.19]. ***Movement of the thick marker during $CrSi_2$ formation compared to that of a thin marker on both non-epitaxial and epitaxial Pd_2Si.***

The effect of a thick marker on the degree of interface roughness is depicted in **figure [4.20]**.

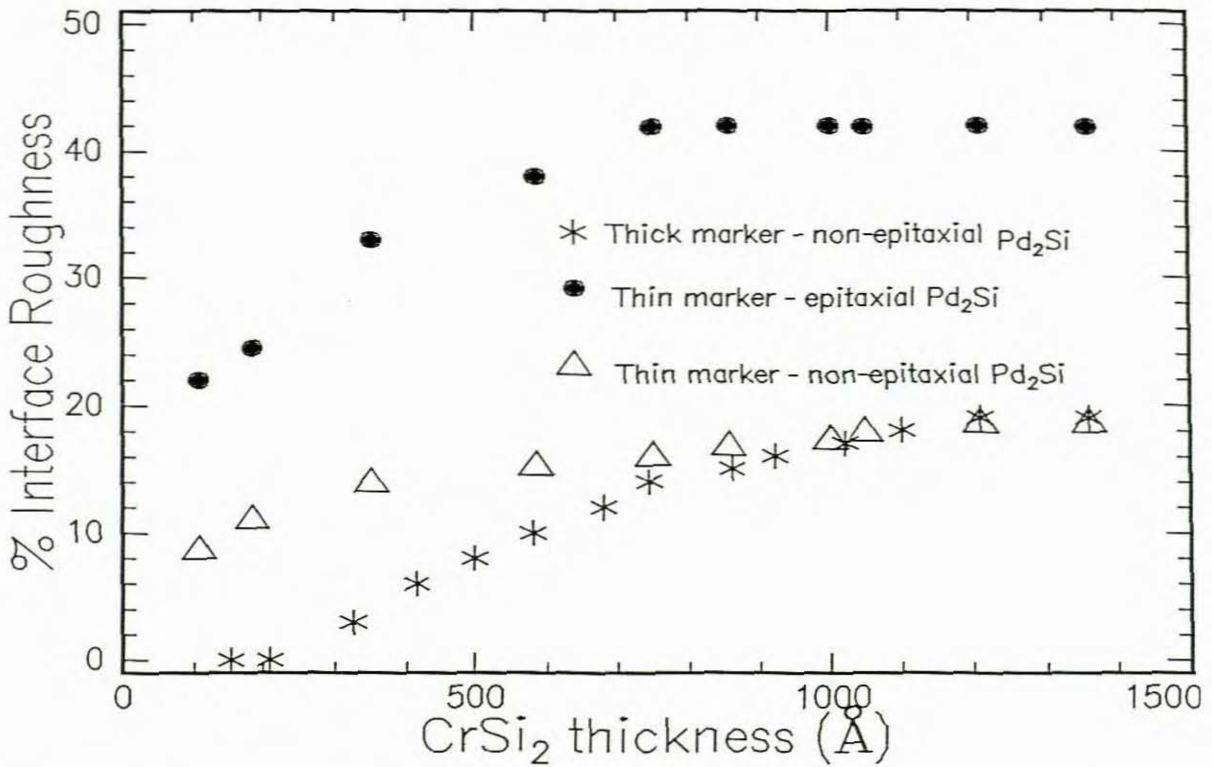

Figure [4.20]. ***Comparison of the degree of the Si | Pd_2Si interface roughness (lateral non-uniformity) for the $CrSi_2$ formation on different substrates, using a thick Ta marker (12Å) and thin Ta marker (6Å).***

The time taken for the growth to start was exceptionally longer than when a thin marker was used on both non-epitaxial and epitaxial substrates. **Figure [4.20]** indicates that the Ta marker thickness does not have an effect on the interface roughness, except in the initial stages.

4.5 Comparison of Results

4.5.1 Kinetics

Growth rates of $CrSi_2$ at 425^0C on non-epitaxial and epitaxial Pd_2Si using a thin (5Å) marker were found to be 17.4 Åmin^{-1} and 14.7 Åmin^{-1} respectively, differing marginally. In the presence of the thick marker (10Å), the growth rate is 16.7Åmin^{-1} and does not differ significantly. However, the time taken for growth to initiate with the thick marker is

longer for the thin marker case. The activation energy of 2.1 eV for growth on the non-epitaxial Pd_2Si, given in **figure [4.2]**, does not differ much from that of epitaxial Pd_2Si, that is 1.9 eV, shown in **figure [4.9].**

4.5.2 Diffusion mechanism

The degree of silicon diffusion in the polycrystalline layer during $CrSi_2$ formation, illustrated in **figure [4.5]** is marginally higher than for growth on epitaxial Pd_2Si, shown in **figure [4.12]**. This can be ascribed to the larger number of grain boundaries in polycrystalline Pd_2Si. With an increase in marker thickness the palladium diffusion mechanism (maximum ~ 50 %) increased significantly since the marker is apparently a greater barrier to silicon diffusion as compared to palladium diffusion. This indicates that the diffusion of silicon through the marker decreases with the increase in Ta marker thickness. As the reaction proceeds however, the silicon diffusion mechanism becomes dominant.

4.5.3 Interface roughness

The degree of lateral non-uniformity of the Si | Pd_2Si interface for non-epitaxial Pd_2Si, depicted in **figure [4.7]**, is much less than for epitaxial Pd_2Si, illustrated **in figure [4.14]**. This is primarily due to the orientation of Pd_2Si on the substrate. Pd_2Si grows non-epitaxially on Si<111> and epitaxially on Si <100>. Thus $CrSi_2$ formation on epitaxial Pd_2Si leads to a non-uniform Si <111> | Pd_2Si interface, but on polycrystalline Pd_2Si the effect is much smaller. This can be ascribed to the fact that there are much less paths for silicon diffusion through epitaxial Pd_2Si, leading to local pitting of silicon at the Si<111> | Pd_2Si interface. The degree of interface roughness however increases with the increase in the temperature at which the reaction takes place. With the increase in marker thickness, the interface roughness decreased significantly relative to the thin marker. In this instance (approximately 50% of) the silicon was derived primarily from the Pd_2Si layer in

front of the marker. Hence a small amount of silicon passed the back Pd_2Si layer, thus the layer remained comparatively uniform.

4.6 Diffusion in the $CrSi_2$ layer

To ascertain the diffusion mechanism in the $CrSi_2$ layer a Ta marker was inserted in this layer. The reaction however did not proceed at the reaction temperatures previously stated (less than 500^0C). The sample had to be annealed at temperatures of about 800^0C before $CrSi_2$ formation on Pd_2Si started to take place. **Figure [4.21]** illustrates the RBS spectra of the as deposited and the annealed samples showing that silicon is the diffusing species, due to the movement of the Ta marker to a lower channel position. The fact that higher temperatures have to be used to initiate $CrSi_2$ formation indicates that the Ta marker is a greater barrier to Si diffusion than to Pd diffusion.

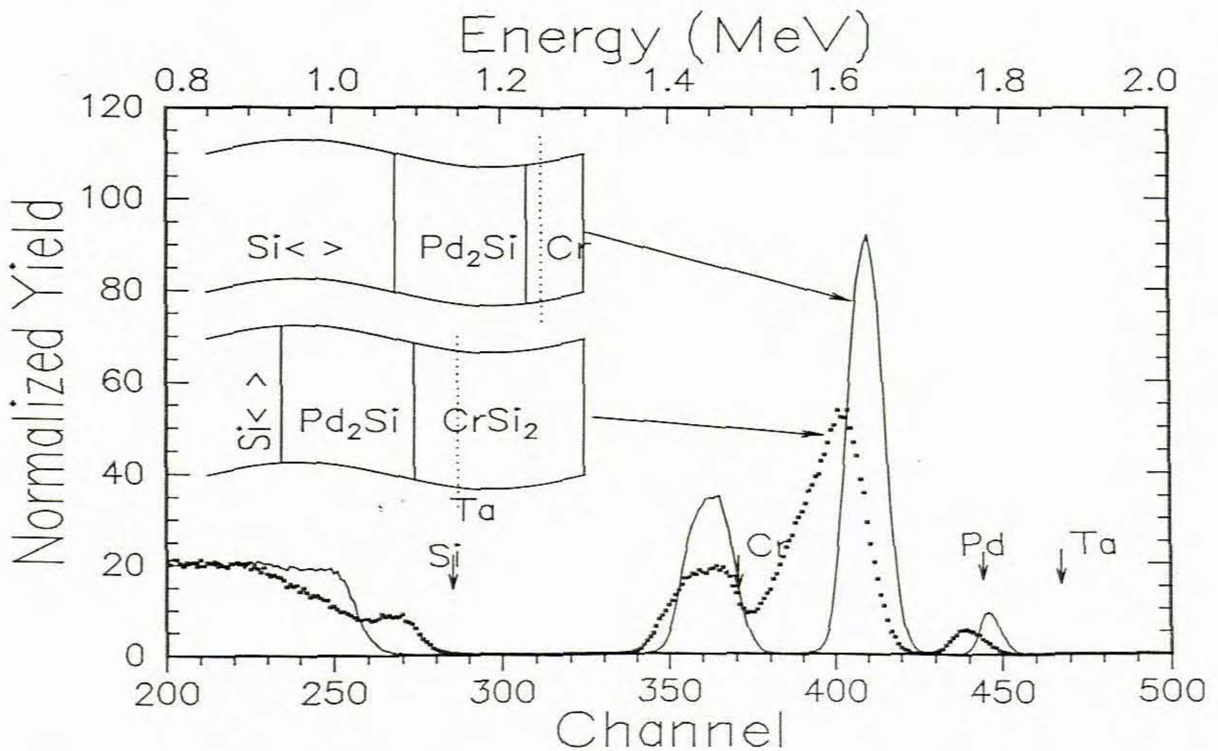

Figure [4.21]. ***RBS spectra indicating silicon diffusion in the $CrSi_2$ layer during formation at 800^0C. The continuous line represents the as deposited sample and the dotted line the annealed sample.***

CHAPTER 5
SUMMARY AND CONCLUSION

5.1 Summary

As silicon integrated circuit technology reaches higher levels of integration and complexity it has become necessary to use more than one metal for metallisation. It has thus become necessary to obtain a basic knowledge of solid-state interaction in silicon bi-metal thin-film structures. In this investigation the Si <>| Pd | Cr system has been investigated. At about 200^{0}C, it was found that palladium reacts with the silicon to form Pd_2Si, while at temperatures above 400^{0}C the silicide $CrSi_2$ forms on top of the Pd_2Si layer. The kinetics of $CrSi_2$ formation was determined on epitaxial and non-epitaxial Pd_2Si. By placing thin Ta marker layers in the Pd_2Si and $CrSi_2$ layers the diffusing species and diffusion mechanism were determined during $CrSi_2$ formation on Pd_2Si.

Rutherford Backscattering Spectrometry was used for sample characterisation and computer simulations of RBS spectra were effected using the software program RUMP. The simulations were done to optimise the thickness of the individual layers that were to be deposited on the substrate. The Pd_2Si layer thickness was optimised to serve as a reservoir of silicon should the palladium diffusion mechanism be the dominant diffusion mechanism. In the instance of the silicon diffusion mechanism optimisation of the Pd_2Si layer thickness is not required since the silicon would be derived from the substrate. The tantalum marker position in the Pd_2Si layer should be optimised in order to yield a well-resolved spectrum. The thickness of the Cr layer depends, in the case of the palladium diffusion mechanism occurring, on the thickness of the Pd_2Si layer. Hence the maximum

thickness of Cr that can be deposited depends on the Pd_2Si layer thickness. In the case of a silicon diffusion mechanism the Cr layer thickness can vary. Further simulations were then done to observe the movement of the marker in both instances of the silicon diffusion mechanism and the palladium diffusion mechanism taking place. To investigate the diffusion in the $CrSi_2$ layer, simulations were done for both the cases where silicon or palladium is the diffusing species. Theoretical plots of the marker position were generated to serve as a guide to identify the diffusing species.

The chemical system, Si < >| Pd | Cr, was subjected to a heating process at temperatures of 400, 425, 450, 475, 500 and 550 ^{0}C. At the temperature of 550 ^{0}C the $CrSi_2$ layer was completely formed before the temperature could be reached. At 500 ^{0}C the $CrSi_2$ formation was completed within 60 seconds and therefore did not yield reliable and significant data.

The growth of $CrSi_2$ was then determined at the reaction temperatures of 400, 425, 450 and 475 ^{0}C where first a thin (5Å) and then a thick (10Å) marker were inserted in the Pd_2Si layer. At these temperatures it was found that:

- The percentage silicon diffusion mechanism for $CrSi_2$ formation on both epitaxial Pd_2Si and non-epitaxial Pd_2Si increased as the reaction proceeded. Hence, at the relatively high temperatures of 450 and 475 ^{0}C for growth on both non-epitaxial and epitaxial Pd_2Si, silicon was the only diffusing species. For $CrSi_2$ growth on non-epitaxial Pd_2Si, the initial % silicon diffusion was slightly higher than in the case of $CrSi_2$ growth on epitaxial Pd_2Si. This can be ascribed to the fact that the silicon diffusion occurs by means of grain boundary diffusion, which is not in the case of palladium. Some initial palladium diffusion was found to occur until a $CrSi_2$ layer thickness of approximately 300Å formed. This initial palladium diffusion is independent of the temperature at which the reaction proceeds. The % silicon diffusion mechanism increases to 100%

after the $CrSi_2$ layer reaches a thickness of 300-500Å. When a thick (10Å) marker was inserted in the Pd_2Si layer, the % palladium diffusion (60%) increased markedly as compared to the case of the thin (5Å) marker. This is because in the case of the thick marker no silicon diffusion occurs in the early stages of $CrSi_2$ formation, silicon is obtained from the dissociation of Pd_2Si and not derived from the substrate. No movement of the thin (5Å) marker within the $CrSi_2$ layer was observed. This indicates that silicon is the diffusing species in $CrSi_2$. The $CrSi_2$ formation was only found to take place at temperatures as high as 800^0C, which indicates that the Ta marker is a barrier to the silicon diffusion.

- The growth rate of $CrSi_2$ on non-epitaxial Pd_2Si was marginally faster than the growth on epitaxial Pd_2Si. This can be attributed to the fact that there are more grain boundaries along which Si diffusion can take place. The Arrhenius plot indicated a high activation energy of about 2.0 ± 0.1 eV for the reaction on both the substrates, which is indicative of the difficulty with which the reaction proceeded. In the presence of a thick (10Å) marker, the growth rate ($16.7Åmin^{-1}$) was slightly less than the growth rate of $CrSi_2$ on non-epitaxial Pd_2Si and slightly more than the growth rate ($15.8Åmin^{-1}$) on epitaxial Pd_2Si ($17.8\ Åmin^{-1}$) with a thin (5Å) marker at the temperature of 425^0C.. However, the marker markedly affected the kinetics of the Si < >| Pd | Cr system, when placed in the $CrSi_2$ layer. in that the reaction could only proceed at the temperature of 800^0C.
- The degree of interface roughness or lateral non-uniformity of the Si<>|Pd_2Si interface, in the case of the thin marker, increased as the reaction temperature increased. The percentage interface roughness (~20%) for growth on the non-epitaxial Pd_2Si was significantly less than the percentage interface roughness (~40%) for growth on the epitaxial Pd_2Si. This is directly related to the orientation of the different substrates. When a thick

(10Å) marker was inserted in the Pd_2Si layer formed on Si <100>, the degree of interface roughness remained relatively constant (less than 10 %) during the initial stages of $CrSi_2$ formation compared to the degree of interface roughness (~20%) during $CrSi_2$ growth in the presence of the thin marker. This is due to palladium diffusion occurring in the early stages of $CrSi_2$ formation. In these early stages of $CrSi_2$ formation the silicon is obtained from the dissociation of Pd_2Si and not derived directly from the substrate, leading to less interface roughness of the Si <100 > | Pd_2Si interface.

5.2 Conclusion

The investigation of the chemical system, Si < >| Pd | Cr, in this study, indicates that when the structure is subjected to heating, that the silicon diffusion in the Pd_2Si layer is dominant during $CrSi_2$ formation on Pd_2Si. The data obtained at the various reaction temperatures shows that the extent of the roughness of the Si < > | Pd_2Si interface is temperature dependent, hence a certain degree of control can be exercised as to the lateral non-uniformity. When inserting a thick (10Å) Ta marker the diffusion mechanism is affected in that the palladium diffusion mechanism increased noticeably. The thickness of the marker can therefore be used to control the diffusing species. By placing the Ta marker in the $CrSi_2$ layer, it was found that silicon and not chromium diffuses in the $CrSi_2$ layer.

APPENDIX A

1. K values for RBS

Table [6.1] lists the kinematic factor K_M for elements heavier than sodium (Na).

Table [6.1]. ***List of K values and the densities of elements heavier than Na.***

Element Symbol	Atomic Number	K value	Density $gm.cm^{-3}$
Mg	12	0.5205	1.74
Al	13	0.5558	2.70
Si	14	0.5690	2.33
P	15	0.6001	1.82
S	16	0.6107	2.07
Ca	20	0.6745	1.53
Sc	21	0.7041	2.99
Ti	22	0.7196	4.51
V	23	0.7339	6.09
Cr	24	0.7385	7.19
Mn	25	0.7507	7.47
Fe	26	0.7542	7.87
Co	27	0.7647	8.9
Ni	28	0.7655	8.91
Cu	29	0.7805	8.93
Zn	30	0.7859	7.13
Zr	40	0.8415	6.51
Mo	42	0.8487	10.22
Pd	46	0.8625	12.00
Ag	47	0.8643	10.50
Ta	73	0.9167	16.66
Au	79	0.9232	19.28

APPENDIX B

Thicknesses that react

Silicides are formed when metals on a silicon substrate react with the substrate. Since the densities of the elements vary, it is necessary to know the mass ratios of the reactants and the products.

In the formation of Pd_2Si on a silicon substrate, the reaction can be written as

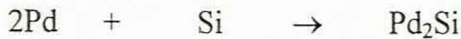

$$2Pd \quad + \quad Si \quad \rightarrow \quad Pd_2Si$$

Dividing the moles of the elements by the density yields

$2Pd$	+	Si	$\rightarrow$	Pd_2Si
$\frac{2 \times 106.40}{12.00}$		$\frac{28.10}{2.33}$		$\frac{240.9}{9.57}$
17.73		12.06		25.18
1		0.68		1.42

These calculations indicate that 1Å of palladium will react with 0.68Å of silicon to form 1.42Å of palladium silicide. **Table [6.2]** lists the for Pd_2Si, Cr and Ta that would react to form silicides.

Table [6.2]. Thickness of the metals of Pd, Cr and Ta that would react with silicon to form the corresponding silicides.

Symbol of Metal	Thickness that would react				
Pd	2Pd	+	Si	→	Pd_2Si
	1		0.68		1.42
	Pd	+	Si	→	PdSi
	1		1.36		1.97
Cr	Cr	+	2Si	→	$CrSi_2$
	1		3.34		3.00
	Cr	+	Si	→	CrSi
	1		1.67		2.04
	5Cr	+	3Si	→	Cr_5Si_3
	1		1		1.91
Ta	Ta	+	2Si	→	$TaSi_2$
	1		2.21		2.40
	2Ta	+	Si	→	Ta_2Si
	1		0.55		1.32
	3Ta	+	Si	→	Ta_3Si
	1		0.37		1.24

BIBLIOGRAPHY

ATKINS, P.W. 1995: Physical Chemistry London: Oxford University Press.

BAXI, H.C. & MASSALSKI, T.B. 1991: The Pd-Si (Palladium-Silicon) System. Journal of Phase Equilibria. vol. 12, no.3, pp. 349-356.

BOTHA, A.P., PRETORIUS, R., & KRITZINGER, S. 1981: Determination of the diffusing species and mechanism of diffusion during $CrSi_2$ formation, using ^{31}Si as a marker. Applied Physics Letters, vol. 40, no.5, pp. 412-414.

COMRIE, C.M & EGAN, J.M. 1989: Diffusion of Silicon in Pd_2Si during growth. Journal of Vacuum Science Technology. vol. A7, no. 1492, pp. 1492-1496

COMRIE, C.M.; EGAN, J.C.; LIU, J.C. & MAYER, J.W. 1988: An investigation into the mechanism of epitaxial Pd_2Si formation. South African Journal of Science, vol. 84, pp. 688 – 689.

COMRIE, C.M.; LIU, J.C., HUNG, L.S. & MAYER, J.W. 1988: Reordering of polycrystalline Pd_2Si on epitaxial Pd_2Si. Journal of Applied Physics, vol. 63, no. 7, pp. 2402 –2404.

COTTON, F.A., WILKINSON, F.R.S. & Gauss, P.L. 1987: Inorganic Chemistry. London: Interscience Publishers.

FARMER, J., WANDT, M. A. E. & PRETORIUS, R. 1990: Radioactive metal tracer investigation of Pd_2Si formation. Applied Physics Letters, vol. 56, no. 17, pp 1643-1645

HO, K. T., LIEN, C.-D., SHRETER, U. & NICOLET, M.-A. 1985: An inert marker study for palladium silicide formation: Si moves in polycrystalline Pd_2Si. Journal of Applied Physics. vol. 57, no. 2, pp 227-231

HONG, S.Q., COMRIE, C.M., RUSSELL, S.W. & MAYER, J.W. 1991: Phase formation in Cu-Si and Cu-Ge. Journal of Applied Physics, vol 70, no. 7, pp 3655-3660

KUBASCHEWSKI, O. & ALCOCK, C.B. 1979: Metallurigcal Thermochemistry. New York: Pergamon.

LIEN, C.-D., NICOLET, M-A. & PAI, C.S. 1985: A structure marker study for Pd_2Si formation: Pd moves en epitaxial Pd_2Si. Journal of Applied Physics, vol. 57, no. 2, pp. 224-226.

LIPTROT, G.F. 1983: Modern Inorganic Chemistry. London: Bell and Hyman.

MIEDEMA, A.R., de CHATEL, P.F. & de BOER, F.R. 1979: Cohesion in alloys – Fundamentals of a semi-empirical model. Physica 100B, pp. 1 – 28.

MOFFAT, W.G. 1997 (Updated as issued): Handbook of Binary Phase Diagrams. New York: Genium Publishing Company.

NATAN, M. & DUNCAN, S.W. 1985: Microstructure and growth kinetics of $CrSi_2$ on Silicon<100> studied using Cross-sectional transmission electron microscopic. Thin Solid Films, vol. 123, pp. 69-85.

NICOLET, M-A. & LAU, S.S. 1983: Formation and characterisation of Transition-Metal Silicides. VLSI Electronics: Microstructure Science, Vol. 6.

PRETORIUS, R., MARAIS, T.K. & THERON, C.C. 1992: Thin film compound formation sequence: An effective heat of formation model. Material Science and Engineering, vol. 30, pp. 1-83.

PRETORIUS, R., OLOWOLAFE, J.O. & MAYER, J.W. 1978: Radio-active silicon tracer studies of the formation of $CrSi_2$ on Pd_2Si and PtSi. Philosophical Magazine A, vol. 37, no. 3, pp. 327-336.

SCHMALZRIED, H. 1981: Solid State reactions. Weinheim: Verlag Chemie.

TU, K.-N., MAYER, J.W. & FELDMAN, L.C. 1992: Electronic Thin Film Science for Electrical Engineers and Material Scientists. New York: Macmillan Publishing Company.

WEI, C.S., VAN DER SPIEGEL & SANTIAGO, J.J. 1988: Growth kinetics of Palladium Silicide formed by Rapid thermal Annealing. Journal of the Electrochemical Society, vol. 135, no. 2, pp. 446-451.

WEST, A.R., 1984: Solid State Chemistry and its Applications. Chicago: Wiley and Sons.

ZINGU, E.C., COMRIE, C.W. & PRETORIUS, R. 1983: The effect of the interposed silicide thickness of growth in bilayer silicide thin-film structures: The Si<111>/Pd_2Si/Cr system. Journal of Applied Physics. vol. 54, no. 5, pp. 2392-2401.

ZINGU, E.C., COMRIE, C.W., MAYER, J. & PRETORIUS, R. 1984: Mobility of Pd and Si in Pd_2Si. Physical Review B. vol. 30, no. 10, pp. 5916-5922.